Aus der Medizinischen Klinik und Poliklinik III
der Ludwig-Maximilians-Universität München
Direktor: Prof. Dr. Dr. Michael von Bergwelt

Dissertation

zum Erwerb des Doctor of Philosophy (Ph.D.) an

der Medizinischen Fakultät der

Ludwig-Maximilians-Universität zu München

The Molecular Ontogeny of Follicular Lymphoma: Identification and Functional Characterization of Selected Truncal Gene Mutations

vorgelegt von:

William David Keay

aus:

Brighton, United Kingdom

Jahr: 2023

First evaluator (1. TAC member):   Prof. Dr. med. Oliver Weigert

Second evaluator (2. TAC member):   apl. Prof. Dr. med. Karsten Spiekermann

Third evaluator: Priv. Doz. Dr. Tobias Birnbaum

Fourth evaluator: apl. Prof. Dr. Ralf Schmidmaier

Dean: **Prof. Dr. med. Thomas Gudermann**

date of the defense:

01.02.2023

Table of Contents

Abstract

Background: Advanced-stage follicular lymphoma (FL) is considered incurable, with patients typically suffering from a chronic relapsing clinical course. Relapsed FL is thought to originate from common progenitor cells (CPCs) through divergent evolution. CPCs typically contain the hallmark *BCL2*/*IGH* translocation, in addition to other recurrent mutations. Targeting CPC-defining, early acquired (i.e., truncal) mutations offers the chance to eradicate/cure the disease.

Aim: To define and functionally characterize early acquired mutations in FL.

Results: We hypothesized that CPC-defining mutations can be acquired before the FL-hallmark *BCL2*/*IGH* translocation in hematopoietic stem and progenitor cells (HSPCs). To directly define the molecular ontogeny of FL, we used highly sensitive mutation detection of purified *BCL2*/*IGH*-negative (*BCL2*/*IGH*⁻) HSPCs from leukapheresis samples of 3 patients in clinical remission. However, using complementary approaches, we did not identify CPC-defining mutations in *BCL2*/*IGH*⁻ progenitor cells. Vice versa, we identified B cells harboring the FL-specific *BCL2*/*IGH* translocation but without CPC-defining mutations in one informative case.

We next used indirect approaches to identify truncal mutations for functional characterization. Using cancer cell fraction corrected (CCF)-variant allele frequency (VAF) from FL patients, we identified *STAT6* (based on a previous study) and *IKZF3* (based on our own data) as truncal events by high clonality. Previous work from our group (Boesl et al.) provided the first insights into the biology of *STAT6* mutations, however, the mechanisms remained incompletely understood. In my thesis, I significantly contributed to this work by showing that *STAT6* mutations drive a self-reinforcing microcircuit. Specifically, I showed that in the presence of interleukin-4 (IL-4) (i) $STAT6^{D419G}$ mutations are gain-of-function (by serial replating pre-B cell colony-forming-units (CFU) assays), that (ii) $STAT6^{D419G}$ (but not $STAT6^{WT}$) binds to the PARP14 promoter and activates gene expression of PARP14 (which is a component of the STAT6 enhanceosome), and that (iii) increased nuclear accumulation of phosphorylated $STAT6^{D419G}$ drives increased expression of known STAT6 target genes, including *FCER2*, *CCL17*, *CCL22*, as well as *PARP14* itself.

Finally, using our own available DNA sequencing data, we identified *IKZF3* mutations as truncal events by high clonality. Of note, mutations cluster in distinct hotspots, mostly L162R and S215R. To

model early and later mutation acquisition, I utilized Cre-Lox recombination restricted *IKZF3* expression in lineage negative (lin-) HSPCs from Emu-BCL2/Vav-Cre mice (IKZF3 expression before B-lineage commitment) vs. Emu-BCL2/Mb1-Cre mice (*IKZF3* expression in B-lineage committed cells). My results indicate that *IKZF3*^{S215R} mutations are primarily gain-of-function (i.e. provide a serial replating phenotype) when expressed in HSPCs. In contrast, *IKZF3*^{L162R} mutations provide a serial replating phenotype when expressed in pre-B cells. Phenotypic analysis of IKZF3^{L162R} mouse pre-B CFUs identified them to be in a highly proliferative differentiation state (B220$^+$ CD24^{++} CD43$^+$), characterized by ongoing pre-BCR signaling and increased SYK expression. In primary human FL-like B cells, we confirmed this phenotype, with IKZF3^{L162R} cells showing increased SYK expression and an increased proliferative rate. RNA sequencing analysis of *IKZF3*^{L162R} FL-like B cells vs. *IKZF3*^{WT} identified B cell proliferation and activation to be enriched.

Discussion and conclusion: The absence of mutations in HSPCs suggests that in human FL, the *BCL2*/*IGH* translocation can precede the acquisition of CPC-defining mutations. We also identified *BCL2*/*IGH*$^+$ cells in a patient in ongoing clinical remission but without CPC-defining mutations. The absence of CPC-defining mutations suggests that these cells are not contributing to relapse.

In the second part of my thesis, I studied early acquired *STAT6* mutations. My results significantly contributed to further characterizing the *STAT6* mutation phenotype. We propose that the *STAT6*^{D419G} gain-of-function phenotype is strictly dependent on IL-4. STAT6^{D419G} but not STAT6^{WT} aberrantly increases *PARP14* levels in lymphoma cells. Increased PARP14 levels then contribute to increased assembly/stabilization of the STAT6 enhanceosome complex, resulting in increased STAT6-dependent gene expression and thereby amplifying an IL-4 driven self-reinforcing microcircuit. Therefore, PARP14 represents an attractive therapeutic target in *STAT6*^{MUT} FL.

Lastly, I identified IKZF3 with mutation-specific phenotypes when expressed in HSPCs vs. B cells. My results indicate that *IKZF3*^{L162R} induces proliferative expansion of pre-B cells and FL-like mature B cells, characterized by increased BCR signaling and SYK expression. Further functional experiments are required to better define the precise mechanism.

List of Figures

List of Tables

Abbreviations

ANOVA- analysis of variance

BCA- bicinchoninic acid assay

BCRs- B cell receptors

BLL- B-cell acute lymphoblastic leukemia

Bp- Base pairs

BTK- Bruton-tyrosine kinase

CCL17- C-C motif chemokine ligand 17

CCL22- C-C motif chemokine ligand 22

cDNA-complementary deoxyribonucleic acid

CFUs- Colony forming units

CML- Chronic myeloid leukemia

CMV- Cytomegalovirus

CPC- Common progenitor cell

CREBBP- CREB binding protein

Cre- Cre recombinase

CRISPR- Clustered regularly interspaced short palindromic repeats

CT- Computed tomography

ddPCR- Digital droplet polymerase chain reaction

DLBCL- Diffuse large cell B cell lymphoma

DMEM- Dulbecco's modified eagle's medium

DMSO- Dimethyl sulfoxide

dNTP- Deoxynucleotide triphosphates

DTT- Dithiothreitol

e.g.- For example

ECL- Enhanced chemiluminescence

EDTA- Ethylenediamine tetraacetic acid

ERK1/2- Extracellular signal-regulated kinase

EV- Empty vector

FACS- Fluorescence-activated cell sorting

FAS- Fas cell surface death receptor

FBS- Fetal bovine serum

FC- Flow cytometry or fold change

FCER2 (CD23)- Fc Epsilon Receptor II.

FDC- Follicular dendritic cell

FFPE- Formalin fixed paraffin embedded

FFS- Failure-free survival

FL- Follicular Lymphoma

FLIPI- Follicular lymphoma international prognostic index

g- G force

GAPDH- Glyceraldehyde-3-phosphate dehydrogenase

GC- Germinal center B cell

GFP- Green fluorescent protein

Gy- Gray

h- Hour

HSC- Hematopoietic stem cells

HSPC- Hematopoietic stem and progenitor cells

IGH- Immunoglobulin heavy locus

IKZF1- IKAROS family zinc finer 1

IKZF3- IKAROS family zinc finger 3

IMDM- Iscove's modified Dulbecco's medium

IP- Immunoprecipitation

IPBase- Insect version of the piggyBac transposase

IRES-Internal ribosomal entry site

k/d- shRNA Knockdown

KMT2D- Lysine methyltransferase 2D

KO-Knockout

LMNCs- Leukapheresis-derived mononuclear cells

LN- Lymph node

LoxP- Locus of X-over P1

MACS- Magnetic-activated cell sorting

MBR- BCL2/IGH major breakpoint region

mcr- *BCL2/IGH* minor cluster region

mg- Milligram

mL- Milliliter

MLP- Multilymphoid progenitor cells

MPP- Multipotent progenitor cells

MRD- Minimal residual disease

MSCV- Murine stem cell virus

MUT- Mutant

n.a.- Not applicable

n.d.- Not detectable

NDN, non-templated nucleotides

NGS- Next-generation sequencing

OS- Overall survival

PARP14- Poly(adp-ribose) polymerase family member 14

PB- PiggyBac

PBMCs- Peripheral mononuclear cells

PCR- Polymerase chain reaction

PEI- Polyethylenimine

POD- Progression of disease

qChIP- Quantitative chromatin immunoprecipitation

QIseq- Quantitative insertion site sequencing

qPCR- Quantitative polymerase chain reaction

R-CHOP- CD20 antibody + cyclophosphamide, doxorubicin (hydroxydaunomycin), vincristine
(Oncovin), and prednisone

Rpm- Revolutions per minute

RPMI- Roswell Park Memorial Institute

SA- Splice acceptor

SB- Sleeping beauty transposon

SD-Splice donor

SHM-Somatic hypermutation

STAT6- Signal transducer and activator of transcription 6

SYK- Spleen tyrosine kinase

T_{FH}- T follicular helper cell

UMI- Unique molecular identifiers

V- Volts

VAF- Variant allele frequency

VDJ- Variable, diversity, joining

Vs.-Versus

β-Tubulin- Beta tubulin

°C- degree Celsius

1. Introduction

1.1 Follicular lymphoma- A clinical perspective

1.1.1 Clinical features

Follicular Lymphoma (FL) is the second most common non-Hodgkin lymphoma in western countries, with an incidence of 3-5 in 100,000 in Europe (1). FL is a very heterogeneous disease with patients typically presenting with painless lymphadenopathy, and frequently disease infiltration of the bone marrow, and less commonly in other organs (2). The majority of FL patients are older, with a median age of diagnosis of 65 years old (3).

To make the diagnosis of FL, a tumor biopsy and evaluation by a hematopathologist is required. Histological grades 1-3a are considered indolent lymphomas, grade 3b is considered a form of aggressive lymphoma. Initial evaluations include a careful physical exam, blood tests, bone marrow biopsies, and a computed tomography (CT) scan with or without PET-imaging. Clinical staging by the Ann Arbor classification (4), as well as the patients' performance status and comorbidities are the main determinants to select the most appropriate approaches for patient management (5).

Most patients present with advanced-stage disease (Ann Arbor III, IV, e.g., LN affected above and below the diaphragm or diffuse infiltration of the bone marrow or other extranodal sites, respectively). Unlike patients with limited-stage disease (Ann Arbor I or II), these patients cannot be cured by irradiation-based therapies. Whilst most patients will respond well to frontline therapies and have long overall survival (median OS > 15-20 years), subsets of patients have early treatment failures and remarkably poor outcomes (1).

1.1.2 Treatment

The first step in determining the most appropriate treatment approach in FL is to distinguish limited-stage from advanced-stage disease. Less than 20% of patients present with limited-stage disease, but these patients should be offered involved-field radiotherapy (IFRT)-based treatment in a curative intent (6). In some cases, however, radiotherapy is not feasible (e.g., technically not possible or in patients with bulky disease). Asymptomatic patients with advanced-stage or patients with limited stage disease that cannot be irradiated should receive watch and wait (5, 7). Symptomatic patients with advanced-stage disease or limited-stage disease that cannot be irradiated should be offered standard CD20 antibody-based immunochemotherapies (rituximab or obinutuzumab in combination

with either CHOP (cyclophosphamide, doxorubicin, vincristine, and prednisone), bendamustine, or - less commonly- CVP (cyclophosphamide, vincristine, and prednisone). If these patients are considered ineligible for standard chemotherapy, they can be offered dose-reduced chemotherapy in combination with CD20 antibodies, CD20 antibody monotherapy, or best supportive care. A summary of some of the available treatment options available to FL patients is depicted in Figure 1.
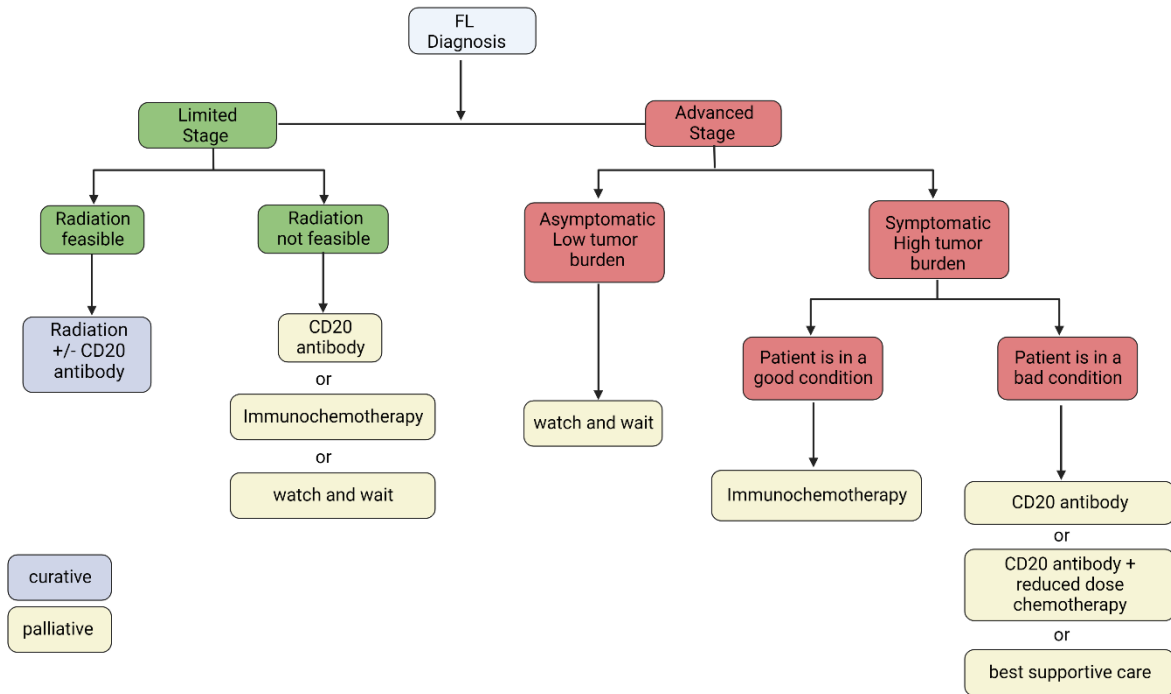
Figure 1- Follicular lymphoma therapeutic decisions.

Adapted from- (5, 7, 8).

In addition to standard immunochemotherapies and in later lines of treatment, novel treatments (approved or in ongoing clinical evaluation) include molecular targeting compounds such as PI3K inhibitors (e.g., idelalisib, copanlisib), EZH2 inhibitors (e.g. tazemetostat), BTK inhibitors (e.g. ibrutinib), and immunomodulatory drugs (IMiDs, e.g. lenalidomide). Others include novel immunotherapies such as anti-CD19 antibodies (e.g. tafasitamab), bispecific T cell engagers (BiTEs, e.g. mosunetuzumab), and chimeric antigen receptor (CAR) T cells (e.g. lisocabtagene maraleucel), amongst others. However, clinically it remains a challenge to identify patient subsets who will benefit most from particular treatments.

1.1.3 Prognosis and risk stratification

To identify patients at risk of early disease progression, prognostic tools have been developed for prospective risk stratification. The follicular lymphoma international prognostic index (FLIPI) is one of the most common and is based on five adverse clinical factors (**Table 1**) (9). The FLIPI categorizes patients into low, intermediate, and high-risk groups with different 5-year OS (91%, 78%, and 53%) (9). Other clinical risk models, such as the FLIPI-2 (10) and the PRIMA-PI (11) have been developed subsequently, yet these tools are (i) purely prognostic, (ii) are not used to guide treatment options in current clinical practice, and (iii) inherently cannot account for the underlying distinct biology of the individual disease.

The m7-FLIPI improves patient risk stratification by integrating biological factors. These include the mutation status of 7 recurrently mutated genes (*EZH2*, *ARID1A*, *MEF2B*, *EP300*, *FOXO1*, *CREBBP*, *CARD11*) and also FLIPI and ECOG (Eastern Cooperative Oncology Group (ECOG) performance status) (12, 13). Other studies have incorporated gene expression profiles, with a recent study incorporating the expression profiles of 23 genes as a predictor of survival (14, 15).

To date, none of these prognostic approaches have made it into routine diagnostics. In addition, with increasing numbers of promising treatment options, including molecular and immune targeting therapies, a better understanding of the underlying biology is needed to guide individualized treatment approaches with high activity and low toxicity.

	FLIPI (Solal-Celigny et al. *2004*) (9).	FLIPI-2 (Federico et al. *2008*) (10).	PRIMA-PI (Bachy et al. 2018) (11).	m7-FLIPI (Pastore et al. 2015) (13).
Risk factor	Age > 60 years - Stage III/IV - hemoglobin < 12 g/dL - > 4 affected Lymph node regions - elevated serum LDH	Age > 60 years - Elevated β2-microglobulin - hemoglobin < 12 g/dl - bone marrow infiltration - Longest diameter of the largest affected lymph node > 6 cm	β2-microglobulin > 3 mg/l - Bone marrow infiltration	FLIPI: high risk - ECOG > 1 - Non-silent mutations in: - *ARID1A* - *MEF2B* - *FOXO1* - *CARD11* - *CREBBP* - *EP300* - *EZH2*
Calculation	One point per risk factor	Each risk factor gets one point	Staggered weighting of risk factors	Sum of risk factors with individual weighting (https://www.german-lymphoma-alliance.de/Scores.html)
Classification	**Risk:** 0-1 points: low 2 points: intermediate 3-5 points: high	**Risk:** 0 points: low 1-2 points: intermediate 3-5 points: high	**Risk:** β2-microglobulin ≤ 3 mg/l: -KM infiltration: intermediate β2-microglobulin > 3 mg/l: high - None KM infiltration: low	**Risk:** > 0.8: high < 0.8: low

Table 1- Risk stratification in follicular lymphoma.
Modified from (8).

1.2   Follicular lymphoma- A molecular perspective

1.2.1   Germinal center (GC) derived lymphomas

FL is thought to develop in cells transitioning the GC and has a B cell biology phenotypically similar to GC B cells (16). GCs are formed upon antigen challenge, which activates B cells that undergo somatic hypermutation and proliferation to generate high-affinity B cell receptors (BCRs). GCs consist of dark zones, which are characterized by rapidly proliferating B cells, and light zones where B cells interact with follicular dendritic cells (FDCs) and T follicular helper cells (T_{FH}) (**Fig. 2**) (17, 18). B cells undergo rounds of selection of their BCR by diversifying their immunoglobulin genes by activation of the enzyme, activation-induced cytidine deaminase (AID), and somatic hypermutations (19-22). The majority of GC cells will undergo negative selection, but some will differentiate into antibody-secreting plasma cells or memory B cells, while others will undergo further rounds of somatic hypermutation (16).
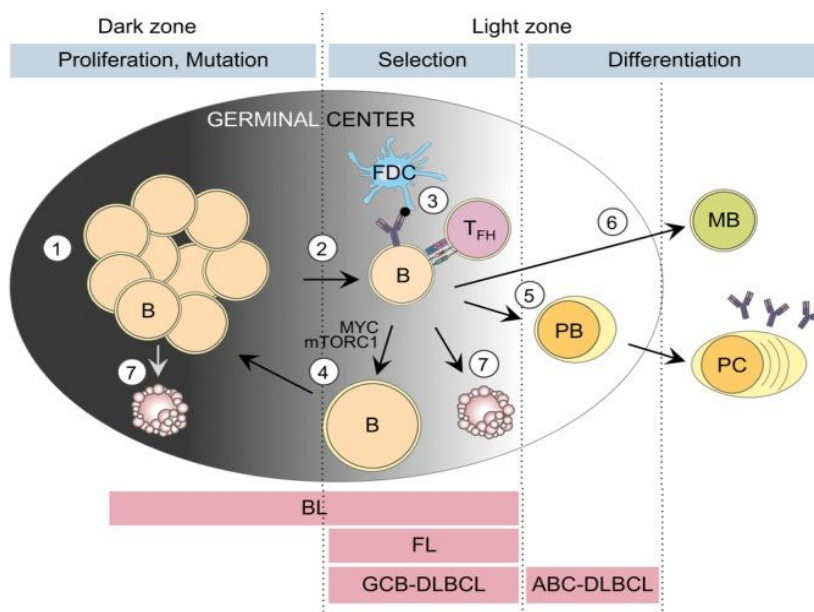
Figure 2- Germinal center (GC) derived lymphoma.

(1) GCs are formed in the dark zone when B cells become activated by antigens. GC B cells proliferate and somatically mutate their immunoglobulin genes. **(2)** After proliferating, GC B cells transit into the light zone. **(3)** B cell selection takes place in the light zone via affinity to a specific antigen, by interaction with follicular T-helper cells (T_{FH}) and with follicular dendritic cells (FDCs). **(4)** Those cells positively selected activate MYC and mTORC1 metabolic programs, transit to the dark zone, and undergo proliferative expansion and further selection. **(5)** Positively selected cells may first differentiate into plasmablasts (PB) before further differentiating into antibody-secreting plasma cells (PC), or **(6)** they differentiate into memory B cells (MB). **(7)** B cells that are not selected or have unfavorable somatic mutations undergo apoptosis. The relation between GC B cell-derived lymphomas and their GC cell of origin is shown, which is based on transcriptional, genetic, and other profiles. Modified from (16).

The hallmark lesion of FL is the *BCL2/IGH* translocation (t(14;18), hereafter *BCL2/IGH*), which is present in 85% of cases of advanced FL. This translocation leads to increased expression of anti-apoptotic BCL2. The translocation is thought to occur in pre/pro B cells in the bone marrow undergoing VDJ (variable, diversity, joining) recombination (23). It is, however, not enough to develop FL. In fact, the *BCL2/IGH* translocation is present in healthy individuals with increasing prevalence with age (24, 25). Whilst the translocation is commonly considered an early transformative event in the pathogenesis of FL; additional mutations are required to develop the disease. (26, 27). These mutations are thought to primarily be acquired in the GC reaction (28).

1.2.2 Gene mutations in follicular lymphoma

1.2.2.1 Mutational landscape

Genetic aberrations in FL are now well known, yet when each individual mutation is acquired (the molecular ontogeny) and how they contribute to FL development and pathogenesis is poorly described. Epigenetic dysregulation is common amongst hematological malignancies. In FL, the most common mutations affect *CREBBP* and *KMT2D,* which involve posttranslational modifications of histones and are found in over 50% of cases (29).
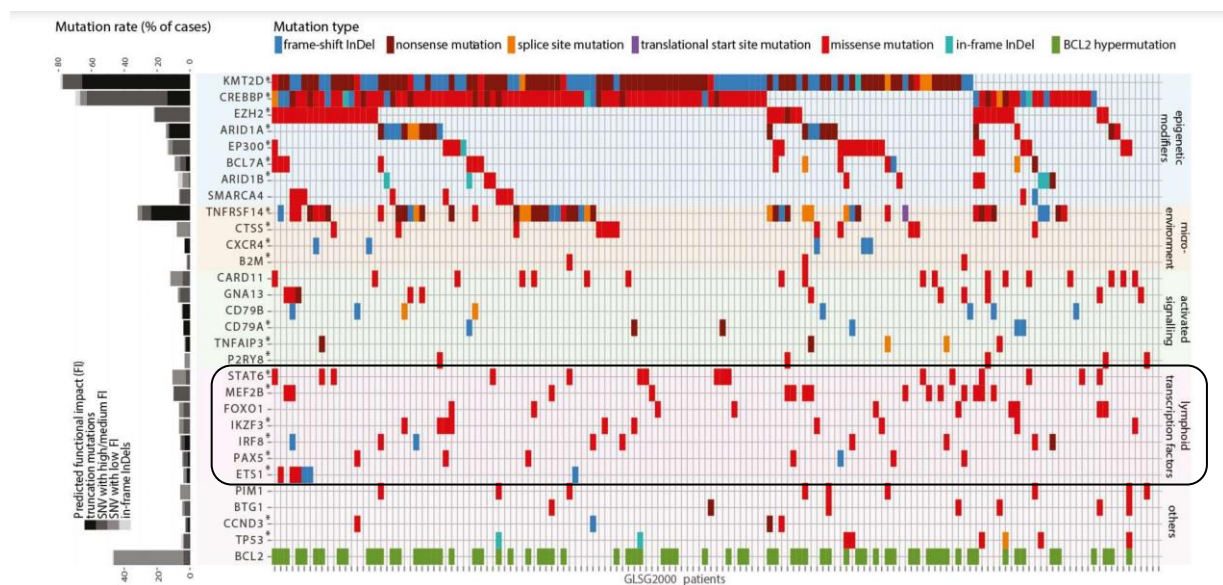
Figure 3- Landscape of somatic mutations in FL.

The mutation profiles from 151 patients from the German Low-Grade Lymphoma Study Group 2000 (GLSG2000) study are displayed. The colors indicate the different type of mutated genes. **Right**-Mutations are categorized as indicated. **Left**- Mutational rate given as a percentage of cases. Asterix indicates 22 significantly mutated genes as calculated by MutSigCV (Broad Institute). Modified from (13).

1.2.2.2 Transcription factors

Lymphomas are heavily dependent on a highly ordered transcriptional program (30). Transcription factors are some of the most recurrently mutated genes in FL (**Fig. 3**, indicated by the box). Commonly mutated transcription factors include *STAT6*, *MEF2B*, *FOXO1,* and *IKZF3* (13, 31-33).

Signal transducer and activator of transcription 6 (STAT6)

Signal transducer and activator of transcription 6 (*STAT6*) is found highly recurrently mutated in FL with a frequency of around 13% (34). FL is dependent on the tumor microenvironment (TME) for growth, which is enriched in IL-4 secreting T_{FH} cells (35). IL-4 binds to its receptor IL4R on lymphoma cells, recruits JAK1/3, and activates STAT6 by phosphorylation of Y641. Activation of STAT6 leads to nuclear translocation, where it can regulate transcription via direct binding to DNA. IL-4 drives STAT6-dependent expression by releasing transcriptional repressors (e.g., HDAC2 and HDAC3) and promoting the recruitment of activators (e.g., NCOA1, NCOA2, and EP300), including PARP14, which form the STAT6 enhanceosome complex (36-39).

Previous work from our lab identified *PARP14* in RNA sequencing analyses as the top differentially expressed gene in IL-4-stimulated $STAT6^{MUT}$ vs. $STAT6^{WT}$ overexpressing lymphoma cell lines (40, 41). Luciferase assays revealed activation of the PARP14 promoter by $STAT6^{MUT}$ and not by $STAT6^{WT}$. Inhibition of PARP14 attenuated $STAT6^{MUT}$ gain-of-function phenotype. These results indicate that PARP14 is a novel $STAT6^{MUT}$ target gene, however, the mechanism is not fully understood.

IKAROS family zinc finger 3 (IKZF3)

Another transcription factor recurrently mutated in FL is IKAROS family zinc finger 3 (*IKZF3*). Interestingly, it is mutated not only in FL but also in multiple other diseases, including B cell acute lymphoblastic leukemia (B-ALL), chronic myeloid leukemia (CML), and other types of lymphoma (42-45). Some specific hotspot mutations such as $IKZF3^{L162R}$ and $IKZF3^{S215R}$ can be found in both FL, chronic lymphocytic leukemia (CLL), and diffuse large B cell lymphoma (DLBCL), with other mutations disease-specific (46).

IKZF3's function is essential for B cell development (47). It can form homodimers or heterodimers with other transcription factor family members, such as Ikaros (*IKZF1*). *IKZF1* is expressed in hematopoietic stem cells and is required for pre-B cell development. Pre-BCR signaling then induces high expression of IKZF3, which interacts with IKZF1, regulating pre-B cell transcription (48, 49). *Ikzf3*

is also important for mature B cells, with deficient mice showing increased numbers of B cell precursors, abnormal autoantibody production, and breakdown of tolerance (50). Recent studies have identified and functionally characterized *IKZF3* driver mutations in CLL (43). Identical mutations have been identified in FL, yet their contribution to FL pathogenesis has not been explored (13).

1.3   The tumor microenvironment (TME)

FL grows in follicles surrounded by various cells of the TME. Early studies revealed the importance of the TME for primary FL cells, with researchers unable to cultivate FL cells even with adding cytokines or feeder layers. Additionally, expression profiling showed that signatures from non-tumor immune cells were linked to disease behavior (14, 51-54). Crosstalk between cells of the microenvironment and FL cells is dynamic and promotes tumor growth, prevents apoptosis, and encourages immune dysregulation for the tumor's advantage (55). Furthermore, signals from the cells of the immune microenvironment have been shown to be predictive of patient outcomes (14, 15, 51).

FL cells are dependent on cells of the microenvironment for homing into follicles. FL cells express high levels of CXCR4 and CXCR5 and are attracted into follicles by the secretion of cytokines and chemokines from T_{FH} cells. This includes CXCL13, IL-4, and IL-21, which promote the growth of GC B cells (56). IL-4 (and CD40L) also induce FL cells to secrete CCL17 and CCL22, which results in further T_{reg} recruitment and IL-4-producing T_{FH} cells (57). Thus, FL cells exploit the immune microenvironment to promote tumor survival and proliferation (**Fig. 4**).

In recent years, several studies have shown that gain-of-function mutations can promote biological mechanisms that exploit the microenvironment to promote lymphomagenesis. E.g., cathepsin S (*CTSS*) is recurrently mutated or amplified in 20% of FL cases. CTSS is important for MHC class II processing and presentation with mutation or copy number gain leading to increased interaction and recruitment of CD4+ T_{FH} cells, thus inducing a supportive microenvironment that promotes tumor growth (58, 59). Other mutations such as *EZH2* have been shown to have a reduced dependency on T_{FH} cell help (60). In summary, in recent years, it has become increasingly clear that tumor cells exploit the immune microenvironment to their advantage.
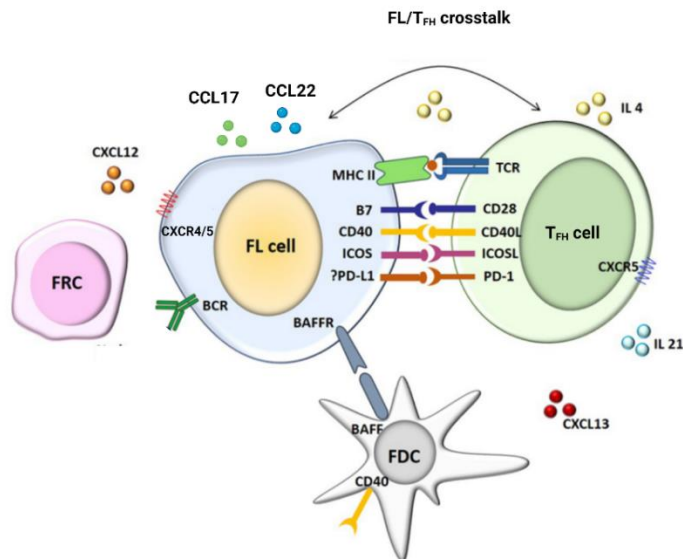
Figure 4- Follicular lymphoma cells are dependent on the tumor microenvironment.

FL cells interact with cells of the microenvironment with continuous crosstalk. T_{FH} cells interact with their T cell receptor, with the B cells MHC class II molecules. CD40/40L interaction together with other costimulatory molecules trigger B and T cell activation. Subsets of stomal cells secrete chemokines CXCL12 and CXCL13, which attract FL cells via chemokine receptors CXCR4/5. T_{FH} cells secrete IL-4, IL-21, and CXCL13 promoting growth. B cell activating factor is secreted by FDCs and binds to BAFFR on FL cells. FL cells secrete chemokines CCL17 and CCL22, resulting in further T cell recruitment and IL-4 secretion. Modified from (61). **Abbreviations-** FL, follicular lymphoma; T_{FH}, T follicular helper cells; FDC, follicular dendritic cell; FRC, follicular reticular cell; BAFF, B cell activating factor.

1.4 The molecular ontogeny of follicular lymphoma

The molecular ontogeny of FL is defined as the sequence of events that lead to the development of the disease and subsequent relapses/histological transformation. Common progenitor cells (CPCs) carry some but not all mutations required for a malignant transformation. The targeting of truncal early acquired mutations (CPCs, the presumed origin of relapse) is clinically important as it could offer the chance to eradicate the disease. By definition, CPC-defining mutations are (somatic) alterations that are shared in both the initial and relapsed tumors. This includes the hallmark *BCL2*/*IGH* translocation and other additional recurrent mutations (*CREBBP*, *KMT2D*, and *EP300)* (62, 63).

1.5   Aims of this project

Traditionally, the *BCL2*/*IGH* translocation is considered the first CPC-defining event in lymphomagenesis, and is thought to occur in early pre/pro B cells due to erroneous VDJ recombination (64). However, our group previously challenged this model, reporting *EP300* mutations in CD34$^+$CD19$^-$CD10$^-$ cells collected from a patient that went on to develop FL 8 years later (65). Furthermore, Horton et al. recently showed that *Crebbp* loss in mice HSPCs can promote lymphomagenesis (66). This project aimed to define the timing of mutation acquisition (ontogeny) in FL. Specifically, we wanted to determine if somatic mutations can be acquired before the *BCL2*/*IGH* translocation in HSPCs. Furthermore, we wanted to functionally characterize these early acquired (truncal) mutations, as therapies targeting CPC-defining mutations hold promise of eradicating the disease and curing patients.

To address this, we had the following aims:

(1) Defining the Molecular Ontogeny of FL:

    a.   To identify patients with FL and available diagnostic tumor biopsies as well as HSPC-enriched leukapheresis-derived mononuclear cell (LMNC) products.

    b.   To define the mutation profile of the diagnostic FL biopsies.

    c.   To purify progenitor and mature cell fractions from LMNCs and perform highly-sensitive mutation detection.

    d.   To perform colony forming unit (CFU) assays as a complementary approach to functionally amplify self-renewing progenitor cells from LMNCs, and perform highly sensitive mutation detection.

(2) Functional characterization of early acquired mutations:

    a.   If we are unable to identify FL-associated mutations that are acquired before the *BCL2*/*IGH* translocation, we will infer early acquired (truncal) mutations by high cancer-cell fraction (CCF)-corrected clonality, using our own available DNA sequencing and copy number data.

    b.   To functionally characterize these candidate mutations using representative ex vivo FL model systems.

2. Material and Methods

2.1 Material

2.1.1 Reagents

Reagent	Supplier
Western blotting	
Bolt MOPS buffer 20x	Thermo Fisher Scientific, Waltham, Massachusetts, USA
Bolt LDS Sample buffer 4x	Thermo Fisher Scientific, Waltham, Massachusetts, USA
Bolt sample reducing agent 10x	Thermo Fisher Scientific, Waltham, Massachusetts, USA
Bolt™ 4 bis 12 %, Bis-Tris, 1,0 mm, mini-protein-gel, 10 Wells	Invitrogen, Waltham, Massachusetts, USA
4–15% Mini-PROTEAN® TGX™ Precast Protein Gels	Bio-Rad, Hercules, California, USA
4x Laemmli sample buffer	Bio-Rad, Hercules, California, USA
Dithiothreitol (DTT)	Bio-Rad, Hercules, California, USA
Milk powder	Sigma Aldrich, St. Louis, Missouri, USA
Phosphatase inhibitor cocktail 2	Sigma-Aldrich, St. Louis, Missouri, USA
Phosphatase inhibitor cocktail 3	Sigma-Aldrich, St. Louis, Missouri, USA
Protease inhibitor	Sigma-Aldrich, St. Louis, Missouri, USA
Stripping buffer	Thermo Fisher Scientific, Waltham, Massachusetts, USA
Magic Mark XP	Thermo Fisher Scientific, Waltham, Massachusetts, USA
Page Ruler	Thermo Fisher Scientific, Waltham, Massachusetts, USA
Methanol	Sigma-Aldrich, St. Louis, Missouri, USA
Transfer stacks	Merck Millipore, Massachusetts, Burlington, USA
Transfer sandwich	Invitrogen, Waltham, Massachusetts, USA
Restore plus stripping	Thermo Fisher Scientific, Waltham, Massachusetts, USA
Tris-buffered saline (TBS)	Thermo Fisher Scientific, Waltham, Massachusetts, USA
Tween	Sigma-Aldrich, St. Louis, Missouri, USA
Immunoprecipitation	
FLAG-M2 magnetic beads	Sigma-Aldrich, St. Louis, Missouri, USA
FLAG-M2 affinity gel	Sigma-Aldrich, St. Louis, Missouri, USA
5x Passive lysis buffer	Promega, Madison, Wisconsin, USA
ChIP-grade magnetic beads	Cell Signaling Technology, Danvers, Massachusetts, United States
10x SDS	Invitrogen, Waltham, Massachusetts, USA
Cell Culture	
FBS	Pan Biotech, Aidenbach, Germany
Penicillin streptomycin	Thermo Fisher Scientific, Waltham, Massachusetts, USA
Anti Anti	Thermo Fisher Scientific, Waltham, Massachusetts, USA

Stable glutamine	Thermo Fisher Scientific, Waltham, Massachusetts, USA
PBS	Thermo Fisher Scientific, Waltham, Massachusetts, USA
H20	Thermo Fisher Scientific, Waltham, Massachusetts, USA
IL-4 (mouse and human)	Miltenyi Biotec, Cologne, Germany
DMSO	Sigma-Aldrich, St. Louis, Missouri, USA
EDTA 0.5 M pH 8.0	Merck Millipore, Massachusetts, Burlington, USA
Trypan Blue	Invitrogen, Waltham, Massachusetts, USA
Trypsin EDTA	BioChrom, Cambridge, United Kingdom
Sodium selenite	Thermo Fisher Scientific, Waltham, Massachusetts, USA
Cyclosporin	Novartis, Basel, Switzerland
Hanks balanced salt solution	Thermo Fisher Scientific, Waltham, Massachusetts, USA
Media	
Iscove's Modified Dulbecco's Medium (IMDM)	PAN Biotech, Aidenbach, Germany, Capricon, Scientific, Düsseldorf, Germany
Dulbecco's Modified Eagle's Medium (DMEM)	PAN Biotech, Aidenbach, Germany, Capricon, Scientific, Düsseldorf, Germany
Roswell Park Memorial Institute Medium (RPMI 1640)	PAN Biotech, Aidenbach, Germany, Capricon, Scientific, Düsseldorf, Germany
Advanced RPMI	Thermo Fisher Scientific, Waltham, Massachusetts, USA
Opti-minimum essential medium (MEM)	Thermo Fisher Scientific, Waltham, Massachusetts, USA
Restriction enzymes	
DpnI	NEB, Ipswich, Massachusetts, USA
BsrgI	NEB, Ipswich, Massachusetts, USA
HindIII	NEB, Ipswich, Massachusetts, USA
Nco1	NEB, Ipswich, Massachusetts, USA
Quantitative polymerase chain reaction (qPCR)	
Fast SYBR green master mix	Bio-Rad, Hercules, California, USA
Taqman advanced fast master mix	Invitrogen, Waltham, Massachusetts, USA
Tri reagent	Zymo Research, Irvine, USA
Other Applications	
1% Formaldehyde	Thermo Fisher Scientific, Waltham, Massachusetts, USA
10x TRIS-Borat-EDTA (TBE)	Life Technologies, California/USA
1kb Plus Ladder	NEB, Ipswich, Massachusetts, USA
2 Log Ladder	NEB, Ipswich, Massachusetts, USA
50bp ladder	NEB, Ipswich, Massachusetts, USA
Gel loading dye purple (6x),	NEB, Ipswich, Massachusetts, USA
Agarose	Bioline, London, United Kingdom
Beta mercaptoethanol	Sigma-Aldrich, St. Louis, Missouri, USA
CRISPR-Cas9 oligonucleotides / primers	Integrated DNA Technologies (IDT) Coralville, Iowa, USA
ddPCR customized	Bio-Rad, Hercules, California, USA

mutation assays	
ddPCR supermix for probes	Bio-Rad, Hercules, California, USA
Ethylenglykol-disuccinat-di-(N-succinimidyl)-ester (EGS) crosslinker	Sigma-Aldrich, St. Louis, Missouri, USA
Exonuclease I	NEB, Ipswich, Massachusetts, USA
Ficoll-Paque	GE Healthcare, Chicago, Illinois, USA
gBlocks	Integrated DNA Technologies (IDT) Coralville, Iowa, USA
Glycine	Sigma-Aldrich, St. Louis, Missouri, USA
NaCl	Sigma-Aldrich, St. Louis, Missouri, USA
One shot ccdb survival competent cells	Invitrogen, Waltham, Massachusetts, USA
One shot top 10 competent cells	Invitrogen, Waltham, Massachusetts, USA
Passive lysis buffer	Promega, Madison, Wisconsin, USA
Polyethylenimine (PEI)	Sigma-Aldrich, St. Louis, Missouri, USA
Polybrene	Merck Millipore, Massachusetts, Burlington, USA
Primers	Metabion, Planegg, Bayern, Germany
Protease K	Bioline, Toronto, Ontario, Canada
RNAse	Qiagen, Hilden, Germany
Rnase away	Carl Roth, Karlsruhe, Germany
ROTI Safe GelStain	Carl Roth, Karlsruhe, Germany
RLT buffer	Qiagen, Hilden, Germany
SOC medium	Invitrogen, Waltham, Massachusetts, USA
TAE buffer	Invitrogen, Waltham, Massachusetts, USA
TBE buffer	Invitrogen, Waltham, Massachusetts, USA
TE (Tris-HCL-EDTA)	Thermo Fisher Scientific, Waltham, Massachusetts, USA
Tri reagent	Zymo Research Irvine, California, USA

Table 2- List of laboratory reagents.

2.1.2   Lab consumables

Consumable	Supplier
15 mL, 50 mL falcons	Sarstedt, Nümbrecht, Germany
2, 5, and 25 mL stripettes	Corning, New York, USA
5 mL Polystyrene Round-bottom tube	Corning, New York, USA
6, 12, 24 well plates, standard	Sarstedt, Nümbrecht, Germany
6, 12, 24 well plates, suspension	Sarstedt, Nümbrecht, Germany
Adhesive seals	Bio-Rad, Hercules, California, USA
Bacterial cell spreaders	Carl Roth, Karlsruhe, Germany
Duran bottles	Schott, Mainz, Germany
Micro tubes (1.5 mL, 2 mL)	Sarstedt, Nümbrecht, Germany
Microplate 96-well	Greiner bio-one, Kremsmünste, Austria
Millex filters (0.22 µm, 0.45 µm) PVDF	Merck Millipore, Massachusetts, Burlington, USA
Parafilm	Sigma-Aldrich, St. Louis, Missouri, USA
PCR tubes	Brand, Wertheim, Germnay
Pipette tips	Biozym, Hessisch Oldendorf, Germany
Protein/ DNA low-binding tubes	Sarstedt, Nümbrecht, Germany
qPCR Plates	Bio-Rad, Hercules, California, USA
Tissue culture flasks, standard	Sarstedt, Nümbrecht, Germany
Tissue culture flasks, suspension	Sarstedt, Nümbrecht, Germany

Table 3- Lab consumables.

2.1.3 Laboratory devices

Device	Supplier
BD ARIA II sorter	Becton, Dickinson, and Company (BD), Franklin Lakes, New Jersey, United States
BD FACS Canto II	Becton, Dickinson, and Company (BD), Franklin Lakes, New Jersey, United States
Bioanalyser	Agilent, Santa Clara, California USA
Bioruptor pico	Diagenode, Liège, Belgium
Centrifuge 5415 D	Eppendorf, Hamburg, Germany
Centrifuge 5424 R	Eppendorf, Hamburg, Germany
CO_2 incubator	Binder, Tuttlingen, Germany
DMi8 widefield fluorescence microscope	Leica, Wetzlar, Germany
EasySep magnet	Stemcell Technologies, Vancouver, Canada
Electroporation cuvette	Peqlab Biotechnologie GmbH, Erlangen
Electroporator	Bio-Rad, Hercules, California, USA
Fusion SL (SL4), (Vilber Lourmat)	Peqlab Biotechnologie, Erlangen, Germany
GloMax® discover multimode microplate reader	Promega, Madison, Wisconsin, USA
Gel Scanner- EBOX VX2	Vilber Lourmat Eberhardzell Germany
HERA safe sterile workbench	Thermo Fisher Scientific, Waltham, USA
Light microscopy Tubus, Modell FSA	Leitz, Wetzlar, Germany
Magnetic-activated cell sorting	Miltenyi Biotec, Bergisch Gladbach, Germany
Micro scales	Sartorius, Göttingen, Germany
Microwave	Siemens, Munich, Germany
Mini incubator	Labnet, Edison, New Jersey, USA
Mini trans-blot® cell	Bio-Rad, Hercules, California, USA
Multifuge X1R	Thermo Fisher Scientific, Waltham/USA
Nanodrop 1000 spectrophotometer	Peqlab Biotechnologie, Erlangen, Germany
Nucleofector 2b	Lonza Group AG, Basel, Switzerland
PCR machine	Bio-Rad, Hercules, California, USA
Pierce power blotter/stainer	Thermo Fisher Scientific, Waltham, USA
Pipettes research plus 2.5 µl, 10 µl, 100 µl, 200 µl, 1000 µl	Eppendorf, Hamburg, Germany
PowerPac	Bio-Rad, Hercules, California, USA
qPCR machine	Bio-Rad, Hercules, California, USA
Qubit 3.0	Invitrogen, California, USA

Fluorometer	
QX200 ddPCR system	Bio-Rad, Hercules, California, USA
RS-TR05 tube roller	Phoenix instruments, Texas, USA
Shaker DRS-12	NeoLab, Heidelberg, Germany
Thermomixer 5436	Eppendorf, Hamburg, Germnay
Thermomixer C	Eppendorf, Hamburg, Germnay

Table 4- Laboratory devices.

2.1.4 Cell lines

Cell Lines	Species	Media	Cell type
HEK 293T	Human	DMEM + 10% FBS	Embryonic kidney cells
OCI-Ly1	Human	IMDM + 10% FBS	B cell lymphoma
OCI-Ly8	Human	IMDM + 10% FBS	B cell lymphoma
Karpas 422	Human	RPMI + 10% FBS	B cell lymphoma
SU-DHL-4	Human	RPMI + 10% FBS	B cell lymphoma
SU-DHL-5	Human	RPMI + 10% FBS	B cell lymphoma
SU-DHL-16	Human	RPMI + 10% FBS	B cell lymphoma
DB	Human	RPMI + 10% FBS	B lymphoma blasts
YK6- CD40L-IL21	Human	RPMI + 10% FBS	Follicular dendritic cells
Rec1	Human	RPMI + 10% FBS	Mantle cell lymphoma
B3	Mouse	IMDM +10% FBS	pre-B cells
GC B Cells	Human	Advanced RPMI + 20% FBS, 1% Stable Glutamine + 1 % Penicillin/Streptomycin	Tonsil-derived germinal center B cells

Table 5- Cell lines.

2.1.5   Cloning and expression constructs

Construct	Reference/ Plasmid ID
pDONR221	Invitrogen, Waltham, Massachusetts, USA
IKZF3 pDONR-221	Harvard repository ID- HsCD00079542
pMSCV-IRES-GFP	Addgene plasmid #20672
pHAGE-CMV-MCS-IRES-ZsGreen	Harvard repository ID EvNO00061605
pMSCV-STAT6^{WT} or STAT6^{D419G}- IRES GFP	Boesl et al., (40)
pUMVC/ pCAT	Addgene plasmid #8454
pCMV-VSV-G	Addgene plasmid #8454
psPAX2	Addgene plasmid #12260
pCL-Eco	Addgene plasmid #12371
pMSCV-IKZF3^{WT}, or IKZF3^{L162R}, or IKZF3^{S215R}- IRES GFP	This thesis
pMSCV- IKZF3^{WT}, or IKZF3^{L162R}, or IKZF3^{S215R}, or GFP-STOP-DEST-IRES-Puro 2a- Thy1.1 WPRE	Marc Schmidt Supprian
pLKO shRNA 1 (IKZF3)	Sigma ID- TRCN000414188
pLKO shRNA 2 (IKZF3)	Sigma ID- TRCN000436593
TRC2 pLKO.5-puro	Sigma ID -SHC216
pLKO-RFP-IKZF3-sh2	Addgene plasmid #69043
pLKO-RFP-IKZF3-sh3	Addgene plasmid #69044
pLKO-RFP-shCntrl	Addgene plasmid #69040
pSpCas9(BB)-2A-GFP (PX458)	Addgene plasmid #48138
phCMV-GaLV MTR	Addgene plasmid #163612
pHIT60	Addgene plasmid #35614
MSCV-BCL6-2A-BCL2-IRES-hCD2	Addgene plasmid #135305
pRL (Renilla Luciferase)	Promega, Madison, Wisconsin, USA
pGL3 Basic	Promega, Madison, Wisconsin, USA

Table 6- Plasmid constructs used in this study.

2.1.6   Kits

Kits	Supplier
Bicinchoninic acid (BCA) assay	Thermo Fisher Scientific, Waltham, Massachusetts, USA
Complementary DNA (cDNA) synthesis	Bio-Rad, Hercules, California, USA
Clarity-enhanced chemiluminescence (ECL)	Bio-Rad, Hercules, California, USA
Clarity max ECL	Bio-Rad, Hercules, California, USA
Cell line nucleofector kit V	Lonza Group AG, Basel, Switzerland
Dual Glow luciferase system	Promega, Madison, Wisconsin, USA
EasySep human CD34 positive Selection kit,	Stem Cell Technologies, Vancouver, Canada
EasySep human progenitor cell enrichment kit,	Stem Cell Technologies, Vancouver, Canada
Gateway BP clonase II	Invitrogen, Waltham, Massachusetts, USA
Gateway LR clonase II	Invitrogen, Waltham, Massachusetts, USA
Gel extraction	Qiagen, Hilden, Germany
KOD hot start DNA polymerase	Novagen, Merck Millipore, Massachusetts, Burlington, USA
NEBNext® multiplex oligos for Illumina	New England Biolabs (NEB), Ipswich, Massachusetts, United States
NEBNext® Ultra™ II DNA Library Prep Kit for Illumina	New England Biolabs (NEB), Ipswich, Massachusetts, United States
NE-PER nuclear and cytoplasmic extraction kit	Thermo Fisher Scientific, Waltham, Massachusetts, USA
PCR cleanup kit	Qiagen, Hilden, Germany
Phusion high-fidelity DNA polymerase	NEB, Ipswich, Massachusetts, USA
Pierce ECL	Thermo Fisher Scientific, Waltham, Massachusetts, USA
Pure yield plasmid midiprep kit	Promega, Madison, Wisconsin, USA
Pure yield plasmid miniprep kit	Promega, Madison, Wisconsin, USA
Quick ligation kit	NEB, Ipswich, Massachusetts, USA
QIAamp DNA Blood kit	Qiagen, Hilden, Germany
RNA extraction	Zymo Research, Irvine, California, USA
Zymo RNA extraction	Zymo Research, Irvine, USA

Table 7- Kits.

2.1.7   Antibodies

2.1.7.1   Western blotting

Antibodies	Supplier	Clone	Dilution	Product Number
FLAG® M2	Sigma-Aldrich	M2	1:2500	F3165
BCL2	Santa Cruz Technology	100	1:1000	Sc-509
BCL6	Cell Signaling Technology	D412V	1:1000	14895S
Beta Tubulin	Cell Signaling Technology	9F3	1:1000	2128S
GAPDH	Invitrogen	6C5	1:20 000	AM4300
IKZF1	Cell Signaling Technology	D6N9Y	1:1000	14859s
IKZF3	Cell Signaling Technology	D1C1E	1:1000	15103S
Lamin B1	Abcam	EPR8985(B)	1:2500	ab133741
LYN	Cell Signaling Technology	C13F9	1:1000	2796S
PARP14	Sigma- Aldrich		1:250	HPA012063
pLYN Y397	Abcam		1:1000	Ab226778
pP44/42 MAPK	Cell Signaling Technology		1:1000	9101
pStat6 (Tyr641)	Cell Signaling Technology		1:2000	9361
pSYK Tyr323	Cell Signaling Technology		1:1000	2715S
STAT6	Cell Signaling Technology		1:2000	9362
SYK	Cell Signaling Technology	D3Z1E	1:1000	13198
α-Tubulin	Sigma-Aldrich	DM1A	1:20 000	T6199
Anti-Rabbit IgG (HRP conjugate)	Promega		1:5000	W4011
Anti-Mouse IgG (HRP conjugate)	Promega		1:5000	W4021

Table 8- Antibodies used for Western blotting.

p= antibody detecting the phosphorylated protein.

2.1.7.2   Quantitative chromatin immunoprecipitation (qChIP)

Table 9- Quantitative chromatin immunoprecipitation (qChIP) and ChIPseq antibodies.

Name	Supplier	Clone	Product number	Dilution
STAT6	Cell Signaling Technology	D3H4	5397S	1:50
FLAG	Sigma-Aldrich	M2	F3165	1:50
Histone H3	Cell Signaling Technology	Polyclonal	2650S	1:50
IgG XP Isotype Control	Cell Signaling Technology	DA1E	3900S	Lot-dependent concentration of STAT6

2.1.7.3 Flow cytometry

Marker	Species	Fluorochrome	Vendor / Clone	Dilution
CD45	Human	PE	BD H130	1:100
CD45RA	Human	FITC	BD H100	1:100
CD34	Human	APC-Cy7	Thermo Fisher 581	1:100
CD38	Human	PE-Cy7	Biolegend HB-7	1:100
CD90	Human	Qdot 605	Biolegend OX-7	1:100
CD10	Human	APC	Thermo Fisher eBioCB-CALLA (CB-CALLA)	1:100
CD19	Human	FITC	BD HIB19	1:100
CD3	Human	APC	BD HIT3a	1:100
CD15	Human	PE-Cy7	Biolegend W6D3	1:100
CD90.1 Mouse	Mouse	APC	Biolegend OX7	1:200
CD19	Mouse	PE-Cy7	Biolegend PE Vivo 770	1:250
CD45R B220	Mouse	PerCP	Biolegend, RA3-6B2	1:50
CD43	Human or Mouse	BV421	Biolegend, S7	1:100
CD44	Human or Mouse	FITC	Biolegend, IM7	1:100
CD24	Mouse	PE	Biolegend, 30F1	1:100
IgD	Mouse	BV510	Biolegend, 11-26c. 2a	1:100
IgM	Mouse	APC/Cy7	Biolegend, RMM-1	1:100
CD43	Mouse	APC	Biolegend, S11	1:100
CD19	Human	FITC	Biolegend, HIB19	1:200
CD19	Human	APC	Biolegend, V CD19.11	1:200

Table 10- Antibodies used for flow cytometry.

2.1.8　　　Primer sequences and protocols

2.1.8.1　　　Primer sequences and nested PCR protocol for *BCL2/IGH*

Primer / Probe	Forward / Reverse	Remark
Nested PCR		
BCL2/IGH MBR	CAGCCTTGAAACATTGATGG / ACCTGAGGAGACGGTGACC TCTATGGTGGTTTGACCTTTAG / ACCAGGGTCCCTTGGCCCCA	First amplification Second amplification
BCL2/IGH mcr	CGTGCTGGTACCACTCCTG / ACCTGAGGAGACGGTGACC CCTGGCTTCCTTCCCTCTG / ACCAGGGTCCCTTGGCCCCA	First amplification Second amplification

Table 11- Nested PCR primers for major and minor BCL2/IGH breakpoints.

Abbreviations- MBR, major breakpoint region; mcr, minor cluster region.

1st PCR	Temperature / Time (min)
Initial denaturation	94°C / 3
27 Cycles	94°C / 1
	55°C / 1
	72°C/ 1
Final extension	72°C / 10

2nd PCR	Temperature / Time (min)
Initial denaturation	94°C / 3
30 Cycles	94°C / 1
	58°C / 1
	72°C / 1
Final extension	72°C / 10

Table 12- PCR protocol for *BCL2/IGH* major breakpoint region (MBR).

1st PCR	Temperature / Time (min)
1 Cycle	94°C / 3
	58°C / 1
	72°C / 1
30 Cycles	94°C / 1
	58°C / 1
	72°C / 30 sec
Final extension	72°C / 10

2nd PCR	Temperature / Time (min)
1 Cycle	94°C / 3
	60°C / 1
	72°C / 1
30 Cycles	94°C / 1
	60°C / 1
	72°C / 30 sec
Final extension	72°C / 10

Table 13- PCR protocol for *BCL2/IGH* minor cluster region (mcr).

2.1.8.2 Quantitative polymerase chain reaction protocol and primer sequences for *BCL2/IGH*

Primer / Probe	Forward / Reverse
RT-qPCR	
BCL2/IGH MBR forward / *JH* consensus	CTATGGTGGTTTGACCTTTAGAG / CCTGAGGAGACGGTGACC
Probe for MBR	FAM-CTGTTTCAACACAGACCCACCCAGAG-TAMRA
*m*cr forward/ JH consensus	CATTGAGTTATTTGTCTTTTGATTAACTTG / CCTGAGGAGACGGTGACC
Probe for *mcr*	FAM-AGAGCTCTTTGTATATTCAGGAAATTAGCACTTTGG- TAMRA
GAPDH	CAAAGCTGGTGTGGGAGG / CTCCTGGAAGATGGTGATGG
Probe *GAPDH*	JOE- CAAGCTTCCCGTTCTCAGCC-BHQ-1

Table 14- qPCR Primer sequences for major and minor *BCL2/IGH* breakpoints.

Abbreviations- MBR, major breakpoint region; mcr, minor cluster region; RT-qPCR, real-time quantitative polymerase chain reaction.

	Temperature / Time (min)
Initial denaturation	50°C / 2
	95°C / 10
45 Cycles	95°C / 15 sec
	59°C / 1

Table 15- qPCR protocol for *BCL2/IGH* major and minor breakpoints

2.1.8.3 Primer sequences for UMI-aided next-generation sequencing

Table 16- UMI-aided next-generation sequencing primer sequences.

Patient no.	Primer	Forward / Reverse
FL1	*KMT2D* K2548_fs	TCCCTACACGACGCTCTTCCGATCTNNNNNNNNGAGACCAGGCTGAGGGACA / GTTCAGACGTGTGCTCTTCCGATCTNNNNNNNNAGGCAGTAGGGGAGCCTTC
	KMT2D T4787_fs	TCCCTACACGACGCTCTTCCGATCTNNNNNNNNGGTACCCCTAGGACACACCTTG / GTTCAGACGTGTGCTCTTCCGATCTNNNNNNNNAAAAGGGCAAAGGAAGTGAGG
	CREBBP D1435V	TCCCTACACGACGCTCTTCCGATCTNNNNNNNNACGTGGCCGGAAGAAATG / GTTCAGACGTGTGCTCTTCCGATCTNNNNNNNCCTGAGTTAAACATGTGCCTCCTT
	SMARCA4 G883D	TCCCTACACGACGCTCTTCCGATCTNNNNNNNNCGTTGGAAGTACATGATTGTGG / GTTCAGACGTGTGCTCTTCCGATCTNNNNNNNNGCACCTGCGTCAGCTTG
	ARID1A C1968*	TCCCTACACGACGCTCTTCCGATCTNNNNNNNNCCCCACAGTAAGGATGAGACC / GTTCAGACGTGTGCTCTTCCGATCTNNNNNNNCGAATGGTATTGGACACACAGA
	EZH2 Y641S	TCCCTACACGACGCTCTTCCGATCTNNNNNNNNCAGGTTATCAGTGCCTTACCTCTC / GTTCAGACGTGTGCTCTTCCGATCTNNNNNNNCTATTGCTGGCACCATCTGAC
	TP53 T284P	TCCCTACACGACGCTCTTCCGATCTNNNNNNNNGGTGAGGCTCCCCTTTCTT / GTTCAGACGTGTGCTCTTCCGATCTNNNNNNNGCTTTGAGGTGCGTGTTTGT
	TNFAIP3 C607*	TCCCTACACGACGCTCTTCCGATCTNNNNNNNNCTGCCTGTCTCAAGCTGCAC / GTTCAGACGTGTGCTCTTCCGATCTNNNNNNNTGTGCAAAAGCCCTTGTTTTC
	PTEN V85_ss	TCCCTACACGACGCTCTTCCGATCTNNNNNNNNTTGTGCTGAAAGACATTATGACAC / GTTCAGACGTGTGCTCTTCCGATCTNNNNNNNCAGTAAGATACAGTCTATCGGGTTT
FL2	*KMT2D* Q1377R	TCCCTACACGACGCTCTTCCGATCTNNNNNNNNTTCCCATCTATCCTCTCACCAAA / GTTCAGACGTGTGCTCTTCCGATCTNNNNNNNCCGTGGTTCTCTTCTCCAACA
	EP300 H1451Y	TCCCTACACGACGCTCTTCCGATCTNNNNNNNNCAGGGCATATTTGGGCATGT / GTTCAGACGTGTGCTCTTCCGATCTNNNNNNNCATTCCTGCAGTCGCTTGG
	STAT6 D419G	TCCCTACACGACGCTCTTCCGATCTNNNNNNNNTCCCACAGGATAGTGGCTTTG / GTTCAGACGTGTGCTCTTCCGATCTNNNNNNNACCCCTGTCCTCACCCTCTT
FL3	*KMT2D* N5447_ss	TCCCTACACGACGCTCTTCCGATCTNNNNNNNNTCAACGTAGCATCAATCACATGTTC / GTTCAGACGTGTGCTCTTCCGATCTNNNNNNNACAGCCACCACTGCCACTCT
	CREBBP P1476L	TCCCTACACGACGCTCTTCCGATCTNNNNNNNNGTCGTTTTGGCTTGGGTATTTT / GTTCAGACGTGTGCTCTTCCGATCTNNNNNNNGTGGGTCCTGCAGGTATGTG
	FAS K274I	TCCCTACACGACGCTCTTCCGATCTNNNNNNNNAGGCTTTGTTCGAAAGAATGGTG / GTTCAGACGTGTGCTCTTCCGATCTNNNNNNNCCATGAAGTTGATGCCAATTACG

Abbreviations- UMI, Unique molecular identifier.

2.1.8.4   PCR protocol for UMI-aided next-generation sequencing

1st PCR	Temperature / Time (sec)
Initial denaturation	98°C / 30
5 Cycles	98°C / 10
	56°C / 40
	72°C/ 5
Final extension	72°C / 5 minutes

2nd PCR	Temperature / Time (sec)
35 Cycles	94°C / 10
	60°C / 40
	72°C / 15
Final extension	72°C / 5 minutes

2.1.8.5   Digital droplet PCR (ddPCR) primers

Patient number	Primer	Forward / Reverse	Probe WT 5' HEX / 3' IBFQ Probe MUT 5' FAM / 3' IBFQ
FL3	*KMT2D* Q4200_fs	CGCAGCTGTGGGTTTTTG / GTTGGAATCATGCCTACGGT	AGCTGTG+C+TCG+AAG / AGCTGTG+T+GCTCGA
	KMT2D N5447_ss	CGGTCAACGTAGCATCAATC / ACTCTTGTCCCTTCTTCTGC	T+G+CCTTTCTA+GAA+TCG / T+CT+A+A+AATC+GA+GGC
	CREBBP P1476L	GGGTGGCAATGGAAGATGTA / GGTCCTGCAGGTATGTGAC	CA+CT+T+G+GAGGAC / CA+CT+T+A+GAGGACAGG
	FAS K274I	TGAAGCCAAAATAGATGAGATCAA / TCAATGTGTCATACGCTTCTTT	A+GAA+CAG+A+A+AGTT+CA / A+GAA+CAG+A+T+AGTT+CA

Table 17- ddPCR primer sequences.

2.1.8.6   All other primer sequences

Primers	Sequence
Gateway cloning technology primers	
IKZF3 3x FLAG tag Fwd	GGGGACAACTTTGTACAAAAAAGTTGGCCACCATGGACTACAAAGACCATGACGGTGATTATAAAGATCATGACATCGACTACAAGGATGACGATGACAAGGAAGATATACAAACAATTGCGGAACTGAAAAGC
IKZF3 3x FLAG tag Rev	GGGGACAACTTTGTACAAGAAAGTTGGCTACAACTTCAGCAGGGCTCTGTGTTCTC
IKZF3 HA tag Fwd	GGGGACAACTTTGTACAAAAAAGTTGGCATGTACCCATACGATGTTCCAGATTACGCTGATGCTGATGAGGGTCAAGAC
IKZF3 HA tag Rev	GGGGACAACTTTGTACAAGAAAGTTGGGTATCAGCTCATGTGGAAGCGGTG
IKZF1 HA tag Fwd	GGGGACAACTTTGTACAAAAAAGTTGGCATGTACCCATACGATGTTCCAGATTACGCTGATGCTGATGAGGGTCAAGAC
IKZF1 HA tag Rev	GGGGACAACTTTGTACAAGAAAGTTGGGTATCAGCTCATGTGGAAGCGGTG
IKZF3 mutagenesis	
L162R Fwd	CCTCCGCCGCCACATTAAACTGC
L162R Rev	GCGGCGGAGGTTACCTTTCTGAGTAAAAG
S215R Fwd	AGAGAAGATCCCTTGAGGAGCACAAG
S215R Rev	AGGGATCTTCTCTGCTTGTAACTCC
IKZF3 sequencing primers	
Seq 1 Fwd	AAGCCATCAATAACGCCATC
Seq 1 Rev	GGCTCTGTGTTCTCCTCTGG
Additional Fwd	CATGAAGAACGCCAGAATCA
Seq 2 Fwd	TGGAAAATGTGGACAGTGGA
Seq 2 Rev	TGCCACATTGCTTGCTAATC
IKZF1 sequencing primers	
Seq 1 Fwd	CCCCTGTAAGCGATACTCCA
Seq 1 Rev	TGGGAGCCATTCATTTTCTC
Seq 2 Fwd	TCGGGAGAGAAAATGAATGG
Seq 2 Rev	AACGTCGCCAAACGTAAGAG
Seq 3 Fwd	AACGTCGCCAAACGTAAGAG
Seq 3 Rev	TTGCACTCAAAAGGATCACG
Seq 4 Fwd	GCCAGCTACGAGAAGGAGAA
Seq 4 Rev	TTGCACTCAAAAGGATCACG
Quantitative polymerase chain reaction (qPCR)	
GAPDH Fwd	CACCCACTCCTCCACCTTTG
GAPDH Rev	TCTCTCTCTTCCTCTTGTGCTCTTG
PARP14 Fwd	GACTGTCGCTATGTGCTTCAC
PARP14 Rev	GGACAAGCTCTCAGTGATCTCC
SYK Fwd	CATGGAAAAATCTCTCGGGAAGA
CCL17 Fwd	CCAGGGATGCCATCGTTTTTGTAACTGTGC
CCL17 Rev	CCTCACTGTGGCTCTTCTTCGTCCCTGGAA
CCL22 Fwd	ATCGCCTACAGACTGCACTC
CCL22 Rev	GACGGTAACGGACGTAATCAC
shRNA IKZF3 knockdown	
shRNA sigma UTR TRCN000414188	GACAGTCTAAGAGTAAGTAAA
shRNA sigma UTR 2TRCN000436593	ATCTAATCTCCCTAATCTAAA

TRC2 pLKO.5-puro	CCGGGCGCGATAGCGCTAATAATTTCTCGAGAA ATTATTAGCGCTATCGCGCTTTTT (Non-Target shRNA (SHC216)
pLKO-RFP-IKZF3-sh2	GTAACCTCCTCCGCCACATTA (Addgene- 69043)
pLKO-RFP-IKZF3-sh3	GACAGTCTAAGAGTAAGTAAA (Addgene- 69044)
pLKO-RFP-shCntrl	CAACAAGATGAAGAGCACCAA (Addgene- 69040)
IKZF3 CRISPR Fwd	CACCGCAAGCAGAGAAGTTCCCTTG
IKZF3 CRISPR Rev	AAACCAAGGGAACTTCTCTGCTTGC
HR template	TGTGGAACCCCTGAGGGTCACTGAGTGCCCCTTATGTTCTCCTTCTAGTGGAGAA ACCCTACAAATGTGAGTTTTGTGGAAGGAGTTACAAGCAGAGAAGATCCCTTGAA GAGCACAAGGAGCGCTGCCGTACATTTCTTCAGAGCACTGACCCAGGGGACACT GGTGAGttcacgcaacacacgtttagtgagcatctg
Luciferase reporter assay construct	
PARP14_promoter Fwd	CCGCTCGAGGGATGACTCTGCCATTCCTG
PARP14_promoter Rev	CCCAAGCTTCAGAAAACGATCGAGGGATAAAG
SYK_ Fwd	TAAGCAAAGCTTTCAGCCGATTCCCGCCC
SYK Rev	TGCTTACCATGGTTACCTCGGCCGATGAA
qChIP	
PARP14 Fwd	TTTGTAAAGGGTCGGCTTGC
PARP14 Rev	AGATCAAGTCGGCAGCTTTG

Table 18- Primer sequences used in this study.

2.1.9   Available data

Data Type	Study	Citation
Sequencing data	FL ontogeny	(67)
Sequencing data	GLSG2000, BCCA cohort	(13, 67)
Copy number data	GLSG2000	(58)

Table 19- Available data used in this study.

Abbreviations- GLSG2000, German low-grade lymphoma study group 2000; BCCA, British Columbia Cancer Agency-Vancouver Cancer Centre.

2.1.10 Software

Software	Application	Developer	Link
Adobe Illustrator 2020	Illustrations	Adobe	www.adobe.com
Biorender	Illustrations	Biorender	https://biorender.com
Bowtie2 v2.3.4.1	Sequence alignment	(Langmead et al. 2012) (68)	http://bowtie-bio.sourceforge.net/bowtie2/index.shtml
CNV kit	Copy number analysis	(Talevich et al. 2016) (69)	https://github.com/etal/cnvkit
CFX Maestro v2.2	qPCR analysis software	Bio-Rad	www.bio-rad.com
CRISP-ID	CRISPR Cas9 clone analysis	(Dehairs et al. 2016) (70)	http://crispid.gbiomed.kuleuven.be/#cite
Flow Jo v10.7.1	Flow Cytometry analysis	BD Biosciences	www.flowjo.com
FACS Diva v9	Flow Cytometry data acquisition	BD Biosciences	www.bdbiosciences.com
GSEA 4.1.0	Gene set enrichment analysis	Broad Institute	www.gsea-msigdb.org/gsea/index.jsp
GraphPad Prism v9.1	Graphs and statistics	GraphPad software	www.graphpad.com
Grammarly	Spelling and grammar	Grammarly Inc	https://www.grammarly.com
IGV browser	Genome visualization	Broad Institute	https://software.broadinstitute.org/software/igv/
MACS2 v2.2.0	ChIP-seq peak calling	(Feng et al. 2012) (71)	https://github.com/macs3-project/MACS
Microsoft Office Home and Business 2016	Word Processing	Microsoft Corporation	www.microsoft.com
OncoPrinter	Mutation Plot	CBioPortal	https://www.cbioportal.org
OncoScan Console 1.3	Copy number variation	Thermo Fisher Scientific	https://www.thermofisher.com
Primer3 v. 0.4.0	Primer design	Untergrasser et al. 2012 (72)	https://primer3.ut.ee/
SomaticIndel Detector (GATK)	Indel detector	Broad institute	http://gatkforums.broadinstitute.org/
MuTect	Point	Broad Institute (73)	https://software.broadinstitute.org/c

v1.1.4.	mutation detector		ancer/cga/mutect
RStudio Desktop 2022.02.3+4 92(1.1.463/R 3.6.0)	RNA seq analysis	RStudio	https://www.r-project.org/
RNA seq analysis	ggplot2_3.2.0	(Wickham H. 2016) (74)	https://ggplot2.tidyverse.org/
	DESeq2_1.24.0	(Love et al. 2014) (75)	https://bioconductor.org/packages/release/bioc/html/DESeq2.html
	ggpubr_0.2.1	Alboukadel Kassambara	https://rpkgs.datanovia.com/ggpubr/
	fastqc_0.11.8	(Andrews, S. 2010) (76)	https://www.bioinformatics.babraham.ac.uk/projects/fastqc/
	Cutadapt_1.12	(Marcel, M 2011). (77)	https://doi.org/10.14806/ej.17.1.200
	zUMIs_ 2.9.4d	(Parekh et al. 2018) (78)	https://doi.org/10.1093/gigascience/giy059
	STAR (version 2.7.3a	(Dobin et al. 2013) (79)	STAR: https://doi.org/10.1093/bioinformatics/bts635

Table 20- Software used in this study.

2.2   Methods

2.2.1   Patient samples

2.2.1.1   Patient selection

Three FL patient tumor biopsies and autologous leukapheresis products collected at first remission were assayed in this study. Patients were enrolled in the GLSG2000 trial (German low-grade lymphoma study group 2000) (80). An additional leukapheresis product from a patient with multiple myeloma was used as a control sample. We obtained written consent from each of the patients used in this study (LMU #056/00 and #445/13).

2.2.1.2   Mutation and copy number analysis

Several FL patient data sets were available for use in this study and are detailed in section 2.1.9. Mutation analysis of *STAT6* and *IKZF3* was performed by Dr. Verena Passerini and Dr. Michael Mentz, as previously described (13). For the FL ontogeny project, short insertions/deletions (indels) and single nucleotide variants were called with MuTect and Somatic Indel Detector (GATK). We called variants (frameshift, missense, start codon, nonsense, spice site, in-frame insertions, or deletions) with a variant allele frequency of ≥5%.

Genome-wide copy number analysis was performed to correct variant allele frequencies (VAFs) for cancer cell fraction. Dr. Verena Passerini performed this analysis. A total of 146 samples were used, which had corresponding copy number data generated via the Oncoscan FFPE CNV assay platform. Using this data, cancer cell fractions of *IKZF3*^{MUT} or *STAT6*^{MUT} were calculated using the Absolute algorithm, as previously described (81).

2.2.2   Generation of expression constructs

2.2.2.1   Bacterial transformation

IKZF3 pDONR-221 (section- 2.1.5) was purchased from the Harvard plasmid repository and transformed into *E.coli*. Briefly, 50 ng of the plasmid was added to the bacteria on ice and incubated for 30 minutes. Subsequently, a heat shock at 42°C for 30 seconds was performed, the samples were placed on ice for 2 minutes, and then 1 mL of SOC medium was added. Bacteria were then shaken at 260 revolutions per minute (rpm) for 1 hour (h) at 37 °C before being streaked onto kanamycin-containing agar plates (100 μg/mL). 2-3 colonies were picked, and the plasmid was isolated according to the manufacturer's instructions. All plasmids were then confirmed via BsrGI digest (according to

the manufacturer's instructions). BsrGI digestion cuts out the insert of Gateway vectors (**Table 21**). Digestions were analyzed by agarose gel electrophoresis using a 1% Tris Borate EDTA (TBE) gel, stained with ROTI-GelStain, and running the gel at 100 volts (V) for 1h. The correct size fragment was visualized using a UV gel chamber and comparing digestions and controls to a DNA size ladder (section-2.1.3). The bands were then excised (section- 2.1.6) and the DNA was isolated. Sanger sequencing was performed to verify the sequence (Eurofins Genomics).

Component	
DNA	500ng
10x NEB buffer	2.5 µl (1x)
BsrGI	1 µl (10 units)
Nuclease-free water	to 25 µl
Reaction volume	25 µl
Incubation	1 hour
Incubation temperature	37 °C

Table 21- BsrGI-Restriction digest.

2.2.2.2   Gateway recombination cloning

Gateway cloning technology (Invitrogen) is a method to allow the efficient transfer of DNA sequences between vectors. The first part of the process is typically performed to add nucleotide sequences (termed Gateway sites) to a gene sequence of interest. This is usually performed using PCR (**Fig. 5**). A recombination reaction (BP reaction) is then performed where the PCR product is integrated into the donor vector, followed by bacterial transformation. This results in an entry clone. Another recombination reaction (LR) can then be performed with a compatible expression plasmid.
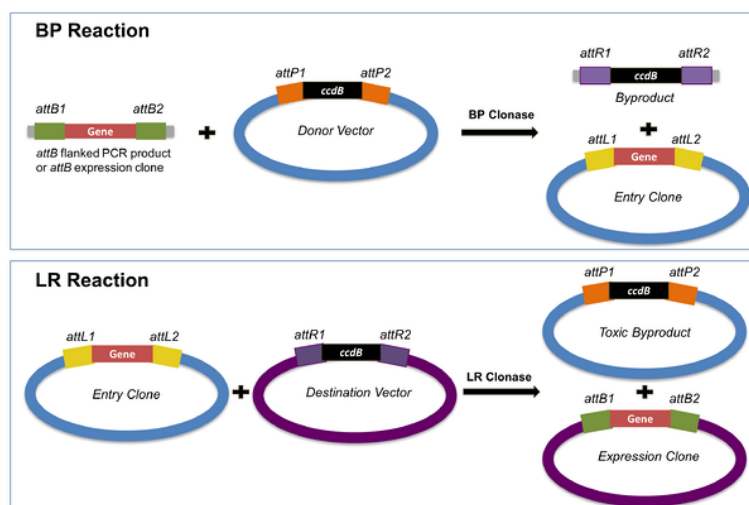
Figure 5- Gateway cloning technology.

The Gateway system consists of the BP and the LR reaction. The BP reaction results in an *att*L flanked entry clone, while the LR reaction creates the expression clone. During the LR reaction, bacterial transformation takes place in ccdB-sensitive bacteria, ensuring only the expression clone is amplified. Figure from (82).

IKZF3 pDONR was purchased as a FUSION gene without a stop codon. Primers were designed to tag the expressed protein (3x-amino acids- DYKDDDDK-Flag-tag, no tag, or human influenza hemagglutinin (HA)-tag) and to add a stop codon. PCRs were carried out using the KOD extreme PCR kit, using 50 ng of IKZF3 pDONR as a template (**Table 22**) (primer sequences- section 2.1.8.6).

	Temperature/time (sec)	Reagent	Concentration
	95°C/ 30	2x extreme buffer	1x
3 cycles per annealing temperature	95°C / 30	2mM dNTPs	0.4 mM
	74, 70, 66, 62, 58, 54 °C	Primers (Fwd+ Rev)	10 µM each
	72°C / 90	Template	50-200 ng
		KOD polymerase	0.4 units
15 cycles	94°C / 30	Nuclease-free water	to 25 µl
	58°C / 40		
	72°C / 90		
Final extension	68°C / 300		
Store	4°C ∞		

Table 22- PCR conditions used for KOD PCR amplification.

To create Gateway clones, *att*B flanked PCR products were mixed with the vector pDONR 223. The BP reaction was performed at 25°C for 2 hours (**Table 23**). The reaction was stopped via the incubation of proteinase K (37 °C, 10 minutes). To select clones with an IKZF3 insert, samples were then transformed into *E.coli,* as previously described (section 2.2.2.1). All clones were verified via Sanger sequencing after the BP reaction or after the LR reaction (Cre-dependent expression constructs).

Component	
attB PCR product	30 ng
pDONR 223	100 ng
TE buffer pH 8	to 5 µl
BP clonase	1 µl (of mix)

Table 23- Gateway BP reaction components.

2.2.2.3   Site-directed mutagenesis

Site-directed mutagenesis primers are detailed in section 2.1.8.6. Primers were designed using Primer3 (72). As a template, 50-200 ng of the gateway Flag-tagged IKZF3 construct was used. PCR was carried out as detailed in Table 22. PCR products were purified using a PCR purification kit, and samples were then treated with Dpn1 to remove the unmutated template, according to the manufacturer's instructions.

2.2.2.4　LR recombination reaction

Lentiviral and retroviral expression plasmids were created from IKZF3 pDONR constructs via the LR recombination reaction (**Table 24**). Two expression plasmids, pMSCV-IRES-GFP, and pHAGE-CMV-MCS-IRES-ZsGreen were used as previously described (58). Cre restricted expression was achieved using a pMSCV-STOP-DEST-IRES-Puro2a-Thy1.1-WPRE vector, which was a kind gift from Marc Schmidt Supprian. LR reactions were performed to transfer pDONR IKZF3^{WT}, IKZF3^{L,162R}, or IKZF3^{S215R} into an expression vector. For a control, we also performed the LR reaction with an *att*B flanked non-coding GFP cassette (a kind gift from Oliver Weigert). The protocol was followed according to the manufacturer's instructions. Following the LR reaction, bacterial transformation was carried out (section-2.2.2.1).

Component	
pHAGE or pMIG GW	300 ng
IKZF3 pDONR 223	200 ng
TE buffer pH 8	2o 5 µl
LR clonase	1 µl (of mix)

Table 24- LR gateway reaction components.

2.2.3　Cell culture

2.2.3.1　Lymphoma cell lines- General maintenance

All cell lines were verified yearly using short tandem repeat analysis (Eurofins Genomics). Cells were stored in cryovials in vapor phase liquid nitrogen and thawed periodically. Cells were incubated at 37 °C with 5% CO_2, and every 3-4 days, cells were passaged before reaching a maximum density of $2x10^6$ cells/mL.

2.2.3.2　Human ex vivo FL-like co-culture model

GC B cells were isolated from human tonsils, as previously described (83), and transduced with a BCL2 and BCL6 expression construct (section- 2.1.5). GC B cell surface phenotype was monitored by flow cytometry (FC) analysis. Cells were cultured on a follicular dendritic cell (FDC) feeder layer (YK6-CD40lg-IL21). The FDC layer provides essential support by expressing CD40L and secreting IL-21 (**Fig. 6**). GC cells were then additionally transduced with *STAT6*^{WT}, *STAT6*^{D419G}, *IKZF3*^{WT}, I*KZF3*^{L162R}, *IKZF3*^{S215R} or an EV control. The culture is referred to as FL-like upon transduction with an FL gene of interest. FL-like B cells were then cultured for 3-4 days before being gently harvested via pipetting up and down. B cells were then washed once with PBS, centrifuged 400 xg for 4 minutes, and resuspended in advanced RPMI+ 20% FBS. Cells were mixed at equal ratios with trypan blue and

counted using a hemocytometer. For one well of a 12-well plate, 0.2×10^6 YK6-CD40lg-IL21 cells were plated in RPMI+ 10% and incubated at 37°C, 5% CO_2 overnight. The medium was then removed, and the wells were washed 1x with 1 mL PBS. FL-like B cells were then plated on top in advanced RPMI+20% FBS at a density of 1×10^6/mL. Cells were incubated at 37°C, 5% CO_2 for 3-4 days. The number of cells cultured was scaled up or down, maintaining a ratio of 1:5 (YK6-CD40lg-IL21:FL like-B cells).

Feeder layers were grown in $175 cm^2$ flasks, and upon reaching confluency, they were treated with mitomycin C (10 μg/mL) for 50 minutes. Cells were then washed in PBS and isolated from the feeder flask via treatment with trypsin EDTA (Ethylenediamine tetraacetic acid) solution 1x (5 mL per flask) for 5 minutes at 37°C, 5% CO_2. RPMI 10% was then used to neutralize the trypsin, and the cells were then counted. Cells were mixed at equal ratios with trypan blue and counted using a hemocytometer. Cells were then centrifuged at 400 xg for 5 minutes. Cells were resuspended in FBS+ 10% DMSO at a density of 2×10^6/mL and stored in cryovials at -80°C until required. Before use, cells were washed once with PBS and then plated at the desired density. For Western blotting, FL-like B cells were depleted from the YK6-CD40lg-IL21 feeders using magnetic-activated cell sorting (MACS). Cell lysis was then performed as described in section 2.2.6.1. For *STAT6* experiments, IL-4 stimulation (10 ng/μl) was added to the co-culture for 24 hours. The cells were subsequently depleted from the feeder layer and analyzed via Western blotting (section-2.2.6) or qPCR (section 2.2.5.3). An identical procedure was carried out for *IKZF3* in the absence of stimulation.
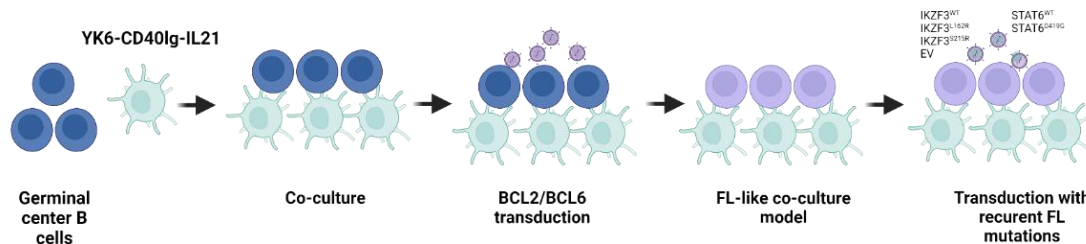
Figure 6- FL-like co-culture model.

GC B cells were isolated from tonsil tissue and co-cultured on FDC feeder cells (YK6-CD40lg-IL-21). Cells were immortalized by *BCL2* and *BCL6* transduction, as previously described (84). Recurrently mutated genes in FL were introduced by retroviral transduction. **Abbreviations-** FL, follicular lymphoma; IL-21, interleukin 21; GC, germinal center B cells; FDC, follicular dendritic cell; BCL2, B cell leukemia/lymphoma 2; BCL6, B cell lymphoma 6, CD40lg, CD40 ligand.

We developed these FL-like co-culture models in collaboration with Dr. Dan Hodson (84). Dr. Carolin Strobl established the protocols in our lab and supported and helped me with all aspects of these experiments.

2.2.3.3   Virus production

HEK 293T cells were used as a packaging cell line to produce retrovirus or lentivirus. 10 μg of IKZF3 expression constructs (pMIG, pHAGE, (pLKO for shRNA knockdown) section 2.1.5) were transfected with psPAX2 (9 μg) and VSV-G (2.5 μg)(lentivirus), or pCAT (8 μg) and VSV-G (2.5 μg) (retrovirus), as previously described (58). An ecotropic packaging vector (pCL-Eco) was used for mice cell transductions (9 μg). Transfection was carried out using PEI (1.5x (total μg of DNA) in a volume of 600 μl of Opti-MEM (section 2.1.1). Before transfection, HEK 293T cells were plated at a density of 4.5 x10^5/ mL in 10 mL in an adherent cell culture plate (58cm^2) and incubated for 1 day in DMEM. DMEM was then replaced with Opti-MEM, and the transfection was performed. Briefly, the required components were mixed in 1.5 mL Eppendorf's in 600 μl of Opti-MEM with the calculated amount of PEI. After 10 minutes of incubation, the mixture was added to the cells. After 6 hours, 1 mL of FBS was added to each plate. The medium was replaced the following day with DMEM+ 10% FBS. The supernatant containing the virus was then harvested after 48h and 72h and filtered using a 0.45 μm filter. The virus was then centrifuged overnight at 24,446 xg, 4°C. The pelleted virus was then split into 8 equal aliquots with a volume of 50 μl of DMEM and stored at -80°C until required.

2.2.3.4   Virus production- Germinal center B cells

Virus production and transduction of tonsil-derived germinal center B cells were performed as previously described in the published protocol (84). All constructs were obtained from the same research group and are listed (section 2.1.5).

2.2.3.5   Transduction

Before transduction, cell viability was checked by Vi-CELL XR (Beckman Coulter). 1x10^6 cells were placed in a 24-well plate in 500 μl of DMEM, with 50 μl concentrated virus and 1μg/mL polybrene. The plate was then centrifuged for 90 minutes at 1500 xg at 4 °C. Plates were incubated at 37°C, 5% CO_2, for 4 hours, before replacing the medium. S2 status was checked after one week via harvesting the supernatant and checking the reinfection of HEK 293T cells by FC analysis.

2.2.3.6   Cell sorting /selection

For fluorescence-activated cell sorting (FACS) of positively transduced cells, 10-20 million cells were washed in PBS, filtered, and sorted using a BD Arai II or a Cytoflex sorter into the appropriate media. After sorting, cells were centrifuged at 500 xg for 4 minutes and replated in fresh medium with anti-anti (1x). Anti-anti antibiotics were used for five days and then omitted.

For puromycin selection of shRNA clones, puromycin kill curves were performed to determine the appropriate dosage. Puromycin was then added to the cells for 5-10 days. In most cases, 10 μg/mL was the appropriate concentration. In highly sensitive cell lines, puromycin was added for 24 hours, removed, and the cells were then washed and replated in media without puromycin. Puromycin was then reapplied later when the cells had greater viability.

2.2.4 Colony forming unit assay (CFU)

2.2.4.1 Hematopoietic stem cells (HSCs)

HSPC-enriched LMNCs were first thawed in RPMI 1640 medium and washed twice in Hanks balanced salt solution containing 2% FBS. A pretreatment with DNase 1 was performed, followed by magnetic cell separation (EasySep Human Progenitor Cell Enrichment Kit or EasySep Human CD34 Positive Selection Kit, Stem Cell Technologies). CD34$^+$ and lin$^-$ cells (20,000-100,000 per plate) were then plated on methylcellulose-medium (MethoCult H4035 Optimum Without EPO, Stem Cell Technologies) and cultured for 14 days at 37°C with 5% CO_2. As CFU assays for human lymphoid progenitors are unavailable, we used MethoCult™ H4035 Optimum Without EPO, which is primarily used for the growth of granulocyte-macrophage progenitor cells (CFU-GM, CFU-G, and CFU-M). In this assay, HSPCs potentially with FL mutations have self-renewal capacity to give rise to CFUs, which consist of at least 20-40 genetically identical cells. We used LMNCs from a patient with multiple myeloma as a control. CFU plates were analyzed individually or pooled (1-4 plates per pool). We analyzed 5 pools of CD34$^+$ and 5 pools of lin$^-$ hematopoietic stem and progenitor cells (HSPC)-derived CFUs per patient.

2.2.4.2 Pre-B cell CFU assay

Emu-BCL2 mice (B6.Cg-Tg(BCL2)36Wehi/J) were obtained from Jackson Laboratory. Heterozygous mice were crossed with Mb1-Cre (cd79atm1(cre)Reth) or Vav Cre-(Tg(Vav1-cre)1Cgp) heterozygous mice (85-87). Mice heterozygous for both transgenes were sacrificed at 6-10 weeks of age using isoflurane and cervical dislocation. Subsequently, femurs were flushed with PBS. Harvested bone marrow cells (1x10^6) were retrovirally transduced. For STAT6 experiments, heterozygous Emu-BCL2 mice cells were used; retrovirally transducing *STAT6*^{WT}, *STAT6*^{D419G}, or EV (all cloned into pMSCV-IRES-GFP), as previously described (58). For Cre lineage-restricted experiments, bone marrow cells from Emu-BCL2-Mb1-Cre or Emu-BCL2-Vav-Cre were retrovirally transduced with pMSCV- IKZF3^{WT}, IKZF3^{L162R}, IKZF3^{S215R}, or GFP-STOP-DEST-IRES-Puro 2a-Thy1.1-WPRE. A non-coding GFP cassette was cloned into the vector as a control (verified by Sanger sequencing) (section 2.1.5). Transductions were carried out as described in section 2.2.3.5. Cells were then incubated for 4 hours (5% CO_2,

37°C), and then plated onto methylcellulose (0.3 x 10^6 cells /mL) that supports the growth of pre-B colony-forming-units (CFUs) (M3630). For STAT6 experiments, methylcellulose was supplemented with mouse IL-4 (10 ng/μl). All Pre-B CFUs were counted according to the manufacturer's guidelines. Every 7 days, cells were washed off and replated onto fresh M3630 methylcellulose medium. We verified successful transductions via FC analysis for GFP. For Cre lineage-restricted experiments, we checked successful transductions via FC analysis for Thy1.1.

2.2.4.3   Ex vivo expansion of human PB-derived B cells

Ex vivo expansion of B cells was performed from a peripheral blood sample collected in 2017, as previously described (88). We performed these experiments in collaboration with Dr. Andreas Moosmann and Dr. Anne-Wiebe Mohr at the Helmholtz Center, Munich. Briefly, a co-culture of PBMCs with fibroblastic L929 cells (murine stably expressing CD40L) was set up. L929 were plated in 96 well plates and irradiated (180 Gy). PBMCs were added at specific densities to the culture (2.5, 5, 10 or 20 × 10^4 cells per well), in 200 μl RPMI 1640 medium containing 10% fetal bovine serum, streptomycin (100 μg/mL), penicillin (100 U/mL), and sodium selenite (100 nM), in addition to recombinant human IL-4 (2 ng/mL) and cyclosporin A (1 μg/mL). Each week B cells were harvested and plated onto a new feeder.

2.2.5   Molecular Biology

2.2.5.1   DNA isolation

DNA isolation of sorted cellular fractions, CD34+/lin- HSPC-derived CFUs, or cell lines was performed using the QIAamp DNA Blood kit, according to the manufacturer's instructions.

2.2.5.2   RNA isolation

RNA isolation was performed using the Zymo RNA isolation kit and the Tri reagent (Trizol-based reagent), according to the manufacturer's instructions. For RNA seq experiments of FL-like B cells, 10,000 cells were sorted into a low bind tube containing 50 μl RLT buffer containing 1% beta-mercaptoethanol (Cytoflex sorter). Samples were then transferred into low-bind Eppendorf plates on dry ice. For mouse pre-B cells 1000, CD19$^+$ GFP$^+$ cells or APC-Thy1.1$^+$ cells were sorted directly into low bind Eppendorf plates (BD Arai II), containing 50 μl RLT buffer with 1% beta-mercaptoethanol. Plates were periodically frozen on dry ice and then transferred into a -80°C freezer before processing. RNA isolation was performed as previously described by Lucas Wange in collaboration with the group of Professor Wolfgang Enard (89, 90). For qPCR expression analysis of

FL-like B cells, approximately 8x10^6 cells were used for RNA isolation using the Zymo RNA isolation kit, as described in the manufacturer's instructions.

2.2.5.3   Expression analysis

cDNA was prepared using 200 ng of RNA as input for the iScript™ cDNA Synthesis Kit (section- 2.1.6). Random hexamers were used for all qPCR expression analyses. Synthesis was carried out according to the manufacturer's instructions, with a 50% volume reduction. After cDNA synthesis, all samples were diluted equally at 1:2 with nuclease-free water.

For gene expression analysis of *IKZF3*, TaqMan quantitative PCR (qPCR) was carried out using the following primers and probes: *IKZF3* (Hs00232635_m1), *B2M* (Hs00187842-m1). The PCR protocol was followed as provided by the manufacturer (Thermo Fisher Scientific).

SYBR green primers were purchased from the company Metabion. Validated SYBR green primers were used from the Harvard Primer Bank (91). qPCR (**Table 25**) was performed on a CX96 touch qPCR machine and analyzed using CFX Maestro v2.2.

Temperature	Time	Cycles
50°C	2 minutes	1
95°C	10 minutes	1
95°C	15 sec	40
60°C	30 sec	
72°C	30 sec	
72°C	10 minutes	
Melt Curve		

Component	Time
SYBR green	1x
cDNA	1 μl
Primers FWD, REV	10 μM each
Nuclease-free water	to 25 μl

Table 25- SYBR green quantitative PCR (qPCR).

2.2.5.4   RNA Sequencing

cDNA preparation and RNA sequencing were performed in collaboration with Professor Wolfgang Enard's group at the LMU. The Prime-Seq protocol is available and published (89, 90). Sequencing was performed using a HiSeq 1500 Illumina system.

Lucas Wange performed pre-processing of the data at the LMU. Briefly, the data quality was first assessed using fastqc (section 2.1.10) (76). Cutadapt was then used to remove sequencing adapters (unpublished), and the data was then processed using zUMIs pipeline (78). The data was subsequently filtered, using a phred score of 20 for both the UMIs and base calls. Subsequently, reads were aligned to the human or mouse genomes (GRCh38/GRCm38) with Gencode gene

annotations (v35/vM25) using spliced transcripts alignment to a reference (STAR) (79). Lastly, the reads per gene and sample were counted using RSubread (92).

Dr. Verena Passerini performed differential gene expression analysis using the DEseq2 tool (section 2.1.10). An adjusted p-value of $p<0.05$ and log FC of ±0.5 were used to define significance. In specific experiments, these parameters were adjusted as indicated in each Figure. Using the Metascape platform, I performed gene annotation, interactome analysis, and network analysis of differentially expressed genes, as previously described (93).

2.2.5.5 Unique molecular identifier (UMI)-aided deep next-generation sequencing
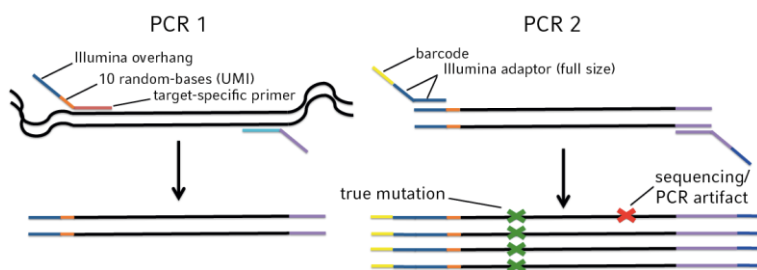
Figure 7- Overview of the unique molecular identifier (UMI) aided next-generation sequencing (NGS) approach.

Figure designed by Dr. Stefan Alig.

500ng of DNA (the equivalent of 10,000 cells) was assayed in quintuplicate using a UMI-aided deep next-generation sequencing approach. This involved a 2 step PCR approach where the first PCR (≤5 cycles; Phusion HF, section 2.1.8.4) amplified the region of interest and introduced a 15-mer UMI barcode (**Fig. 7**). An exonuclease cleanup was then performed to remove excess primers (exonuclease I treatment). The second PCR (35 cycles) then added index primers (single index primers for Illumina). PCR amplicons were then run on a 2% agarose gel in 0.5% TBE for 1 hour, 50V. The correct size amplicon was then excised, and the DNA was extracted (QIAquick gel extraction kit). Sequencing was performed on an Illumina Hi-Seq 1500 with 5 million paired-end 100bp reads per sample. Each sample had a seq depth of approximately 150,000 to 700,000 reads. After deduplication and consensus sequence calling, short insertions/deletions (indels) and single nucleotide variants (SNV) were called with SomaticIndelDetector (GATK) and MuTect.

We called consensus reads where only bases are called where >95% of the reads in a UMI family are identical. This approach considerably reduces background noise (**Fig. 8**).
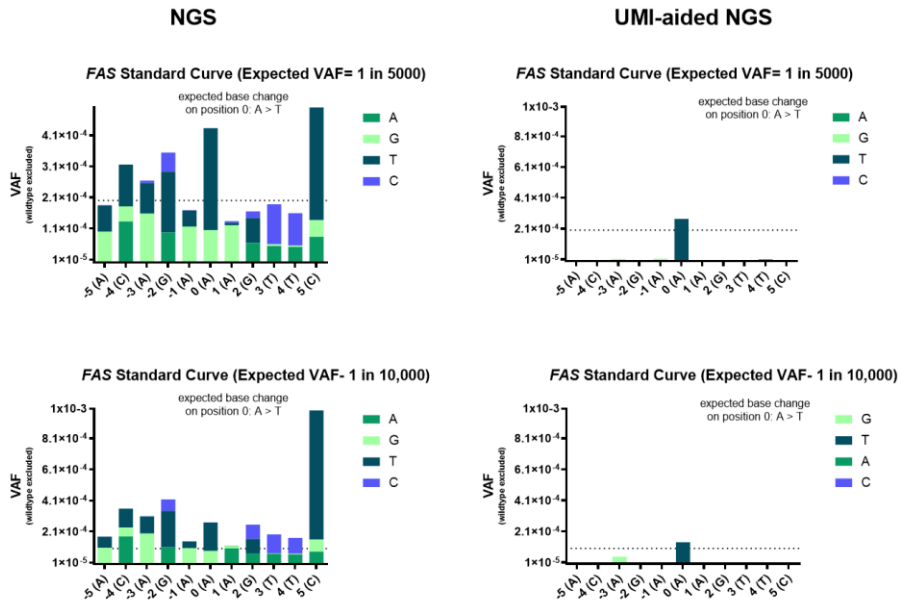
Figure 8- Detecting rare mutations with next-generation sequencing.
Tumor DNA from FL3 was spiked into PBMC healthy donor DNA. Primers were designed to detect a *FAS* (K274I) mutation in FL3. Displayed are the called nucleotides at each position. Position 0 depicts the expected nucleotide change (A > T). **Left-** Nucleotides called without UMI-aided correction. **Right-** Nucleotides called with UMI-aided correction. **Abbreviations**- PBMCS, peripheral blood mononuclear cells; VAF, variant allele frequency; UMI, unique molecular identifier; FAS- Fas Cell Surface Death Receptor; NGS, next generation sequencing.

We performed spike-in experiments to determine sensitivity to detect mutations, mixing healthy genomic DNA isolated from PBMCs and tumor DNA. To ensure consistent detection sensitivity, we performed these experiments using five different mutations (**Fig. 9**).
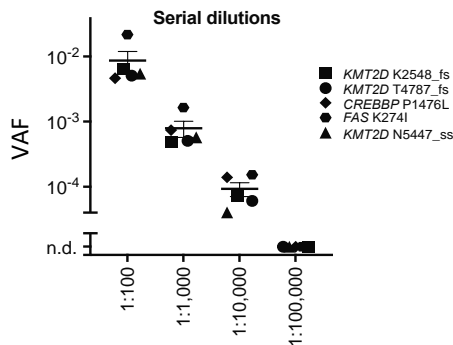
Figure 9- Sensitivity of UMI-aided next-generation sequencing.
Serial dilutions of tumor material for specific mutations mixed with healthy DNA from PBMCs. Error bars depict the standard error of the mean. **Abbreviations-** PBMCS, peripheral blood mononuclear cells; VAF, variant allele frequency; UMI, unique molecular identifier;

Dr. Stefan Alig developed the methodology and sequencing approach and provided valuable instruction for designing and testing the primers, and how to run the analysis pipeline.

2.2.5.6   Digital droplet PCR

For FL3, we analyzed mutations using the QX200 ddPCR system (Bio-Rad laboratories). Ex vivo expanded B cells were assayed in technical duplicate (100 ng), and tumor material from FL3 was used as a control (10 ng). ddPCR was performed in 96 well plates with the ddPCR Supermix for probes (no UTP), in a total volume of 21 µl. Controls included nuclease-free water, gDNA from healthy patient's PBMCs, and gDNA derived from FFPE and gBlocks for positive controls. Data was analyzed on QuantaSoft (Bio-Rad) according to the manufacturer's guidelines (94).

Dr. Sarah Haebe performed ddPCR experiments and analysis in collaboration with the Technical University of Munich (TUM).

2.2.5.7   PCR and Sanger Sequencing of *BCL2/IGH* translocation

PCR (KOD Xtreme Hot Start DNA Polymerase) for *BCL2/IGH* translocation was carried out in a two-step approach. PCR primers spanned the *BCL2/IGH* major breakpoint region (MBR) and the *BCL2/IGH* minor cluster region (mcr) (section 2.1.8). Standard curves for the MBR and mcr were generated using serial dilutions of tumor DNA from FL1 (MBR) and FL3 (mcr). Sanger sequencing was performed at GATC Services (Eurofins Genomics). All primers were designed using Primer3 (section 2.1.10).

2.2.5.8   Quantitative PCR (qPCR) detection of the BCL2/IGH translocation

RT-qPCR (TaqMan) for *BCL2/IGH* MBR and mcr in addition to GAPDH was carried out for CD34^{+} and lin^{-} HSPC-derived CFUs from FL1-FL3. 500 ng of CFUs were tested in duplicate for each of the 5 biological replicates. Probes that hybridize to the *BCL2/IGH* MBR or mcr were utilized (section 2.1.8.2). To determine sensitivity, standard curves were generated of serial dilutions of spiked-in tumor DNA from OCI-Ly1 (MBR) or from the cloned *BCL2/IGH* translocation from FL3 (mcr). Results were analyzed according to published guidelines (95).

2.2.6 Protein analysis

2.2.6.1 Cell lysis

5-10x10^6 cells were harvested, washed in PBS, and lysed in radio immunoprecipitation assay buffer (RIPA). After adding the buffer, cells were placed onto ice for 30 minutes and centrifuged for 30 minutes, 15,000 rpm, 4 °C. The supernatant was then transferred to a fresh tube. The protein concentration was measured using the bicinchoninic acid (BCA) assay as described in the manufacturer's guidelines. The NE/PER Nuclear and cytoplasmic reagents were used following the manufacturer's guidelines for nuclear and cytoplasmic protein extraction.

2.2.6.2 Immunoblotting

Immunoblotting was carried out using two systems. Thermo Fisher Scientific Bolt system, using BOLT pre-cast gels. 60 μg of protein per sample was diluted in lithium dodecyl sulfate (LDS) with a 1X sample reducing agent. Samples were then heated for 10 minutes at 70°C. 4-12% bis-tris gels were used, and the chamber was filled with MOPS buffer. Wells were washed briefly before the protein was loaded. Magic MARK XP Western blot standard was used for protein size comparison. Gels were run for approximately 2 hours, starting at 50V and then increasing to 100V upon migration through the resolving gel.

For the Bio-Rad system, TBX gels were used. Samples were mixed with Laemmli (4x) and dithiothreitol (DTT), which was used as a reducing agent. Gels were run at a constant mini-ampere value of 22 for 130 minutes.

2.2.6.3 Protein transfer

The transfer of proteins from gels to membranes was carried out by two methods. The first was via turbo transfer semi-dry, using power blotter select transfer stacks (PVDF membranes) and according to the manufacturer's instructions. The power blotter settings were 10 minutes 25V. Alternatively, a long transfer was performed using the Bio-Rad wet transfer system (section-2.1.3). For wet transfer, PVDF membranes were activated for 30 seconds in methanol. The transfer stack was assembled according to the manufacturer's instructions, and the transfer was carried out on ice for 2h at a constant voltage of 48V.

Transferred blots were then put into distilled water for 10 minutes before blocking 5% milk (m/v) 1 hour at room temperature. Primary antibodies were added overnight. All blots were then washed 3x

10 minutes (TBS- with 0.1% (V/V) Tween20 (TBS-T), the secondary antibody applied for 1 hour in 5% (m/v) milk, and then washed again (as described) before developing.

Chemiluminescent detection was carried out on a Fusion SL4 imaging system. Blots were incubated with Pierce™ ECL, Clarity Western ECL™, or Clarity Max ECL™ for 1 minute in the dark; excess ECL was removed before image analysis. Following image acquisition, blots were re-washed 3x 5 minutes (TBS-T) and then stripped 15 minutes in stripping buffer. Blots were then re-washed 3x (TBS-T) and blocked for 1 hour with 5% milk (m/v) before adding the next antibody.

2.2.6.4   Immunoprecipitation

For STAT6 immunoprecipitation experiments, STAT6^{WT}, STAT6^{D419G,} or EV cells were initially stimulated with IL-4 (10 ng/mL) for 24 hours. Cells were then lysed using passive lysis buffer (PLB), supplemented with a protease inhibitor cocktail. Cells were lysed for 30 minutes on ice and then centrifuged (30 minutes at 15,596 xg). We used 2.5 mg (calculated by BCA) per IP in a total volume of 5 mL PLB. M2 Flag agarose bead slurry was added to each lysate and then incubated overnight at 4°C. Samples were washed using PLB, rotating for 5 minutes (50 rpm), and then centrifuging (30 seconds, 800 xg). This was repeated three times. To elute the protein, 10x SDS was added to each sample and rotated for 10 minutes. The eluted protein was then removed from the beads via centrifugation (5 minutes, 800 xg), and the elute was heated at 95°C for 5 minutes. The eluted protein and input samples were then analyzed by Western blotting as described (section 2.2.6.2).

2.2.6.5   Quantitative chromatin immunoprecipitation (qChIP)

qChIP was performed using a published protocol with some additional modifications (96). All buffers are listed in the published protocol. 12 x 10^6 STAT6^{WT}, STAT6^{D419G}, or EV cells were seeded and stimulated with IL-4 (10 ng/mL) for 24 hours. PBS was then added to wash the cells (1 mL). To crosslink STAT6 to the DNA, an EGS crosslinker (section 2.1.1) was added for 30 minutes (1.5 mM), lightly shaking. 1% formaldehyde was then added for 10 minutes. For de-crosslinking, 0.125 M glycine was used for 5 minutes. Subsequently, samples were centrifuged (5 minutes, 4000 rpm), and 1 mL cell lysis buffer was added for 10 minutes on ice. Nuclei were then centrifuged, and SDS buffer was added for a further 10 minutes. To shear DNA, sonication was performed using a Bioruptor Pico device for 20 minutes per sample. To verify appropriate DNA fragment size, sonicated products were run on a 1% agarose gel TBE, 100V for 1 hour. DNA concentrations were calculated from the input, and 15 μg of sheared chromatin was used per chromatin immunoprecipitation. Samples were diluted, and the input samples were removed. Antibodies were added according to the

manufacturer's recommendations, and the samples were incubated overnight. To isolate STAT6-bound DNA, ChIP-grade magnetic beads were added to each IP. Samples were incubated for 3 hours, and then the magnetic beads were isolated and washed with high and low salt buffers, lithium chloride (LiCl), and TE (2x). IPs were incubated with SDS buffer for 15 minutes twice to elute the bound protein, each time collecting the supernatant. The eluted samples were then de-crosslinked using NaCl (0.2M) overnight shaking (62°C, 500 rpm). Samples were then treated with RNAse (0.5 mg/mL, 37°C for 2 hours) and Proteinase K (0.1 mg/mL) overnight (42°C), and the DNA was isolated using a PCR purification kit. qPCR was performed as previously described (96).

2.2.6.6   Chromatin immunoprecipitation sequencing (ChIP-seq)

For ChIP-seq experiments, an identical protocol was followed as detailed in section 2.2.6.5. For OCI-Ly1, sonication time was increased to 30 minutes per sample. After purification of the isolated DNA, ChIP-Seq library preparation was carried out using the NEBNext Ultra II DNA kit for Illumina. All isolated DNA was utilized for input, and the samples were processed according to the manufacturer's recommendations. Libraries were analyzed using an Agilent bioanalyzer, and sequencing was performed on a Hi-Seq 1500, with 50bp single-end reads. Reads were aligned using the human genome GRCh38/hg38 and the software package Bowtie2 (97). Reads were visualized using the IGV browser. Peaks were called using MACS2 (71).

2.2.7   Flow cytometry

2.2.7.1   FACS sorting of different hematopoietic lineages.

Before FACS, we first separated leukapheresis-derived mononuclear cells (LMNCs) by Ficoll-Paque gradient density centrifugation, and magnetic cell separation (EasySep Human progenitor cell enrichment), following the manufacturer's recommendations. We then sorted using a BD Aria II. We used a live dead stain and then gated on live lineage negative (lin-) hematopoietic cells (CD45$^+$/CD34$^+$/CD38$^-$) and sorted hematopoietic stem cells (HSC; CD45$^+$/CD34$^+$/CD38$^-$/CD90$^+$/CD45RA$^-$), multilymphoid progenitor cells (MLP; CD45$^+$/CD34$^+$/CD38$^-$/CD90$^{-/low}$/CD45RA$^+$) and multipotent progenitor cells (MPP; CD45$^+$/CD34$^+$/CD38$^-$/CD90$^-$/CD45RA), as previously described (98). T cells (CD45$^+$/CD3$^+$) were sorted from lineage-positive cells.

2.2.7.2   B cell phenotyping

Antibodies used for analyzing GC B cells are listed in section 2.1.7. In each case, cells were washed once in PBS (1 mL), centrifuged (400 xg, 4 minutes), and then stained for 15-30 minutes. Antibody dilutions were scaled up or down depending on the number of cells. After staining, cells were washed 1x with PBS (1 mL) and centrifuged (400 xg, 4 minutes). The supernatant was removed, and the stained cells were resuspended in an appropriate volume with PBS (depending on the cell number). FC was performed on a BD Canto II analyzer.

2.2.8   CRISPR-Cas9

CRISPR-Cas9 was carried out as previously described (58). Karpas 422 or SU-DHL-16 cells were electroporated using the Amaxa Nucleofector II device, program X01. $1x\,10^6$ cells were first washed and incubated in 100 μl of electroporation solution (section 2.1.6). 2 μg of the CRISPR-Cas9 construct and the HDR template were used per electroporation. All sgRNAs were designed using the Benchling CRISPR design online tool (accessed 2020). To disrupt *IKZF3*, sgRNAs were cloned into plasmid pSpCas9(BB)-2A-GFP (PX458, a gift from Feng Zhang, Addgene plasmid #48138) as previously described (58, 99).

2.2.9   Luciferase assay

The luciferase assay was performed using the dual glow luciferase system in HEK 293T cells, as described previously (40). Briefly, 150,000 cells per well in a 12-well adherent cell culture plate were seeded and cultivated overnight at 37°C, 5% CO_2. After 24 hours, 500 ng of IKZF3^{WT}, IKZF3^{MUT}, IKZF1, or an EV control were co-transfected with 500 ng of the SYK promoter. Transfections were carried out using PEI as a transfection reagent (section 2.2.3.3). The SYK promoter was cloned into pGL3 Basic using a 100 ng gDNA template from FL-like B cells, as previously described (40). In addition to the luciferase construct, 40 ng of a pRenilla (pRL) was co-transfected for normalization. Luciferase measurements were taken after 48 hours. The washing of the cells, lysis, and measurement of luciferase was performed as detailed in the manufacturer guidelines, and as previously described (40).

2.2.10   Statistical analysis

All data is from three independent replicates and displayed as the mean +SD unless otherwise specified. Unpaired t-tests were used with Welches correction ($p<0.05$). For multiple comparisons, one-way analysis of variance (ANOVA) was used with Tukey's multiple comparisons test (adjusted p-value <0.05).

3. Results

3.1   The molecular ontogeny of FL

3.1.1   Two models of FL development

The overall goal of this project was to identify early/truncal mutations for subsequent functional analysis. We first wanted to decipher the molecular ontogeny of FL. We hypothesize two different models of FL development. We used the terms 'first hit' and 'subsequent hit' to describe these two models.

In the 'first hit model,' the *BCL2*/*IGH* (t14;18) translocation is the initial event that defines the CPC and FL development (**Fig. 10, left**). Alternatively, mutations might be acquired before the *BCL2*/*IGH* translocation in HSPCs, which subsequently acquire the *BCL2*/*IGH* translocation and become a CPC (**Fig. 10, right**). This 'subsequent hit model' is supported by a recent study by Horton et al., showing that *Crebbp* loss in HSPCs of a mouse can promote lymphomagenesis, with the phenotype altered if *Crebbp* was disrupted at later stages of differentiation (66).
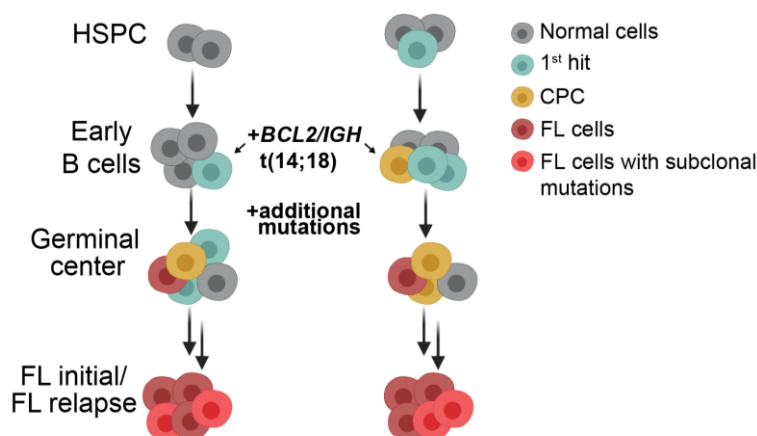
Figure 10- The models of FL evolution.

In the 'first hit model' (**left**), the BCL2/IGH (t14;18) translocation is the initial event that occurs, and upon additional mutations acquired in the germinal center reaction, primary FL develops. In the 'subsequent hit' model (**right**), mutations can be acquired in the HSPCs, which upon *BCL2*/*IGH* translocation form the CPC and develop into FL. Modified from Haebe and Keay et al., 2022 (100). **Abbreviations-** BCL2, B-cell leukemia/lymphoma 2; CPC, common progenitor cell; HSPC, FL- follicular lymphoma, HSPC, hematopoietic stem and progenitor cells; IGH, immunoglobulin heavy locus.

3.1.2 Investigating the 'subsequent hit model' of FL development

For direct verification of the 'subsequent hit model' of FL development, we require samples from FL patients with available purified HSPCs, that lack the *BCL2/IGH* translocation. In this study, we identified three patients with diagnostic biopsies and HSPC-enriched leukapheresis-derived mononuclear cells (LMNCs) from autologous stem cell transplantations collected at first remission. FL1 and FL2 relapsed after R-CHOP, whilst FL3 relapsed after CHOP. As a control, we used a 4th patient's leukapheresis product from a patient that had multiple myeloma.

Using targeted NGS, we profiled the mutational landscape of FL tumors from three patients. The mutation profiles were consistent with a typical FL tumor. FL1 had shared mutations at initial diagnosis and relapse, including *CREBBP* and *KMT2D* (**Fig. 11**). As per definition, these shared mutations are CPC-defining events. FL1 was therefore of high interest to determine if these CPC-defining events could precede the *BCL2/IGH* translocation.
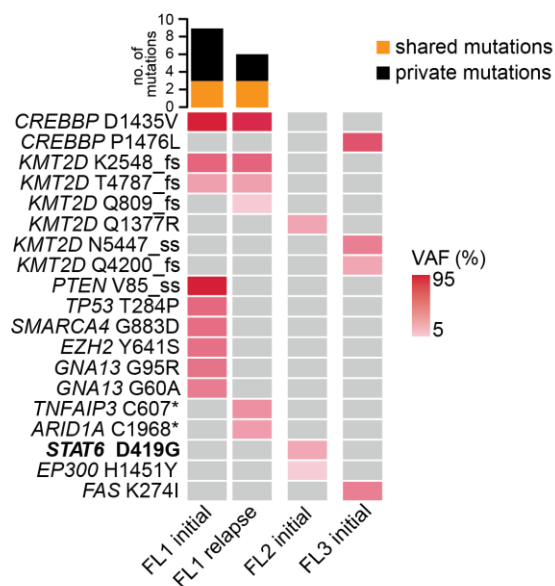
Figure 11- FL mutational profiles.
Oncoprint of non-silent gene mutations in the initial (FL1, 2, and 3) and a relapse tumor biopsy (FL1) from three patients with FL. VAF of each mutation is indicated by color intensity. Modified from Haebe and Keay et al., 2022 (100). **Abbreviations**- FL- follicular lymphoma, VAF- variant allele frequency

To investigate the 'subsequent hit model' and determine if mutations can precede the *BCL2/IGH* translocation, we used two approaches. The first (**Fig. 12**, **upper**) was to sort different cellular fractions and perform highly sensitive NGS.
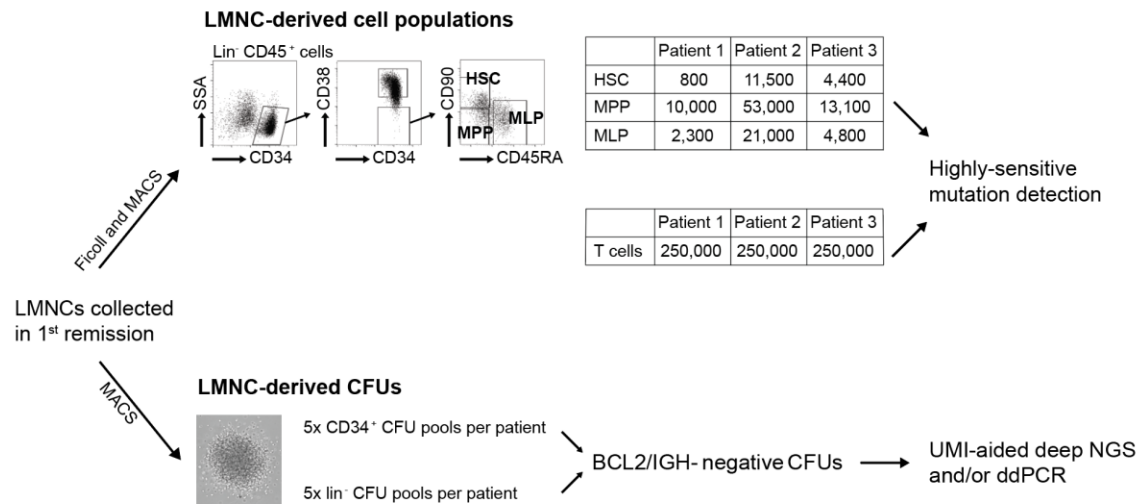
Figure 12- Experimental overview illustrating the two different approaches for detecting mutations in HSPC-enriched LMNCs fractions.

Upper- Representative flow cytometry sorting strategy. The absolute number of sorted cells is shown for each fraction and patient. LMNC-derived T cells and a peripheral blood sample from a healthy individual were used as controls. **Lower-** For each patient, five CD34$^+$ or Lin$^-$ CFU pools were analyzed. Before UMI-aided NGS, every pool was first screened for the BCL2/IGH (t(14;18) translocation via qPCR. Published Figure- from Haebe and Keay et al., 2022 (100). **Abbreviations-** HSPC, hematopoietic stem, and progenitor cells; CFUs, colony forming units; LMNCs, leukapheresis-derived mononuclear cells; HSC, hematopoietic stem cells; MPP, multipotent progenitor cells, MLP, multilymphoid progenitor cells; MACS, magnetic-activated cell sorting; NGS, next-generation sequencing; ddPCR, digital droplet PCR.

For the sorted fractions, we analyzed HSPCs, multi-potent progenitor cells (MPP), multilymphoid progenitor cells (MLP) and included both positive and negative controls. We calculated mutation rate ratios comparing fractions to matched LMNC-derived T cells and a peripheral blood sample from a healthy individual, as previously described (67). However, we did not determine any mutation to be significantly detectable above the background signal. (Data not shown. The data is provided in Haebe and Keay et al., (100) supplementary Table S1).

Due to low cell numbers and difficulty detecting very rare events, we decided to expand LMNCs, isolating CD34$^+$ or lineage-negative (lin$^-$) cells and plating the purified fractions onto methylcellulose (**Fig. 12, Lower**). We then screened the material for the *BCL2/IGH* translocation, establishing a quantitative polymerase chain reaction (qPCR) approach to detect the translocation (section-2.1.8.2). This ensured that our samples did not contain any contaminating B cells with the hallmark FL *BCL2/IGH* translocation. Furthermore, pre/pro B cells can still express low levels of CD34, so we wanted to be sure that we only assayed precursor cells (101).

FL patients have unique *BCL2/IGH* translocations that cluster into a major breakpoint region (MBR), the intermediate cluster region (icr), or a minor cluster region (mcr). These regions define the juxtaposition, including the *BCL2* (18q 21) gene with the *IGH* locus (14q31) (also known as the breakpoint). We used consensus and breakpoint-specific primers to define this region (Sanger sequencing) (102, 103) (**Fig. 13**).

BCL2 (chr. 18) NDN *IGH* (chr. 14)

FL1 GAAATGCAGTGGTGTTTACGAGGCTCCTCAGGTGGTGGTTCGACCCCTG

FL2 ACCCAGAGCCCTCCTGCCCTTCGCTACTACTACTACTACGGTATGGACGT

FL3 AGGAAGGACAATCTCATGGGGGAGA//GTATCTTGACTACTGGGGCCA

Figure 13- *BCL2/IGH* breakpoint regions of FL1-FL3 determined by PCR and Sanger sequencing.

Blue depicts the *BCL2* gene sequence; green indicates NDN (NDN, non-templated nucleotides). Red shows the *IGH* sequence. **Abbreviations**- *BCL2*, B cell leukemia/lymphoma 2; *IGH*, immunoglobulin heavy locus; FL- follicular lymphoma; PCR, polymerase chain reaction.

After defining the patient-specific breakpoint region, we developed a qPCR assay with patient-specific probes to allow us to reliably and sensitively screen CFUs for contaminating BCL2/IGH^{+} cells. We therefore, ensured we only assayed purified HSPCs for the presence of mutations.

FL1 and FL2 CD34^{+} and Lin^{-} derived CFU pools were screened negative (**Fig. 14A**) for *BCL2/IGH*, whilst FL3 CD34^{+} CFU pools were positive (**Fig. 14B, 14C**) and excluded from further analysis. Thus, our results show that translocated FL B cells can persist on methylcellulose for 14 days.
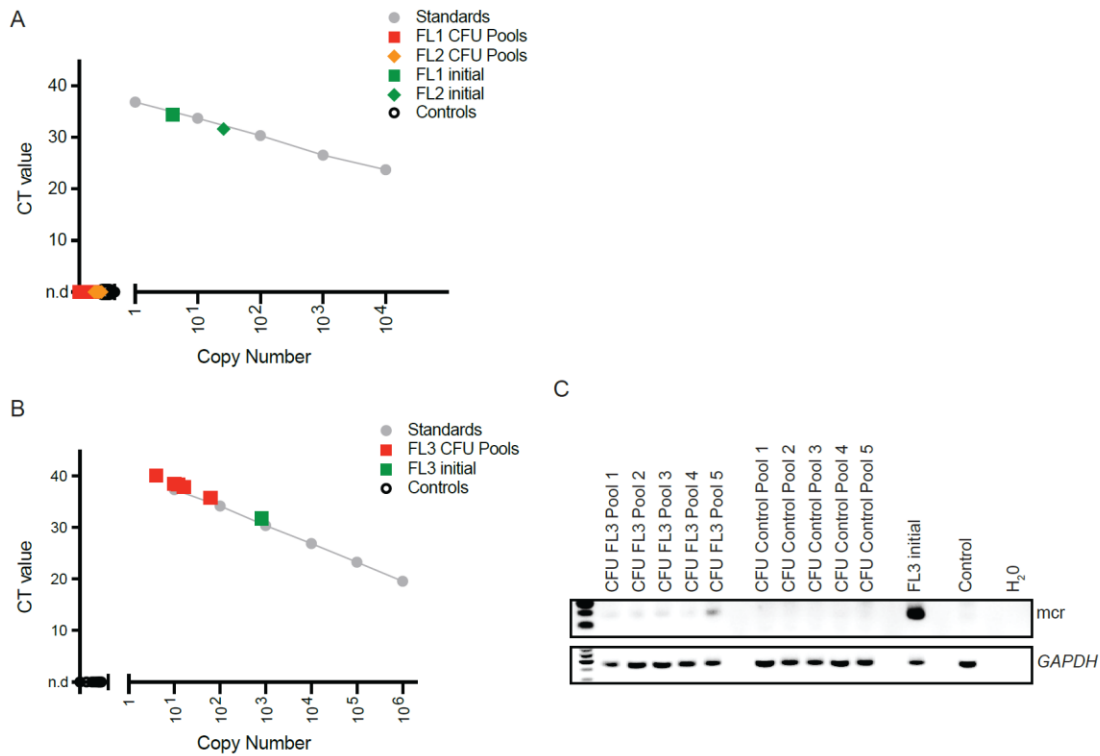
Figure 14- Quantitative PCR (qPCR) analysis of CFU pools for *BCL2/IGH* translocation.

A) qPCR for FL1 and FL2 for the major breakpoint region (MBR), *BCL2/IGH*. Serial dilution (grey) using spike-in DNA from (OCI-Ly1, MBR) in PBMC DNA from healthy donors. Five individual pools were assayed, and five control pools (N=5) were assayed in technical duplicate. Genomic DNA from PBMCs was used as a negative control, and positive controls consisted of tumor DNA from FL1 and FL2. **B)** qPCR for mcr *BCL2/IGH* of FL3. Standard curves were generated using the cloned breakpoint of FL3 (grey). DNA from LMNC-derived CD34+ CFUs was analyzed in technical duplicate and plotted against the standard curve. Five CFU pools were analyzed, with healthy patient gDNA used as a negative control and tumor DNA from FL3 used as a positive control. **C)** qPCR products from LMNC-derived CD34+ CFUs from FL3 visualized by gel electrophoresis. Control pools are derived from LMNC-derived CFUs from a patient with multiple myeloma (CFU Control Pools 1-5). PBMCs from a healthy donor (Negative control) and FL3 were used as a positive control. GAPDH- loading control (177bp), mcr (≈125bp). SD error bars are too small to be shown. Published Figure- from Haebe and Keay et al., 2022 (100). **Abbreviations**- qPCR, quantitative polymerase chain reaction; MBR, major breakpoint region; PBMCS, peripheral blood mononuclear cells; mcr, minor cluster region; CFUs, colony forming units; CT, cycle threshold; SD, standard deviation; LMNCs, leukapheresis-derived mononuclear cells, GAPDH, glyceraldehyde-3-phosphate dehydrogenase.

We next analyzed our highly purified CFUs (confirmed negative for the *BCL2/IGH*) for the presence of mutations. We analyzed five distinct pools of CD34+ and lin⁻ HSPC-derived CFUs. Each of the pools contained a median of 1315 (344–1670) and 779 (566–3115) CFUs. 500 ng of DNA was used, which was equivalent to 10,000 cells. (500 ng genomic DNA, corresponding to ˷500 distinct HSPCs) for each mutation was assayed via UMI-aided NGS in five replicates.

In summary, in both CD34$^+$ and lin$^-$ purified CFU pools, we did not detect any mutations at a limit of detection of 10^{-4} (**Fig. 15 and Table 26**). This included *CREBBP* and *KMT2D,* which are highly recurrent in FL. Our data therefore, does not support our hypothesis that mutations are acquired in HPSCs and subsequently acquire the BCL2/IGH translocation and become a CPC.
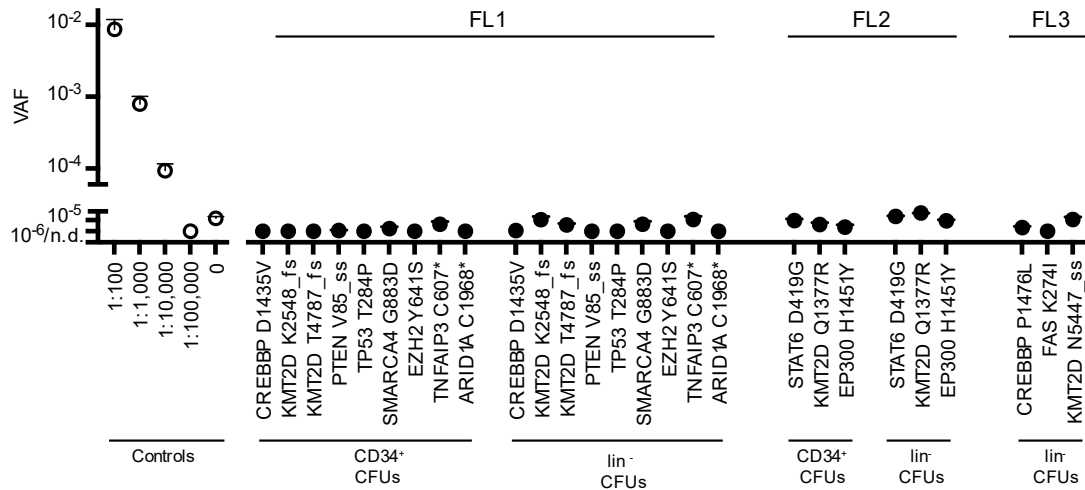
Figure 15- VAF of defined mutations in lin-LMNC and CD34$^+$ derived CFUs from FL1, 2, and 3.

Serial dilutions were performed of tumor material for specific mutations mixed with healthy DNA from PBMCs. Controls included in the standard curve include *KMT2D* K2548_fs, *KMT2D* Q1377R, *KMT2D* N5447_ss, *CREBBP* P1476L, and *FAS* K274I. Negative controls were from CD34$^+$ and lin$^-$ LMNC-derived CFUs from a patient with multiple myeloma. Error bars depict the standard error of the mean. VAF of indicated mutations in CD34$^+$ and lin$^-$ LMNC-derived CFUs from all three patients. Published Figure- from Haebe and Keay et al., 2022 (100). **Abbreviations**- FL1-3, follicular lymphoma patient 1,2 or 3; NGS, next-generation sequencing; n.d., not detectable; UMI, unique molecular identifier; VAF, variant allele frequency; PBMCS, peripheral blood mononuclear cells; CFU, CFUs, colony forming units.

Table 26- Summary of CFU-derived CD34$^+$ or Lin$^-$ CFUs assayed by UMI-aided NGS sequencing.

Patient no.	CD34$^+$ enriched CFUs						Lineage negative CFUs					
	No. of pools (biological replicates)	No. of plates/pool	No. of CFUs / pool (median, min. max.)	BCL2/IGH detection (by qPCR / nested PCR)	gene mutations (tested* / identified**)	UMI-aided sequencing	No. of pools (biological replicates)	No. of plates/pool	No. of CFUs / pool (median, min.-max.)	BCL2/IGH detection (by qPCR / nested PCR)	gene mutations (tested* / identified**)	UMI-aided sequencing
FL1	5	3	1,519 (1,420 - 1,670)	negative (MBR)	9/12	n.d.	5	4	2,488 (2,049 - 3,115)	negative (MBR)	9/12	n.d.
FL2	5	1	411 (344-445)	negative (MBR)	3/3	n.d.	5	2	1,297 (1,168 -- 1,403)	negative (MBR)	3/3	n.d.
FL3	5	n.a.	n.a.	positive (mcr)	n.a.	n.a.	5	2	644 (566 - 779)	negative (mcr)	3/4	n.d.
Control	5	4	1,315 (1,259-1,411)	negative (MBR/mcr)	2/n.a.	n.d.	5	2	749 (618-774)	negative (MBR/mcr)	6/n.a	n.d.

Published Table- from Haebe and Keay et al., 2022 (100). **Abbreviations-** CFU, colony forming units; UMI, unique molecular identifier; HSPC, hematopoietic stem and progenitor cells; mcr, BCL2/IGH minor cluster region; MBR, BCL2/IGH major breakpoint region; n.d., not detectable; n.a., not applicable; NGS, next generation sequencing; *number of mutations tested; ** number mutations identified in the initial tumor.

3.1.3 Investigating the 'first hit model' of FL development

We next investigated the 'first hit model' of lymphomagenesis. The BCL2/IGH translocation is thought to occur in pre/pro B cells; therefore, we focused on FL3, which did not receive any B cell-depleting antibodies (anti-CD20) before LMNC collection. To provide evidence that the *BCL2/IGH* translocation is the 'first hit,' we wanted to identify cells that harbor the translocation but have yet to acquire any CPC-defining mutations (mutations present at diagnosis and relapse).

FL3's BCL2/IGH translocation was detectable at all stages of the disease, including initial diagnosis and relapsed disease. *BCL2/IGH*+ cells in the peripheral blood (PB) were also detectable in ongoing clinical remission 7 and 8 years after allogeneic transplantation. CPC-defining mutations, including *CREBBP,* which was detected at very high VAF in both diagnosis and relapse samples, were not detected in BCL2/IGH positive PBMCs from PB by ddPCR. In addition, we confirmed the absence of the mutations via UMI-aided NGS (**Fig. 16**).
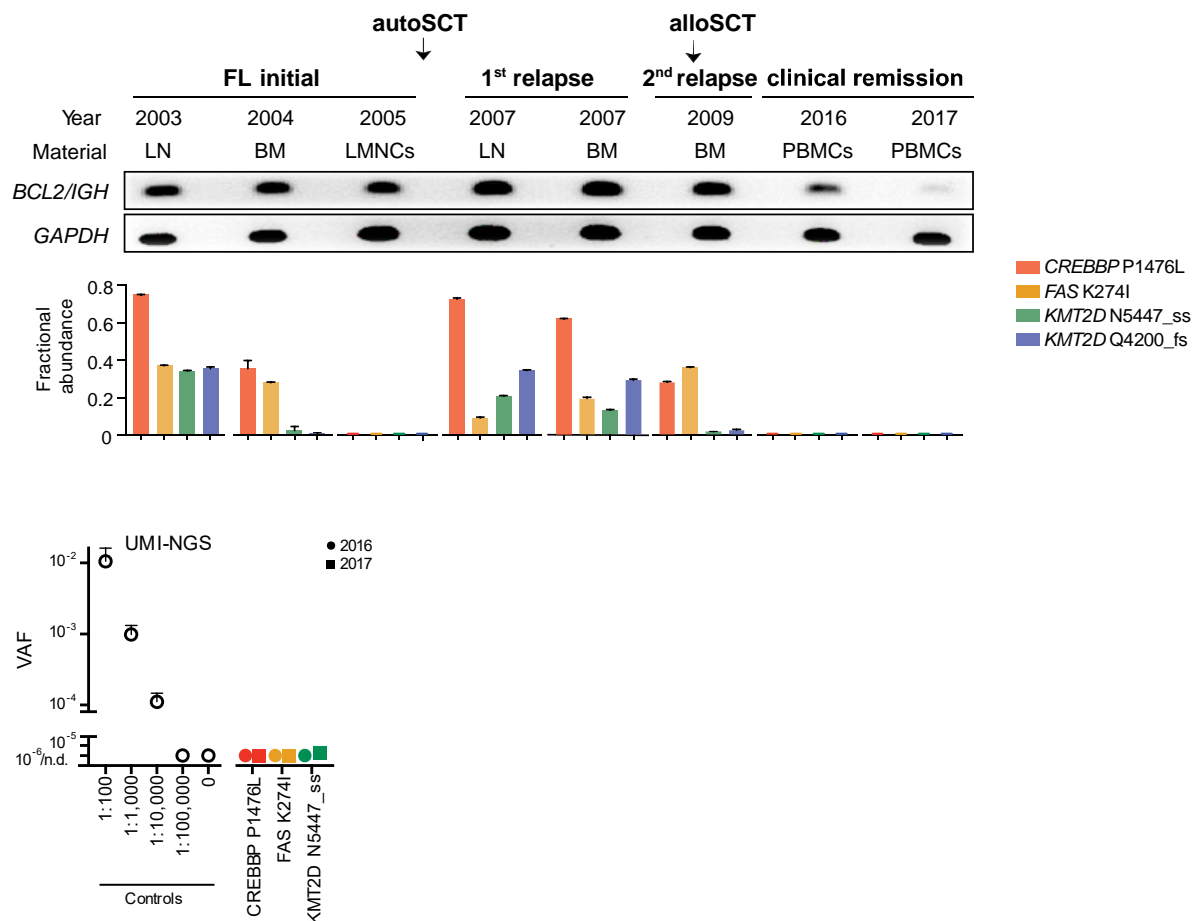

Figure 16- Relapsing FL- An informative case (FL3).
Upper- FL specific analysis of *BCL2/IGH* translocation as determined via PCR. CPC-defining gene mutations were determined via ddPCR. PCR for GAPDH was used as a loading control. **Lower-** VAF of the indicated mutations of peripheral blood samples collected in 2016 and 2017. Serial dilutions

were performed of tumor material for all mutations displayed mixed with healthy DNA from PBMCs. A negative control for each mutation was assayed using gDNA from healthy donor PBMCs. Error bars indicate the standard error of the mean. GAPDH- loading control (177bp), mcr (≈125bp). Published Figure- Modified from Haebe and Keay et al., 2022 (100). **Abbreviations**-NGS, next-generation sequencing; n.d., not detectable; UMI, unique molecular identifier; VAF, variant allele frequency; PBMCS, peripheral blood mononuclear cells alloSCT, allogeneic stem cell transplantation; autoSCT, autologous stem cell transplantation. BCL2, B-cell leukemia/lymphoma 2; BM, bone marrow; GAPDH, glyceraldehyde-3-phosphate dehydrogenase; IGH, immunoglobulin heavy locus; LMNCs, leukapheresis-derived mononuclear cells; LN, lymph node; n.d.

The absence of CPC-defining mutations in the PB samples could be because we are beyond our limit of detection; with a relatively weak band detected for the *BCL2*/*IGH* translocation in the 2017 PB sample by PCR (**Fig. 16**). To rule out a potential incorrect negative result we expanded PB B cells taken from the 2017 PB sample, as previously described (104). We confirmed identical *BCL2*/*IGH* translocation (compared to the initial tumor) via PCR and Sanger sequencing (**Fig. 17A**). We next performed UMI-aided NGS or ddPCR to identify CPC-defining events. However, we did not detect any mutations in *BCL2*/*IGH*-positive ex vivo expanded B cells from two B cell-derived pools via UMI-aided NGS or ddPCR (**Fig. 17B**).
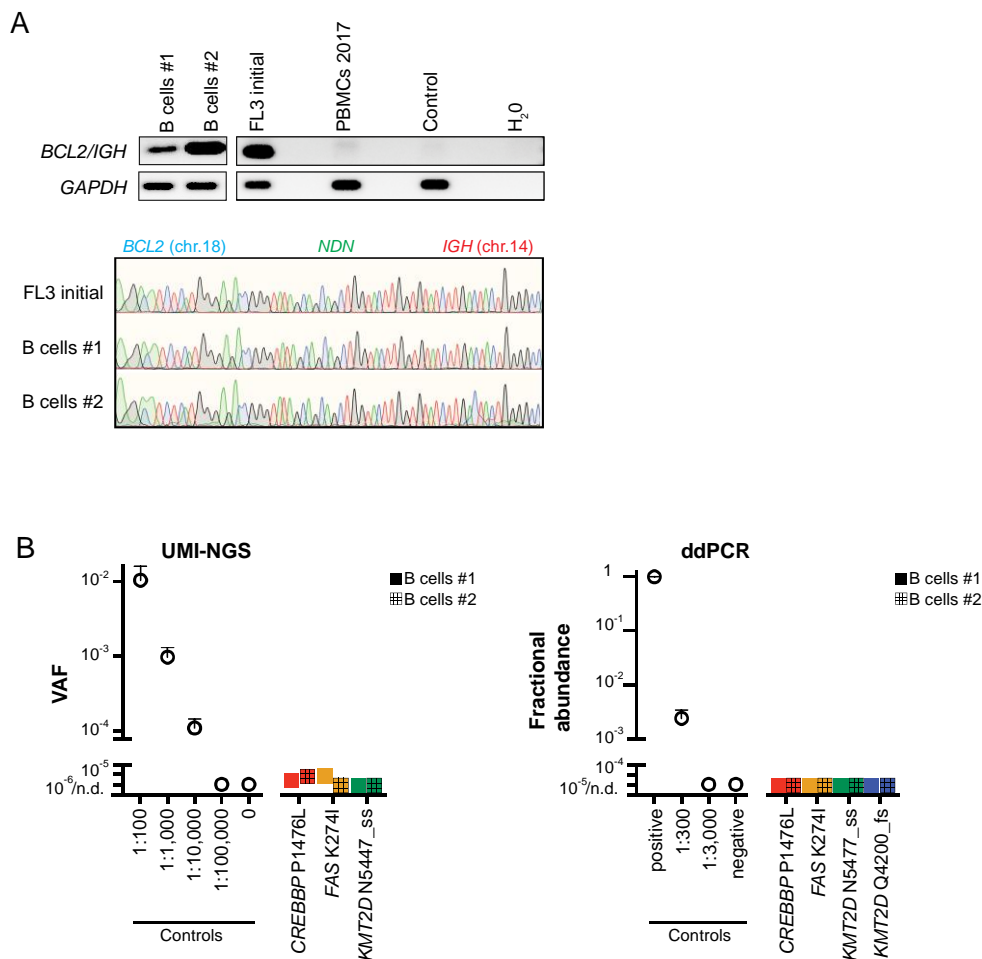

Figure 17- Ex vivo expanded peripheral B cells from FL3.

A) PCR amplification of FL-specific *BCL2/IGH* of two ex vivo expanded B cell lines derived from PBMCs from FL3 taken in 2017. B cells were ex vivo expanded in two independent attempts. As controls, we used genomic DNA from the initial FL3 tumor and the peripheral blood sample collected in 2017 (positive controls), PBMCs from a healthy donor, and H_2O (negative controls). As a loading control, we performed a PCR for GAPDH. GAPDH- loading control (177bp), mcr (≈125bp). Sanger sequencing traces from the *BCL2/IGH* translocations from the initial tumor (FL3) and ex vivo expanded B cells (#1 and #2). **B)** The fractional abundance and VAF from PBMCs were collected in 2016 and 2017 by UMI-NGS (left) and ddPCR (right). Error bars indicate the standard error of the mean. Published Figure- Modified from Haebe and Keay et al., 2022 (100). **Abbreviations**- FL, follicular lymphoma; BCL2, B-cell leukemia/lymphoma 2; ddPCR, digital droplet polymerase chain reaction; NDN, non-templated nucleotides; NGS, next-generation sequencing; PBMCs, peripheral mononuclear cells; GAPDH, glyceraldehyde-3-phosphate dehydrogenase; IGH, immunoglobulin heavy locus; n.d., not detectable; UMI, unique molecular identifier; VAF, variant allele frequency.

In summary, we did not find any mutations in HSPCs from sorted cellular fractions or CD34$^+$/lin$^-$ purified BCL2/IGH$^-$ CFU pools. Our data, therefore, supports the model that in human FL, the *BCL2/IGH* translocation occurs before the acquisition of CPC-defining mutations. In the second section, we identified a patient in clinical remission harboring the BCL2/IGH translocation but without additional mutations. This suggests that BCL2/IGH can persist in the blood and bone marrow during clinical remission. The absence of CPC-defining mutations in these cells suggests they are highly unlikely to be capable of causing relapses.

As we could not identify gene mutations that precede the acquisition of the *BCL2/IGH* translocation, we decided to use alternative approaches to infer early/truncal alterations for functional characterization.

3.2 Functional characterization of recurrent candidate mutations

3.2.1 STAT6

3.2.1.1 Background

Okosun et al. found *STAT6* mutations with a very high VAF of 100%, identifying these mutations as clonal events (105). Kridel et al. analyzed patients at initial diagnosis and relapse, finding a patient with a high VAF *STAT6* mutation at both time points, indicating that some *STAT6* mutations are CPC-defining events (VAF-initial diagnosis-0.47, Relapse-0.44) (106). Another study identified *STAT6* mutations in 9 of 39 (23.1%) transformed FL cases assayed, with 3 patients out of 5 (with available diagnostic specimens), having the same mutations at initial diagnosis (107). These results indicate that some *STAT6* mutations can be truncal and CPC-defining events and are therefore ideal candidates for functional characterization.

Boesl et al. previously functionally characterized *STAT6* mutations in our lab, and in my thesis, I wanted to follow up and complement his work (40). We re-analyzed a previously published cohort to investigate further *STAT6* mutants clonality (German Low-Grade Lymphoma Study Group, GLSG 2000, section 2.1.9). I wanted to further functionally characterize these mutations and refine a mechanism of *STAT6*^MUT lymphoma, previously proposed by Boesl et al. (13).

3.2.1.2 *STAT6* is recurrently mutated in follicular lymphoma

In a cohort of 258 patients with advanced-stage FL, we found *STAT6* mutations in 13% of cases (33 diagnostic biopsies) (**Fig. 18A**) (40). Most mutations clustered in the DNA binding domain and were at position D419 (N = 16, 43%). Using genome-wide copy number data generated from the OncoScan platform from 146 cases, we could correct cancer cell fractions and infer clonality for *STAT6* mutations. In our cohort, 15/146 had *STAT6* mutations with available copy number data. In contrast to Okosun et al., we observed *STAT6* mutations to be clonal in some FL patients and sub-clonal in others (**Fig. 18B**).
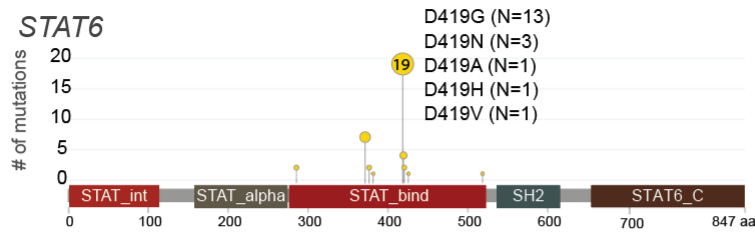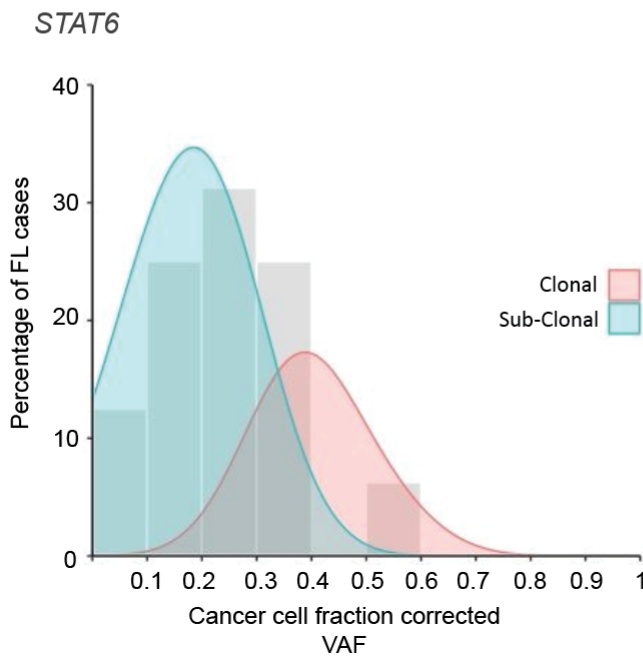
A

B

Figure 18- *STAT6* mutations identified in the GLSG2000 and BCCA cohorts.
A) *STAT6* mutations are displayed as a lollyplot of 258 FL biopsies. **B)** Clonality analysis of *STAT6* mutations from the GLSG2000 cohort (N=146), cancer cell fraction corrected, analysis showing variant allele frequency and percentage of FL cases (13, 40). Figure A is published in the journal *Leukemia* (108). **Abbreviations**- GLSG2000, German low-grade lymphoma study group 2000; VAF, variant allele frequency; BCCA, British Columbia Cancer Agency-Vancouver Cancer Centre; STAT6, signal transducer and activator of transcription 6.

3.2.1.3   *STAT6* mutations are gain-of-function

To test whether *STAT6* DNA binding mutations are gain-of-function, I used a modified version of the pre-B colony formation unit CFU assay, analyzing serial replating capacity. We transduced HSPCs from Emu-BCL2 mice with *STAT6*^WT, *STAT6*^D419G, or an EV control and plated them onto methylcellulose, which supports the growth of pre-B CFUs, supplemented with additional mouse IL-4 (**Fig. 19, left**). IL-4 binds to its receptor (IL-4R) on FL cells, and this recruits JAK1/3 and activates STAT6 by phosphorylation of Y641 (109). From passage 3 onwards, only *STAT6*^D419G conferred a serial

replating phenotype (**Fig. 19, right**). Thus, these results indicate that $STAT6^{D419G}$ mutations confer a gain-of-function phenotype.
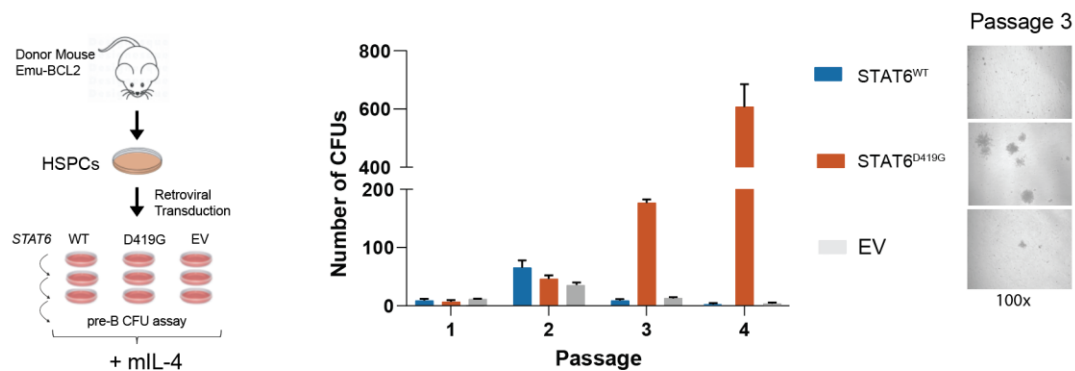

Figure 19- *STAT6* mutations are gain-of-function.

Left- HSPCs from Emu-BCL2 mouse cells were transduced with either $STAT6^{WT}$, $STAT6^{D419G}$, or an empty vector (EV) control and then serially replated on cytokine-supplemented methylcellulose (MethoCult, M3630), with additional mouse IL-4. **Right-** Mouse pre-B CFUs were counted weekly (N = 3, mean + SD). A modified version of this Figure is published in the journal *Leukemia* (108). **Abbreviations-** HSPC, hematopoietic stem and progenitor cells; CFUs, colony forming units; Emu, Immunoglobulin heavy chain enhancer; BCL2, B cell leukemia/lymphoma 2; STAT6, signal transducer and activator of transcription 6; WT, wild type; EV, empty vector, SD, standard deviation.

We have previously shown that $STAT6^{MUT}$ cells require IL-4 for their gain-of-function phenotype (40, 41, 110). To model this phenotype, we used two lymphoma cell lines containing the BCL2/IGH translocation (OCI-Ly8 and OCI-Ly1). RNA seq analysis performed in our lab comparing $STAT6^{MUT}$ vs. $STAT6^{WT}$ cells stimulated with IL-4 revealed PARP14 to be a novel target of STAT6^{MUT} and upregulated in OCI-Ly1 or OCI-Ly8 (40, 110). In this study, we wanted to further functionally characterize STAT6^{MUT} regulation of *PARP14* in order to further define a mechanism.

3.2.1.4   STAT6 and PARP14 directly interact in lymphoma cells

PARP14 was previously described to be a transcriptional switch for STAT6-dependent transcription (38). In this study, they showed that in the presence of IL-4, PARP14 facilitates STAT6 binding to its promoter by releasing of transcriptional repressors, histone deacetylases (HDACs) (38). We hypothesized that STAT6 and PARP14 may directly interact. We confirmed this interaction using immunoprecipitation of 3xFlag tagged STAT6 and probing the membrane for PARP14 (**Fig. 20**).
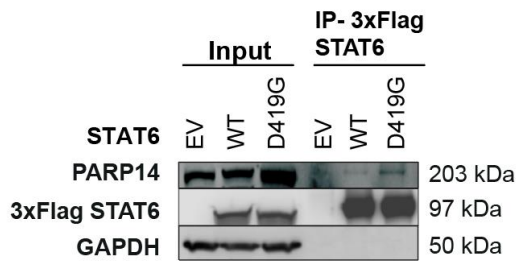
Figure 20- STAT6 and PARP14 directly interact in lymphoma cells.

Immunoprecipitation of 3xFlag tagged STAT6 in OCI-Ly8 cells. Cells were stimulated with IL-4 for 24 hours (10ng/mL). Immunoblotting for PARP14 and STAT6 with GAPDH used as a loading control to verify equal input. This Figure is published in the journal *Leukemia* (108). **Abbreviations**- IL-4, Interleukin 4; WT, wild type; EV, empty vector; STAT6, signal transducer and activator of transcription 6, PARP14, Poly(ADP-ribose) polymerase family member 14; Flag, the brand name for a protein tag with the amino acid sequence DYKDDDDK; GAPDH, glyceraldehyde-3-phosphate dehydrogenase; kDa, kilodaltons; IP, immunoprecipitation.

3.2.1.5 STAT6^{D419G} but not STAT6^{WT} binds specifically to the PARP14 promoter

As we identified previously, increased *PARP14* expression in IL-4 stimulated STAT6^{MUT} OCI-Ly1 and OCI-Ly8 cells, we hypothesized that *STAT6*^{MUT}, but not *STAT6*^{WT} may directly bind to the *PARP14* promoter, regulating expression. To investigate this, we performed chromatin immunoprecipitation sequencing (ChIP-seq). Using OCI-Ly1, we performed ChIP for 3xFlag STAT6^{WT} or 3xFlag STAT6^{D419G}, followed by sequencing.
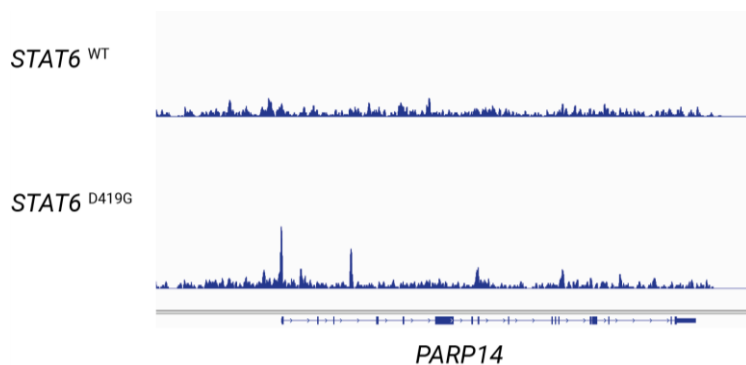
Figure 21- ChIP-seq of OCI-Ly1 lymphoma cells expressing STAT6^{WT} or STAT6^{D419G}.

OCI-Ly1 cells expressing STAT6^{WT} or STAT6^{D419G} were stimulated with IL-4 for 24 hours. ChIP-seq was then carried out for 3x Flag STAT6^{WT} or STAT6^{D419G} (N=2). Representative peaks were viewed via IGV browser. **Abbreviations**-ChIP-seq, Chromatin immunoprecipitation sequencing; STAT6, signal transducer and activator of transcription 6, PARP14, Poly(ADP-ribose) polymerase family member 14.

We observed a higher binding peak for STAT6^{D419G} than STAT6^{WT}, indicating that STAT6^{D419G} binds to the PARP14 promoter (**Fig. 21**). However, we also observed a high level of background signal and

relatively low coverage. Therefore, we opted for quantitative chromatin immunoprecipitation (qChIP) using OCI-Ly8, which had the advantage of (i) reduced sonication time (20 minutes), and (ii) higher PARP14 levels compared to OCI-Ly1.

qChIP analysis of IL-4 stimulated 3xFlag STAT6^{WT}, STAT6^{D419G}, or EV control cells was followed by qPCR for the PARP14 promoter region. We identified increased binding of STAT6^{D419G} to the promoter, with no difference of STAT6^{WT} compared to the EV control (**Fig. 22**). Thus, these results indicate that upon IL-4 stimulation, STAT6^{D419G}, and not STAT6^{WT} binds specifically to the PARP14 promoter.
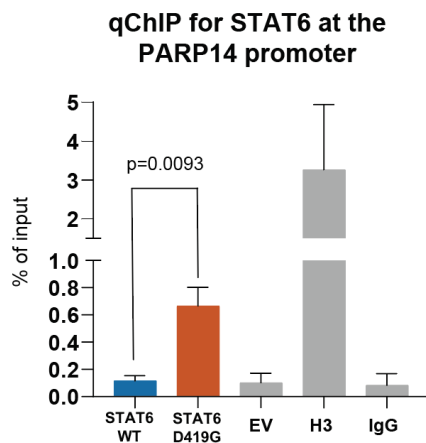
Figure 22- Quantitative chromatin immunoprecipitation for STAT6 at the PARP14 promoter.

Cross-linked chromatin immunoprecipitation (ChIP) of 3xFlag-tagged STAT6^{WT}, STAT6^{D419G}, or EV OCI-Ly8 lymphoma cells after IL-4 stimulation (10ng/mL). H3 and IgG were used as a positive and negative control. Quantitative qPCR was performed for the PARP14 promoter region (N=3, SEM). A modified version of this Figure is published in the journal *Leukemia* (108). **Abbreviations**-qChIP, Quantitative chromatin immunoprecipitation; STAT6, signal transducer and activator of transcription 6, PARP14, Poly(ADP-ribose) polymerase family member 14; H3, Histone 3; IgG. Immunoglobulin G; WT, wild type; EV, empty vector; SEM, standard error of the mean.

3.2.1.6   Validation of our findings using a follicular lymphoma-like co-culture model

To validate our findings, we used a human germinal center B cell co-culture model, as previously described (84). Human tonsil-derived GC B cells are immortalized with BCL2 and BCL6 transduction and require FDC support plus CD40L and IL21 (YK6-CD40lg-IL21) for sustained growth, thus mirroring the dependence of FL cells on the TME (**Fig 23A**). We expressed *STAT6*^{WT}, *STAT6*^{D419G}, or EV, and confirmed protein expression **(Fig. 23B**) and germinal center phenotype (**Fig. 23C**).
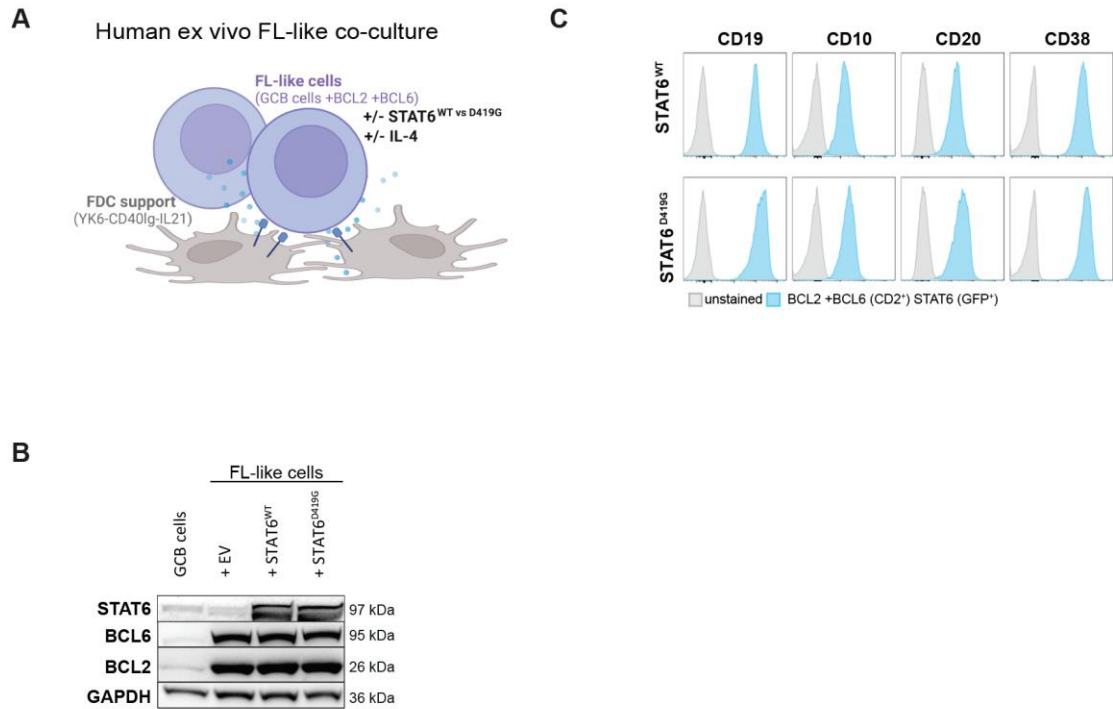
Figure 23- Human ex vivo FL-like co-culture.

A) Overview of the co-culture system. Human tonsil-derived GC B cells expressing BCL2 and BCL6 in addition to STAT6^{WT} STAT6^{D419G} or EV as a control. FL-like cells were co-culture on FDC feeder cells (YK6-CD40lg-IL-21) **B)** Western blot of FL-like B cells. **C)** FC of GC markers of STAT6^{WT} or STAT6^{D419G} FL-like cells. This Figure is published in the journal *Leukemia* (108). **Abbreviations-** FL, follicular lymphoma; IL-4, interleukin 4; GC, germinal center B cells; FDC, follicular dendritic cell; STAT6, signal transducer and activator of transcription 6; BCL2, B cell leukemia/lymphoma 2; BCL6, B cell lymphoma 6, GAPDH, glyceraldehyde-3-phosphate dehydrogenase; WT, wild type; EV, empty vector; kDa, kilodaltons**.**

3.2.1.7   PARP14 is upregulated in FL-like B Cells

We wanted next to validate our previous findings using our FL-like B cell model. We previously showed in OCI-Ly1 and OCI-Ly8 lymphoma cells that IL-4 stimulation increased pSTAT6 and PARP14 only in the nuclear fraction of STAT6^{D419G} cells in comparison to STAT6^{WT} (40). We could confirm this finding using the FL-like GC model (**Fig. 24A**).

We next performed qPCR and could show (as previously described in OCI-ly1 and OCI-Ly8) that upon IL-4 stimulation, *FCER2* (a known STAT6 target gene) is increased in STAT6^{D419G} cells compared to STAT6^{WT} (40) (**Fig. 24B, left**). We also validated increased *PARP14* gene expression (**Fig. 24B, right**).
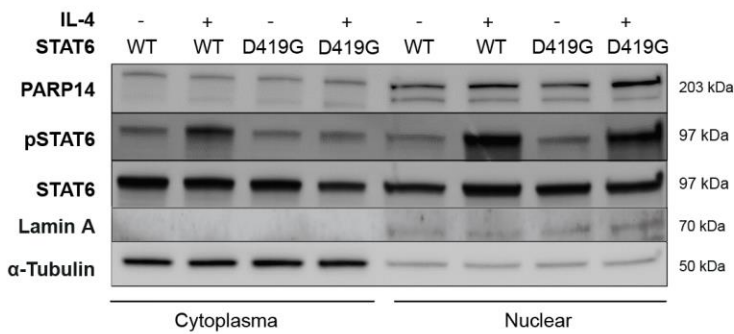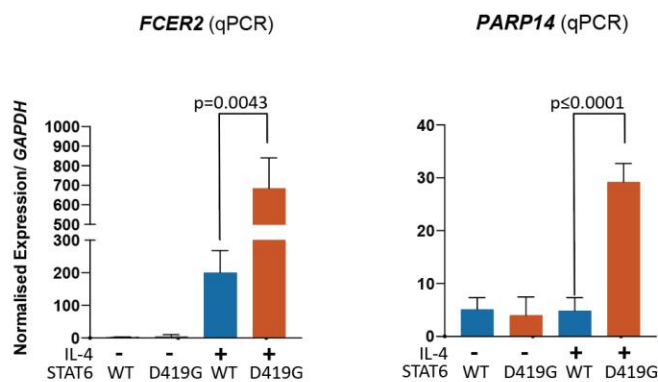
Figure 24- PARP14 is upregulated in STAT6^D419G FL-like B cells.

A) Cytoplasmic and nuclear fraction Western blot analysis of STAT6^WT or STAT6^D419G FL-like B cells stimulated with IL-4. **B)** qPCR analysis of *STAT6*^WT or *STAT6*^D419G FL-like B cells for *FCER2* and *PARP14* (N=4, mean+ SD). A modified version of this Figure is published in the journal *Leukemia* (108). **Abbreviations-** FL, follicular lymphoma; IL-4, interleukin 4; STAT6, signal transducer and activator of transcription 6; pSTAT6, phosphorylated STAT6; WT, wild type; PARP14, Poly(ADP-ribose) polymerase family member 14; *FCER2* (CD23), Fc Epsilon Receptor II; α-Tublin, alpha Tubulin; kDa, kilodaltons; qPCR, quantitative polymerase chain reaction; SD, standard deviation.

3.2.1.8   STAT6^D419G amplifies an IL-4-dependent chemokine response

Previously we analyzed available genome-wide RNA profiling of 106 FL diagnostic biopsies (17 *STAT6*^MUT and 89 *STAT6*^WT) and identified upregulation of known STAT6 target genes in *STAT6*^MUT samples, including *CCL17* and *CCL22* (40, 41, 111). We wanted to test in our FL-like B cells if we could verify this finding. We could indeed show that upon IL-4 stimulation in STAT6^D419G cells, *CCL17* and *CCL22* are upregulated (by qPCR) compared to STAT6^WT cells (**Fig. 25**). This validates our previous finding from primary FL patient material.
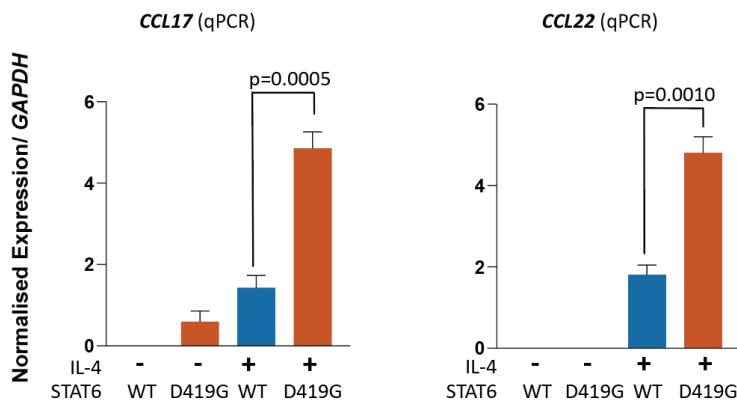
Figure 25- STAT6[D419G] amplifies an IL-4-dependent chemokine response.

qPCR analysis of *CCL17* and *CCL22* expression in STAT6[WT] or STAT6 [D419G] FL-like B cells stimulated with or without IL-4 (N=4, mean+ SD). A modified version of this Figure is published in the journal *Leukemia* (108). **Abbreviations**- *CCL17,* C-C Motif Chemokine Ligand 17; *CCL22,* C-C Motif Chemokine Ligand 22; STAT6, signal transducer and activator of transcription 6; IL-4, interleukin 4, WT, wild type; GAPDH, glyceraldehyde-3-phosphate dehydrogenase; SD, standard deviation; qPCR, quantitative polymerase chain reaction.

In summary, these results significantly contributed to the functional characterization of *STAT6* mutations in FL. I validated previous findings from Boesl et al. and further refined a mechanism of STAT6[MUT] lymphoma that involves increased levels of PARP14. PARP14, therefore, represents a novel therapeutic target of STAT6[MUT] FL (108).

My data however, does not indicate that *STAT6* mutations are amongst the earliest mutations acquired, with both clonal and sub-clonal mutations identified in this study. Therefore, as our original aim was to characterize early acquired events functionally, we decided to focus on another recurrent mutation, *IKZF3*. *IKZF3* mutations are highly clonal and have distinct mutation-specific phenotypes when expressed in HSPCs vs. (early) B cells.

3.2.2   IKZF3

3.2.2.1   Background

Clonal *IKZF3* mutations have been reported in chronic lymphocytic leukemia (CLL). Lazarian et al. identified 10 CLL patients, 4 had *IKZF3* mutations, all of which were clonal events (VAF- >40%) (43). Takahashi et al. also reported clonal *IKZF3* mutations in 2/3 CLL patients with a VAF of >90% (112). Few studies have investigated whether *IKZF3* mutations are early acquired events in the context of FL. Yet, functionally *IKZF3* has an essential role in early B cell development, with expression initiated in early progenitors and increasing upon differentiation into mature B cells (113, 114).

3.2.2.2   *IKZF3* mutations are recurrent and predominantly early/truncal events

We first wanted to identify *IKZF3* mutations in FL patient samples and infer clonality using available data. We re-analyzed two previously published cohorts (GLSG 2000 and BCCA, section 2.1.9) (13). *IKZF3* was mutated in 17/305 patients' diagnostic or relapsed biopsies (6%) (13), (**Fig. 26A**). *IKZF3* mutations cluster into two hotspots, the previously described L162R and a novel hotspot at S215R. Sanger sequencing confirmed that the two hotspot mutations are all heterozygous (**Fig. 26B**).

To assess clonality, we corrected VAF using available copy number data. Of the 146 cases available from the GLSG trial, 14/146 had *IKZF3* mutations, which were in many cases early/truncal due to their high corrected VAF/clonality (11/14, 79%) (**Fig. 26C**).
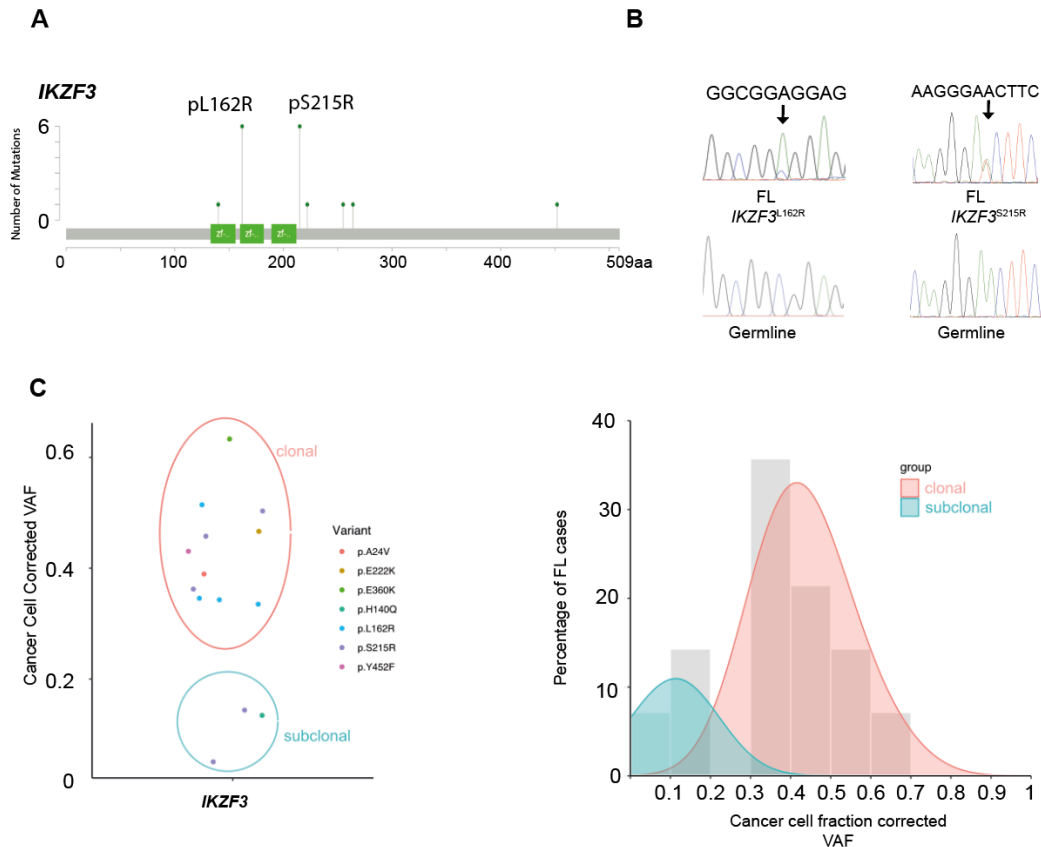
Figure 26- IKZF3 is recurrently mutated in follicular lymphoma.

A) Lolly plot of *IKZF3* mutations from GLSG2000 and BCCA FL cohorts N=305 (13). **B)** Sanger sequencing validation of two hotspot *IKZF3* mutations. **C)** Clonality analysis of *STAT6* mutations from the GLSG2000 cohort (N=146), cancer cell fraction corrected, analysis showing variant allele frequency and percentage of FL cases (13, 40). **Abbreviations**- IKZF3, IKAROS family zinc finger 3; GLSG2000, German low-grade lymphoma study group 2000; VAF, variant allele frequency; BCCA, British Columbia Cancer Agency-Vancouver Cancer Centre.

3.2.2.3 *IKZF3* mutants have distinct phenotypes when expressed in HSPCs vs. early B cells.

To investigate if *IKZF3* mutations are early acquired events, we performed CFU experiments, as previously described, but in addition, we also utilized Cre lineage-restricted mouse strains. This allowed us to express *IKZF3* mutations in early progenitor cells/HSPCs vs. early B cells.

We identified two *IKZF3* mutations recurrently mutated in FL (L162R and S215R). Focusing on these recurrent mutations, we first performed pre-B CFU assays in HSPCs derived from Emu-BCL2 mice. We retrovirally expressed *IKZF3*^WT, *IKZF3*^L162R, *IKZF3*^S215R, or EV control and plated the cells onto methylcellulose (MethoCult, M3630), which supports the differentiation of HSCs into mouse pre-B

CFUs. *IKZF3*[S215R] gave a serial replating phenotype, indicating that the mutation has a gain-of-function phenotype when expressed in HSPCs. In contrast, the other hotspot mutation *IKZF3*[L162R] and the IKZF3[WT] or EV control failed to form pre-B CFUs beyond passage 3 (day- 21) (**Fig. 27**).
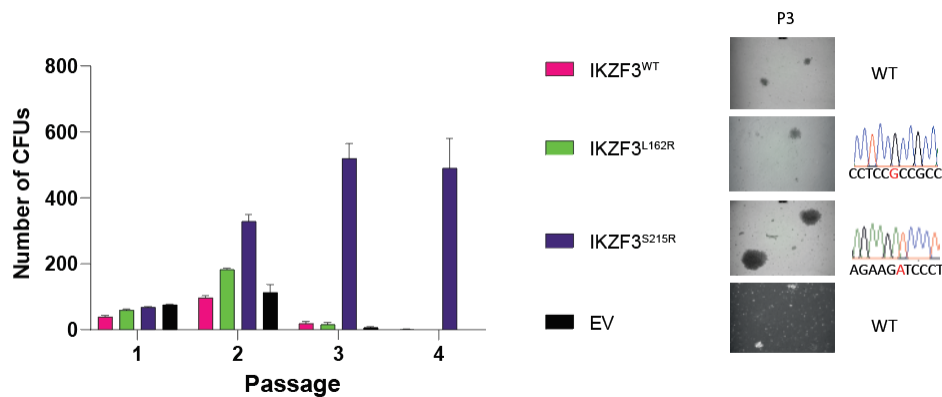
Figure 27- IKZF3[S215R] **mutations are gain-of-function.**

HSPCs from Emu-BCL2 mouse cells were transduced with *IKZF3*[WT], *IKZF3*[MUT], or an EV control and then serially replated on cytokine-supplemented methylcellulose (MethoCult, M3630). Mouse pre-B CFUs were counted weekly. Sanger sequencing of CFUs confirmed integration of the viral construct at passage 3 (Biological N=3, technical N=3, mean + SD). **Abbreviations**- CFUs, colony forming units; IKZF3, IKAROS family zinc finger 3 SD, Emu, Immunoglobulin heavy chain enhancer; BCL2, B cell leukemia/lymphoma; 2 SD, standard deviation; P3, passage 3; EV, empty vector; WT, wild type.

We next wanted to model if there is a difference when *IKZF3* mutations or controls (*IKZF3*[WT] or EV) are expressed in progenitor cells (HSPCs) vs. B lineage-committed cells (early B cells). We utilized two other generated mouse models, Emu-BCL2-Vav-Cre and Emu-BCL2-Mb1-Cre (all heterozygous) (**Fig. 28, left**). The Cre recombinase transgene is expressed under the control of the murine *Vav1* gene regulatory elements and can be utilized to activate gene expression in HSPCs (85). In contrast, *Cd79A* (Mb1) is first expressed in early B cells (86).

We utilized an available Cre-dependent expression construct (**Fig. 28, right**) (kind gift from Marc Schmidt-Supprian). In this construct, a stop codon is placed between loxP sites (locus of X-over P1), with *IKZF3*[WT] or *IKZF3*[MUT] cloned downstream of this codon. The stop codon is removed upon Cre recombinase activity, leading to *IKZF3* expression. As a control, we replaced the ccdB gene (replaced with *IKZF3*[WT] or *IKZF3*[MUT] in the other conditions) with a non-coding GFP cassette (section- 2.2.4.2).
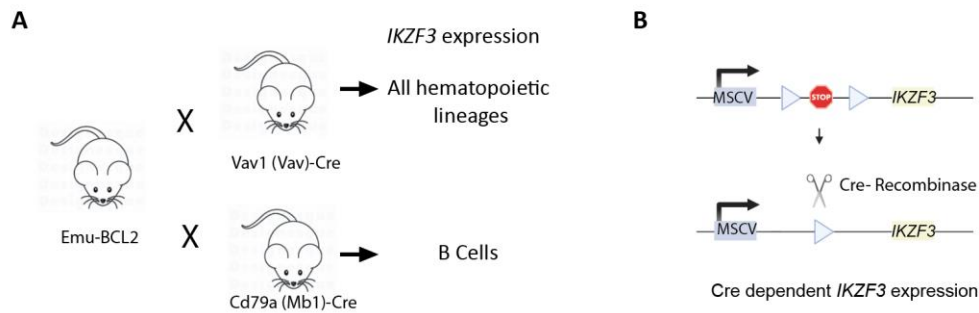
Figure 28- Lineage restricted *IKZF3* expression.

A) Emu-BCL2 mice were crossed with Vav-Cre or Mb1-Cre mice. Heterozygous mice for both alleles were confirmed via PCR. **B)** Cre-dependent *IKZF3* expression construct driven by an MSCV promoter and containing a stop codon between the loxP site (indicated via arrows). *IKZF3*^{WT}, *IKZF3*^{L162R}, *IKZF3*^{S215R}, or GFP control, was cloned downstream of the stop codon. **Abbreviations-** Cre, Cre recombinase*; IKZF3*, IKAROS family zinc finger 3; Emu, Immunoglobulin heavy chain enhancer; BCL2, B cell leukemia/lymphoma 2; loxP, locus of X-over P1; MSCV, Murine stem cell virus.

Analogous to **Fig. 27,** we observed a serial replating capacity of *IKZF3*^{S215R} when expressed in HSPCs under the *Vav1* promoter (Emu-BCL2-Vav-Cre) (**Fig. 29A**). This confirmed our previous findings. In contrast, when we expressed *IKZF3*^{WT} *or IKZF3*^{MUT} in early B cells (Mb1-Cre Emu-BCL2), we saw a serial replating capacity of *IKZF3*^{L162R} mutation (**Fig. 29B**).
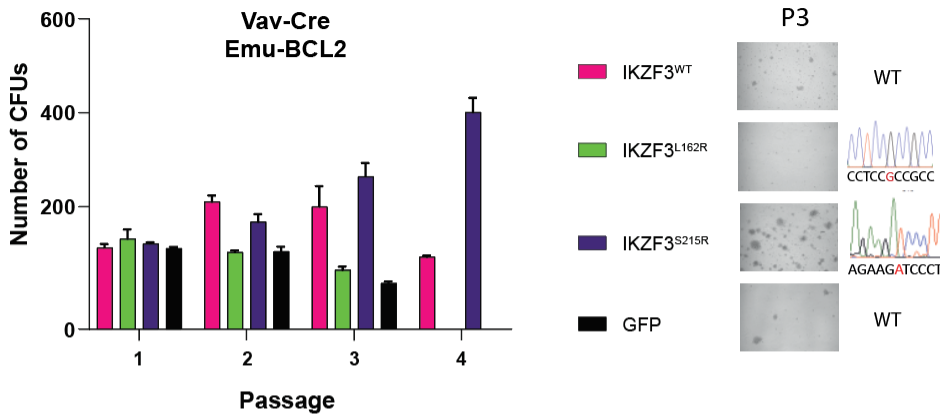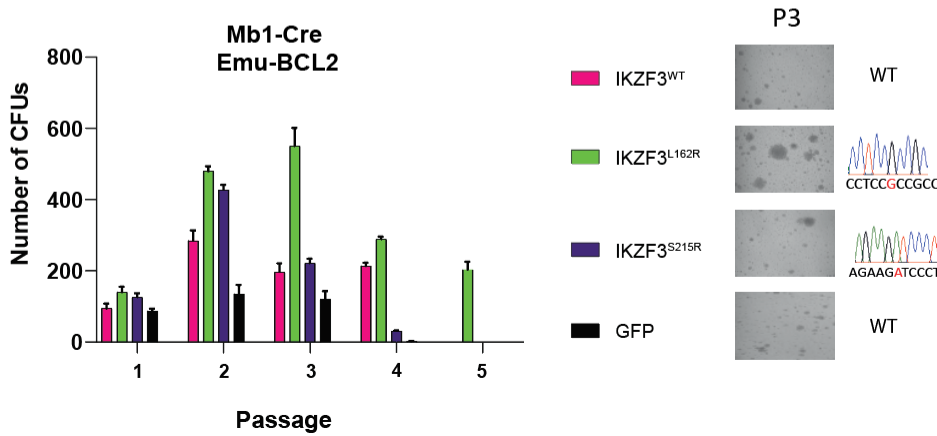
Figure 29- Lineage restricted IKZF3 expression.

A) HSPCs from Emu-BCL2-Vav-Cre mouse cells were transduced with *IKZF3*^WT^, *IKZF3*^MUT^, or a GFP control and then serially replated on cytokine-supplemented methylcellulose. Mouse pre-B CFUs were counted weekly. Sanger sequencing of CFUs confirmed integration of the viral construct at passage 3 (Emu-BCL2-Vav-cre Biological N=3, Technical N=3, mean+ SD). **B)** An identical experiment as described in (A), but using the mouse strain Emu-BCL2-Mb1-Cre (Biological N=4, Technical N=3, mean+ SD). **Abbreviations**- CFUs, colony forming units; Cre, Cre recombinase; IKZF3, IKAROS family zinc finger 3; SD, Emu, Immunoglobulin heavy chain enhancer; BCL2, B cell leukemia/lymphoma 2; SD, standard deviation; EV, empty vector; WT, wild type; P3, passage 3.

These results indicate that specific *IKZF3* mutations have distinct phenotypes when expressed at different stages of B cell development. This is an interesting finding per se; however, we did not identify any *IKZF3* mutations in HSPCs of FL patients (section- 3.1). Therefore, we decided to primarily focus on the *IKZF3*^L162R^ mutation, which had a serial replating phenotype when expressed in early B cells.

3.2.2.4 *IKZF3* expression correlates with copy number

To functionally investigate *IKZF3* in B cells, we identified a panel of lymphoma cell lines that were either *IKZF3*^WT cell lines (Karpas 422, DB, OCI-Ly1, OCI-Ly8, SU-DHL-4, WSU, SU-DHL-5, Jeko) or *IKZF3*^MUT (SU-DHL-16 (*IKZF3*^S215R), Rec1 (*IKZF3*^L162R)). We confirmed IKZF3 protein and RNA expression in each lymphoma cell line (**Fig. 30A, B**). We next correlated the average *IKZF3* expression with the calculated copy number, identifying a positive linear correlation (R^2=0.58, p=0.0187). Cell lines with a copy number >2 had the highest expression. Thus, these results indicate that copy number gain correlates with increased *IKZF3* expression (**Fig. 30C**).
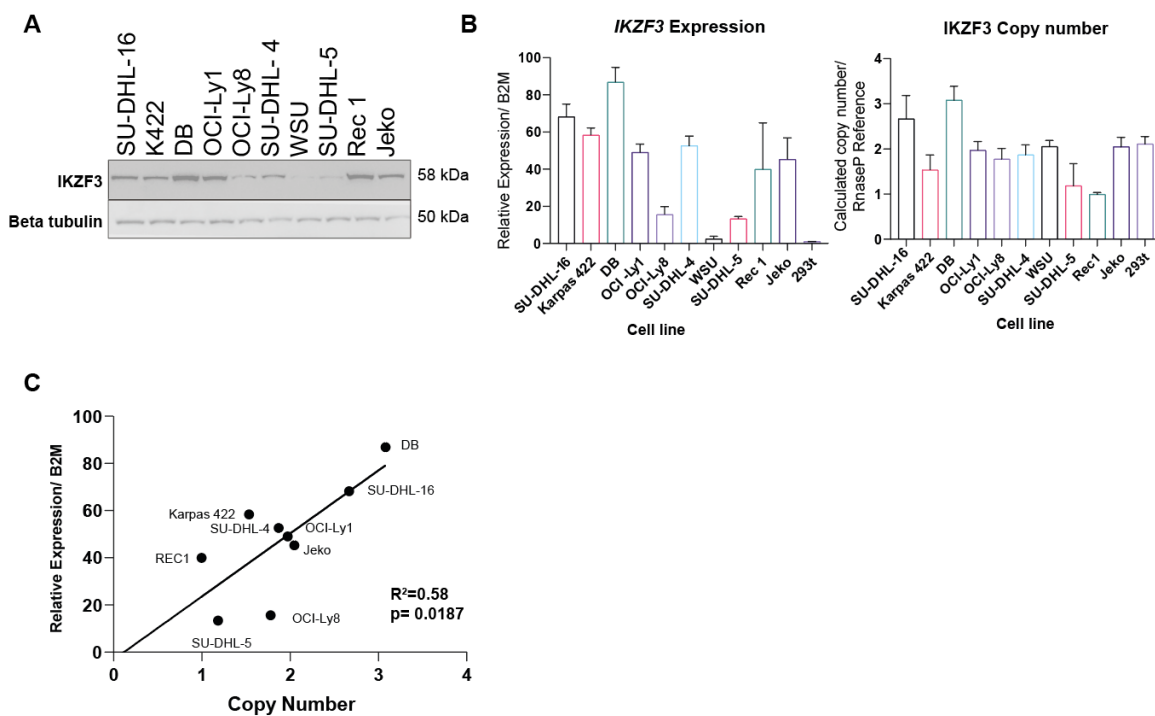
Figure 30- *IKZF3* expression correlates with copy number.

A) Western blot analysis of lymphoma cell lines *IKZF3* expression. **B) Left-** *IKZF3* expression qPCR normalized to *B2M* (N=3 mean +SD). **B) Right-** Calculated copy number relative to RNaseP gene reference. (N=4 mean+ SD). **C)** Correlation between *IKZF3* expression and IKZF3 copy number in lymphoma cell lines (R^2=0.58, p=0.0187). **Abbreviations-** IKZF3, IKAROS family zinc finger 3; B2M, Beta 2 microglobulin; qPCR, quantitative polymerase chain reaction.

3.2.2.5 Knockdown of IKZF3 leads to a selective growth disadvantage in lymphoma cells

To assess if *IKZF3* is an essential gene for lymphoma cell growth, we screened cell lines transducing a previously published RFP-tagged lentiviral shRNA construct targeting IKZF3 (115). We validated IKZF3 knockdown (k/d) in HEK 293T cells (**Fig. 31A**) and selected RFP-sorted lymphoma cell lines (**Fig. 31B**).

Short hairpin RNA (shRNA) 2 was notably more effective than shRNA 3 (**Fig. 31A, B**). Having validated our shRNA constructs, we next wanted to determine if lymphoma cells are dependent on IKZF3 protein expression for growth. We carried out a longitudinal analysis of each RFP tagged shRNA targeting IKZF3 and a scrambled shRNA control that we used to normalize our results (**Fig. 31C**). Knockdown of IKZF3 significantly slowed cellular growth with a decrease in normalized RFP overtime. shRNA 3 showed reduced ability to k/d IKZF3, which also translated into a reduced selective disadvantage compared to shRNA 2. Cell lines with an *IKZF3* mutation or amplification were not more sensitive to IKZF3 k/d. Thus, these results indicate that reduction of IKZF3 protein levels reduces proliferation, irrespective of IKZF3 mutation and copy number status, leading to a selective growth disadvantage in a mixed culture.
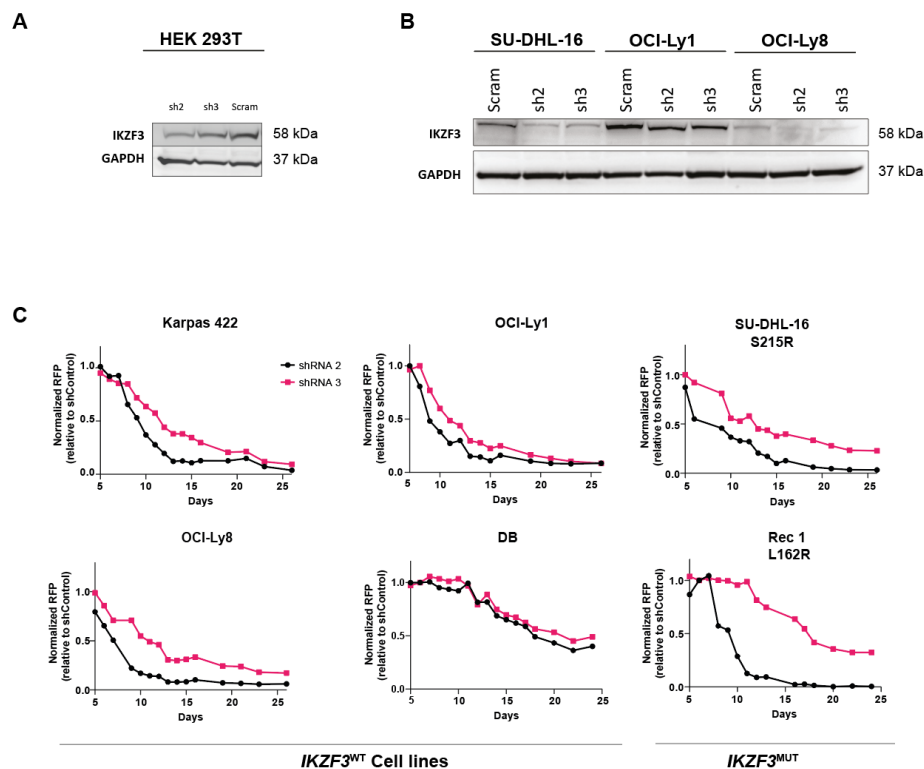
Figure 31- IKZF3 k/d by shRNA leads to a selective growth disadvantage in lymphoma cells.
A) HEK 293T cells exogenously expressing *IKZF3*^WT were lentivirally transduced with two shRNAs (2+3) targeting IKZF3 or a scrambled shRNA control. **B)** SU-DHL-16, OCI-LY1, or OCI-Ly8 were transduced with shRNA constructs described in (A). **C)** shRNA knockdown of IKZF3 measured by flow cytometry for RFP (shRNA IKZF3 RFP) over 25 days. Data is normalized to shControl and shown is 1 representative experiment of 3 biological replicates. **Abbreviations**- shRNA, short hairpin RNA; shControl, shRNA targeting no known human gene; k/d: knockdown IKZF3, IKAROS family zinc finger 3; HEK293T, human embryonic kidney cells.

To further analyze the effect of IKZF3 disruption on cellular growth, we used CRISPR-Cas9 to knock-out endogenous IKZF3. We electroporated Karpas 422 cells with the aim to disrupt a single allele.

Following electroporation, we single-cell sorted GFP+ cells expressing the guide RNA targeting IKZF3 and Cas9. Of the 98 clones we screened by Sanger sequencing, we confirmed reduced protein expression via Western blotting in 4 clones (**Fig. 32A**). No clone showed a complete loss of IKZF3 protein expression, suggesting (similar to **Fig. 31C**) that complete or nearly complete loss of IKZF3 is not tolerated in lymphoma cells. Each clone was hemizygous for IKZF3, with disruption at one allele. One clone (hemizygous clone 3) showed a loss of IKZF3 protein expression **(Fig. 32A, upper panel**); however, when reanalyzed with an additional IKZF3 antibody, the clone was confirmed to have significantly reduced but not absent protein levels (**Fig. 32A, lower panel**).

Our previous data indicated that IKZF3 disruption affects cellular growth leading to a selective growth disadvantage. We therefore, performed a growth curve with our hemizygous K422 clones. Each hemizygous clone grew slower compared to native single-cell-derived clones (NSCC) (**Fig. 32C**), with the level of IKZF3 protein expression correlating with growth rate (**Fig. 32A, B, and C).** We repressed IKZF3^WT-IRES-GFP in hemizygous clone 3 and were able to rescue the reduced growth rate phenotype **(Fig. 32D**).
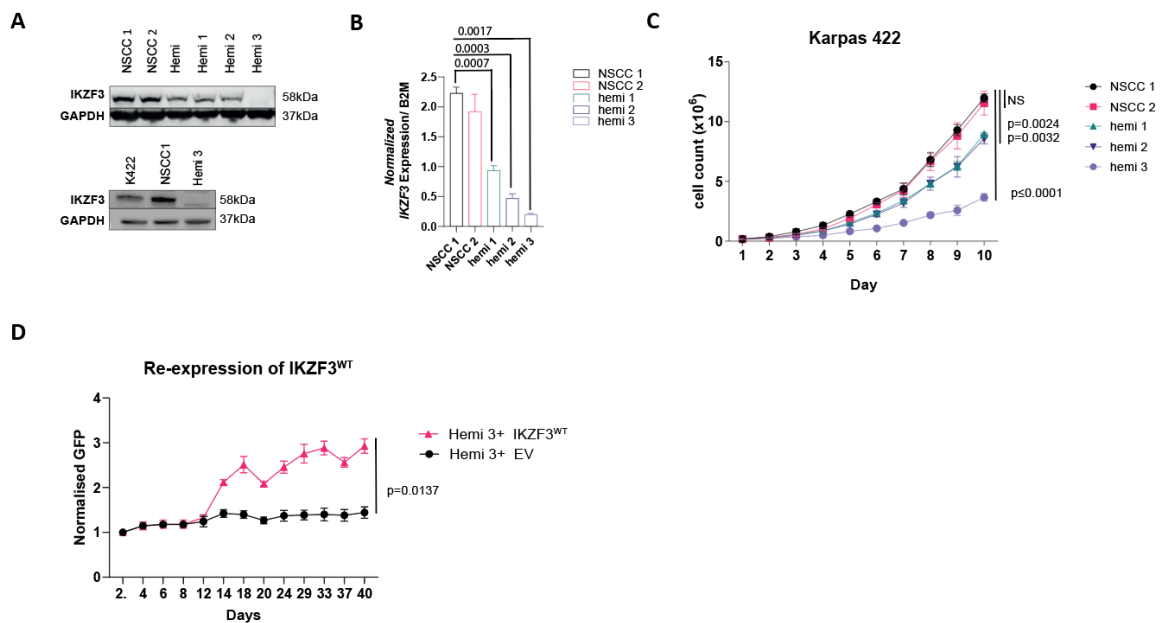
Figure 32- IKZF3 disruption via CRISPR-Cas9 affects cellular growth.

A) Western blotting of CRISPR-Cas9 IKZF3 targeted Karpas 422 clones compared to native single-cell clones with no disruption at the IKZF3 gene locus. **B)** Expression of *IKZF3* in different CRISPR-Cas9 K422 clones normalized to B2M (N=3 mean+ SD). **C)** CRISPR-Cas9 Karpas 422 growth curve (N=3 ±SD). **D)** Re-expression of *IKZF3*^WT or EV control in K422 IKZF3 hemizygous clone 3, and measured for GFP over time via flow cytometry. Normalized to day 2 (N=3 ±SD). **Abbreviations**-IKZF3, IKAROS family zinc finger 3; Hemi, Hemizygous; NSCC, native single cell-derived clone; SD, standard deviation; B2M, Beta 2 microglobulin**;** CRISPR, Clustered regularly interspaced short palindromic repeats; qPCR, quantitative polymerase chain reaction.

We next performed RNA seq analysis comparing hemizygous *IKZF3* clone 3 to an NSCC-derived control (*IKZF3*^{WT}). Principle component analysis (PCCA) showed distinct clustering between conditions (**Fig. 33A**). Gene ontology and Reactome pathway analysis comparing *IKZF3* hemizygous clone 3 with NSCC identified a number of significantly enriched terms, including cell cycle (**Fig. 33B**). This data therefore, supports our previous findings, that disruption of IKZF3 provides a selective growth disadvantage, possibly by disrupting the cell cycle. It is also in line with other studies that have identified the IKZF3/1 complex as a regulator of the cell cycle, colocalizing with DNA replication machinery in cycling cells (50, 116). This phenotype, however, remains to be fully explored functionally, and in this thesis, we wanted to focus more specifically on the impact of *IKZF3* mutations.

A
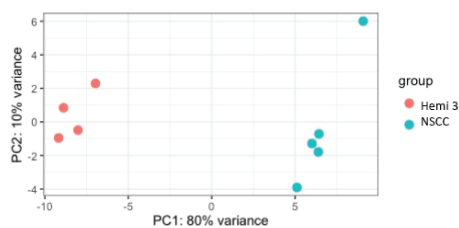
B
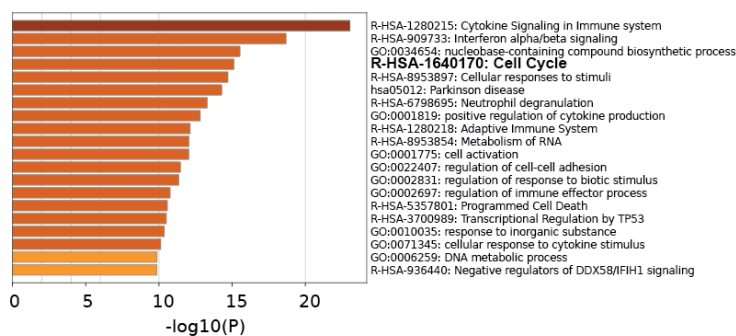
Figure 33- RNA-seq- differential pathway analysis upon IKZF3 disruption.

A) RNA seq analysis was performed on an IKZF3 hemizygous clone vs. an NSCC clone in Karpas 422 cells. Principle component analysis is displayed. **B)** Gene ontology (GO) and Reactome enrichment analysis were performed using the Metascape platform (log$_2$ FC ±0.5, FDR <0.05) (93). **Abbreviations-** IKZF3, IKAROS family zinc finger 3; Hemi, hemizygous; NSCC, native single cell-derived clone; p, p-value.

3.2.2.6   Modeling *IKZF3* mutations in lymphoma cell lines

To functionally investigate IKZF3 mutations, we used SU-DHL-16, which has a heterozygous *IKZF3*^{S215R} mutation. We wanted to correct the mutation using CRISPR-Cas9 mediated homology-directed repair (HDR) to characterize the effect of the mutation functionally. CRISPR-Cas9 introduces double-stranded breaks, which are repaired predominantly by two pathways, non-homologous end joining (NHEJ) or HDR (117, 118). Cells undergo HDR at a much lower frequency than NHEJ (117).

Similar to the previous approach, we electroporated cells with the GFP tagged construct expressing a gRNA targeting *IKZF3* and Cas9, in addition to a double-stranded HDR 200bp *IKZF3*^{WT} template. Of the 126 clones we screened, we identified 6/126 with an insertion or deletion (indel), indicating that they had all undergone NHEJ. We did not identify any clone that had undergone successful HDR. Sanger sequencing analysis using the CRISP-ID tool (section 2.1.10) further revealed in the 6 clones with indels loss of the *IKZF3*^{WT} sequence, with all clones hemizygous for the mutation (*IKZF3*^{S215R}). We again analyzed protein and mRNA expression levels (**Fig. 34A, B**), showing a reduced level. Growth kinetics indicated that the *IKZF3*^{S215R} hemizygous clones grow slower than *IKZF3*^{S215R} heterozygous clones (**Fig. 34C**).

In summary, these results indicate that a certain level of *IKZF3*^{WT} expression is required for normal cellular growth, with lower IKZF3 protein levels resulting in slower growth. However, these results do not explain *IKZF3* mutation's selective advantage in FL.
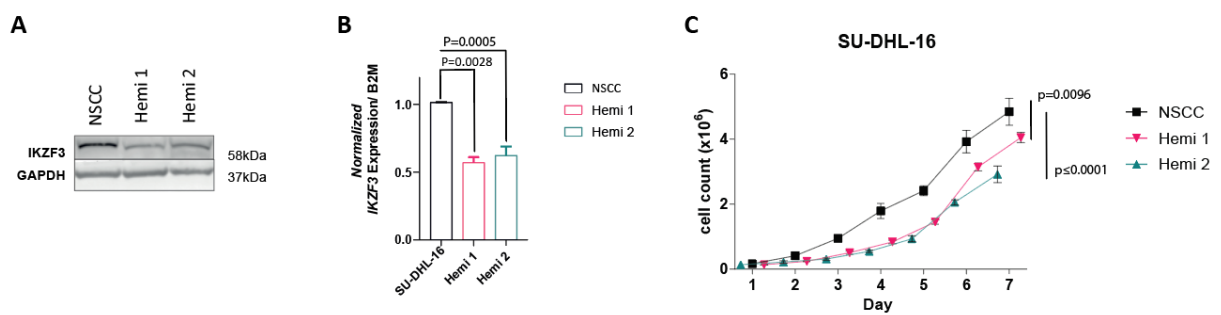
Figure 34- IKZF3 disruption affects growth in SU-DHL-16 lymphoma cells.

A) Western blotting for three single cell-derived SUDHL-16 clones. **B)** qPCR of IKZF3 expression normalized to B2M. (N=3 ±SD). **C)** Growth curve showing total cell count over 7 days comparing NSCC vs. *IKZF3*^{S215R} hemizygous SU-DHL-16 clones (N=6 ±SD). **Abbreviations-** IKZF3, IKAROS family zinc finger 3; Hemi, Hemizygous; NSCC, native single cell-derived clone; B2M, Beta-2 microglobulin; P, p-value; qPCR, quantitative polymerase chain reaction.

3.2.2.7 *IKZF3*[L162R] is gain-of-function when expressed in FL-like B cells

To better model *IKZF3* mutation's selective advantage in FL, we used a human GC B cell co-culture model (section- 2.2.3.2), as previously described (84). As before, we first immortalized GC B cells, retrovirally expressing *BCL2*/*BCL6* and then expressed *IKZF3*[WT] or *IKZF3*[MUT]. Western blotting analysis using an IKZF3 antibody revealed high levels of the endogenous IKZF3 protein (**Fig. 35A, lower IKZF3 band**) and lower levels of retrovirally transduced 3xFlag IKZF3[WT] or IKZF3[MUT] (**Fig. 35A, upper IKZF3 band**). We confirmed the GC phenotype of our FL B cells by FC analysis (**Fig. 35B**).
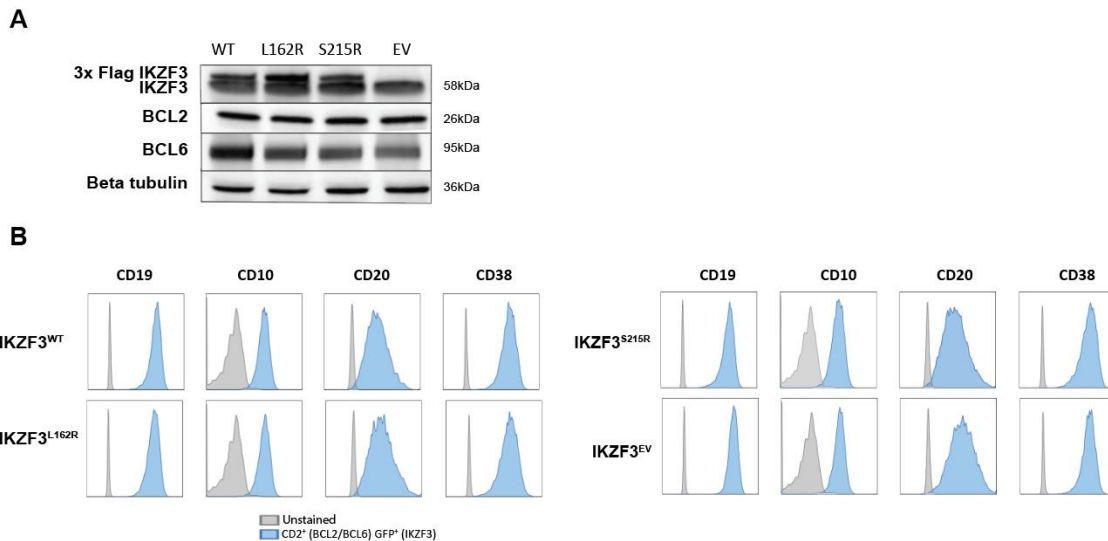
Figure 35- IKZF3[L162R] **has a gain-of-function phenotype in FL-like B cells.**

A) Western blot analysis of human tonsil-derived GC B cells transduced with *BCL2* and *BCL6* in addition to *IKZF3*[WT], *IKZF3*[L162R], *IKZF3*[S215R], or EV as a control. FL-like cells were co-cultured on FDC feeder cells (YK6-CD40lg-IL-21) **B)** FC of GC markers for IKZF3[WT], IKZF3[L162R], IKZF3[S215R], or EV, FL-like cells. **Abbreviations-** FL, follicular lymphoma; GC, germinal center B cells; FDC, follicular dendritic cell; IKZF3, IKAROS family zinc finger 3; BCL2, B cell leukemia/lymphoma 2; BCL6, B cell lymphoma 6; EV, empty vector; WT, wild type; kDa, kilodaltons**.**

We next performed outgrowth experiments, transducing FL-like B cells (BCL2/BCL6^{+}) with *IKZF3*[WT], *IKZF3*[L162R], *IKZF3*[S215R], or an EV control (all IRES-GFP). We measured BCL2/BCL6 (CD2^{+}) and GFP^{+} positive (IKZF3[WT], IKZF3[MUT], or EV) cells over time. In three biological replicates from three different donors, we observed outgrowth of IKZF3[L162R] cells, indicating a gain-of-function phenotype (**Fig. 36A**). This was consistent with our CFU data, where we showed that expression of IKZF3[L162R] in early B cells confers a serial replating phenotype (section 3.2.2.3). IKZF3[WT] and IKZF3[EV] conditions showed similar levels of GFP expression, while we observed a selective disadvantage of IKZF3[S215R] cells in 2/3 replicates, with cells outcompeted over time (**Fig. 36B**).
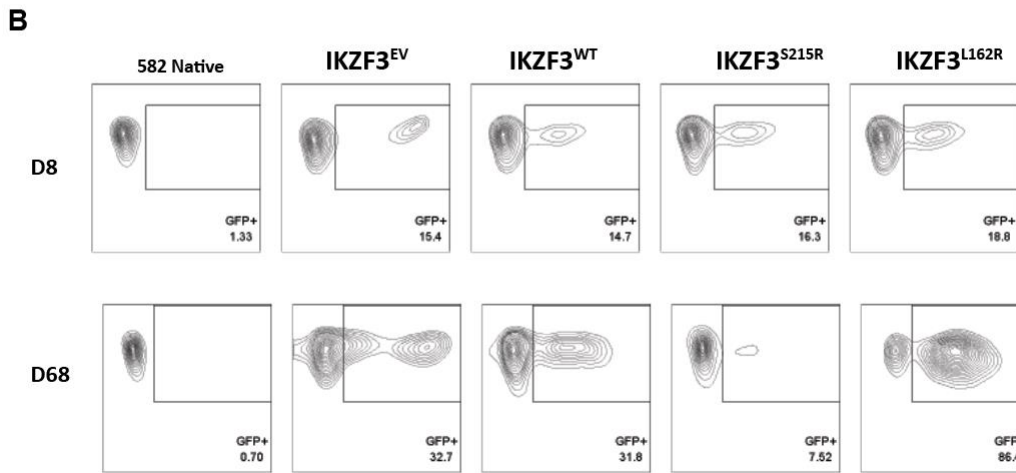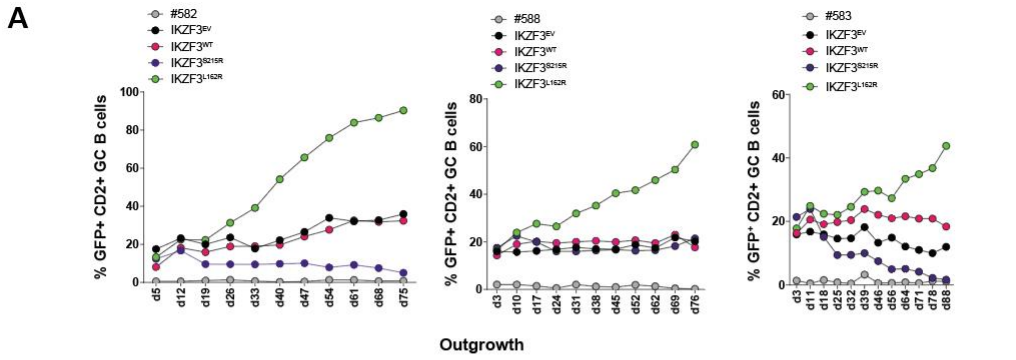
Figure 36- IKZF3^{L162R} confers a gain-of-function phenotype to FL-like B cells.

A) *IKZF3*^{WT} or *IKZF3*^{MUT} expressing germinal center B cells flow cytometry analysis for IKZF3^{WT}, IKZF3^{MUT} or EV (GFP$^+$) and BCL2/BCL6 (CD2$^+$) over time. Independent biological replicates are shown from three independent donors (N=3). **B)** Contour plot showing BCL2/BCL6 GFP$^+$ IKZF3^{WT}, IKZF3^{MUT}, or an EV control at two different time points. **Abbreviations-** FL, follicular lymphoma; GC, germinal center B cells; IKZF3, IKAROS family zinc finger 3; BCL2, B cell leukemia/lymphoma 2; BCL6, B cell lymphoma 6; EV, empty vector; WT, wild type; d, day.

Finally, we performed a competitive outgrowth experiment transducing *IKZF3*^{WT}, *IKZF3*^{L162R}, *IKZF3*^{S215R}, or an EV control (IRES-GFP) with *IKZF3*^{WT} IRES- td-tomatoe. We again observed an outgrowth of IKZF3^{L162R}, confirming our gain-of-function phenotype and our previous data (**Fig. 37**).
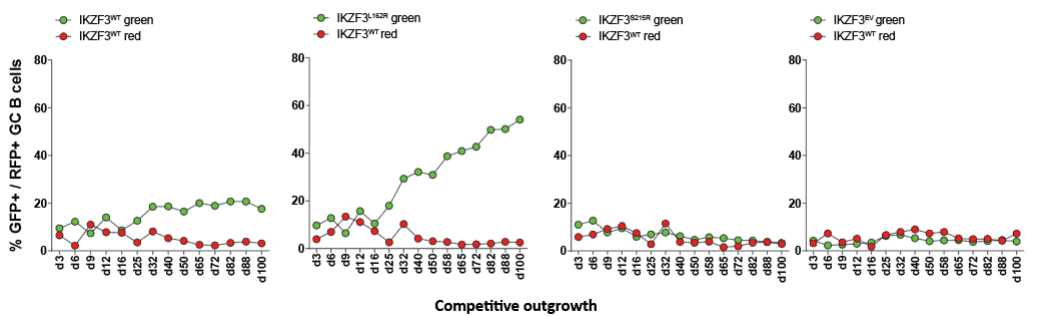
Figure 37- IKZF3^{L162R} FL-like B cells outcompete IKZF3^{WT} B cells.

FL-like B cells (BCL2/BCL6 transduced) were transduced with *IKZF3*^{WT}, *IKZF3*^{L162R}, *IKZF3*^{S215R}, or an EV control (IRES-GFP), in addition to *IKZF3*^{WT}-IRES-tdtomatoe. GFP and RFP were monitored over time. 1 representative experiment of 3 biological replicates. **Abbreviations-** FL, follicular lymphoma; GC, germinal center B cells; IKZF3, IKAROS family zinc finger 3; BCL2, B cell leukemia/lymphoma 2; BCL6, B cell lymphoma 6; EV, empty vector; WT, wild type; d, day; RFP, red fluorescent protein; GFP, green fluorescent protein. tdtomatoe is a bright version of RFP.

3.2.2.8   *IKZF3*^{L162R} regulates B cell activation and proliferation

We wanted next to better functionally analyze IKZF3^{L162R} FL-like B cells. We, therefore, sorted cells at the point of outgrowth (d40-d50). We then performed growth curves, confirming an increased proliferative rate of IKZF3^{L162R} FL-like B cells in 3 biological replicates (**Fig. 38**).
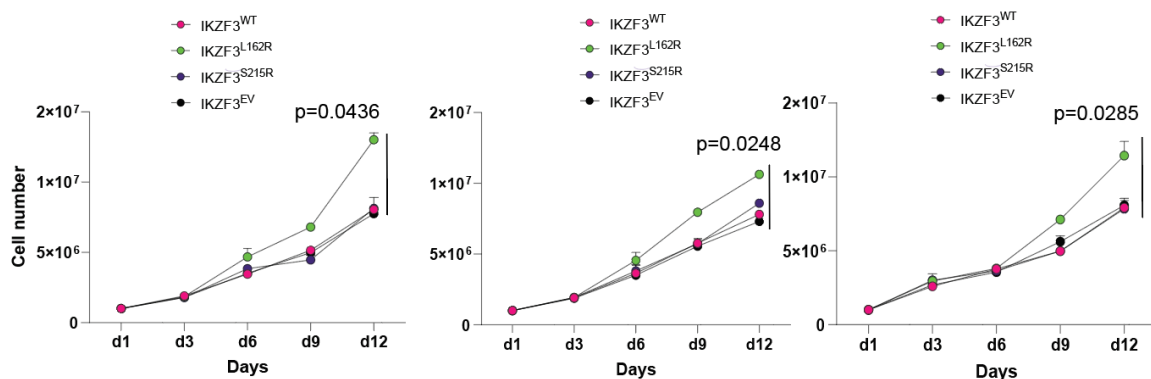
Figure 38- IKZF3^{L162R} FL-like B cells have an increased proliferative rate.

FL-like B Cells expressing IKZF3^{WT}, IKZF3^{L162R}, IKZF3^{S215R}, or EV were sorted by fluorescent activated cell sorting for GFP⁺, and a growth curve was carried out by trypan blue exclusion (technical duplicates are shown ±SEM). **Abbreviations-** FL, follicular lymphoma; IKZF3, IKAROS family zinc finger 3, EV, empty vector; WT, wild type; d, day.

We next performed RNA seq analysis. PCA analysis showed *IKZF3*^{L162R} clustered tightly and distinctly from *IKZF3*^{WT}, *IKZF3*^{S215R}, and EV **(Fig. 39A)**. This indicated a district gene expression profile.

We determined differentially expressed genes (section 2.2.5.4) and then performed network analysis comparing *IKZF3*^{L162R} and *IKZF3*^{WT}, as previously described (93). We identified several uniquely differentially enriched pathways in *IKZF3*^{L162R}, including a number of nodes related to proliferation and B cell activation (**Fig. 39B**). Gene ontology (GO) enrichment analysis confirmed differentially expressed genes in *IKZF3*^{L162R} relating to B cell proliferation and activation (**Fig. 39C**). This data,

therefore, provides further evidence that *IKZF3*[L162R] gain-of-function phenotype is mediated by activating B cells and inducing proliferation. This is in accordance with previous studies that have shown that IKZF3 is able to regulate B cell activation and proliferation (49, 50).
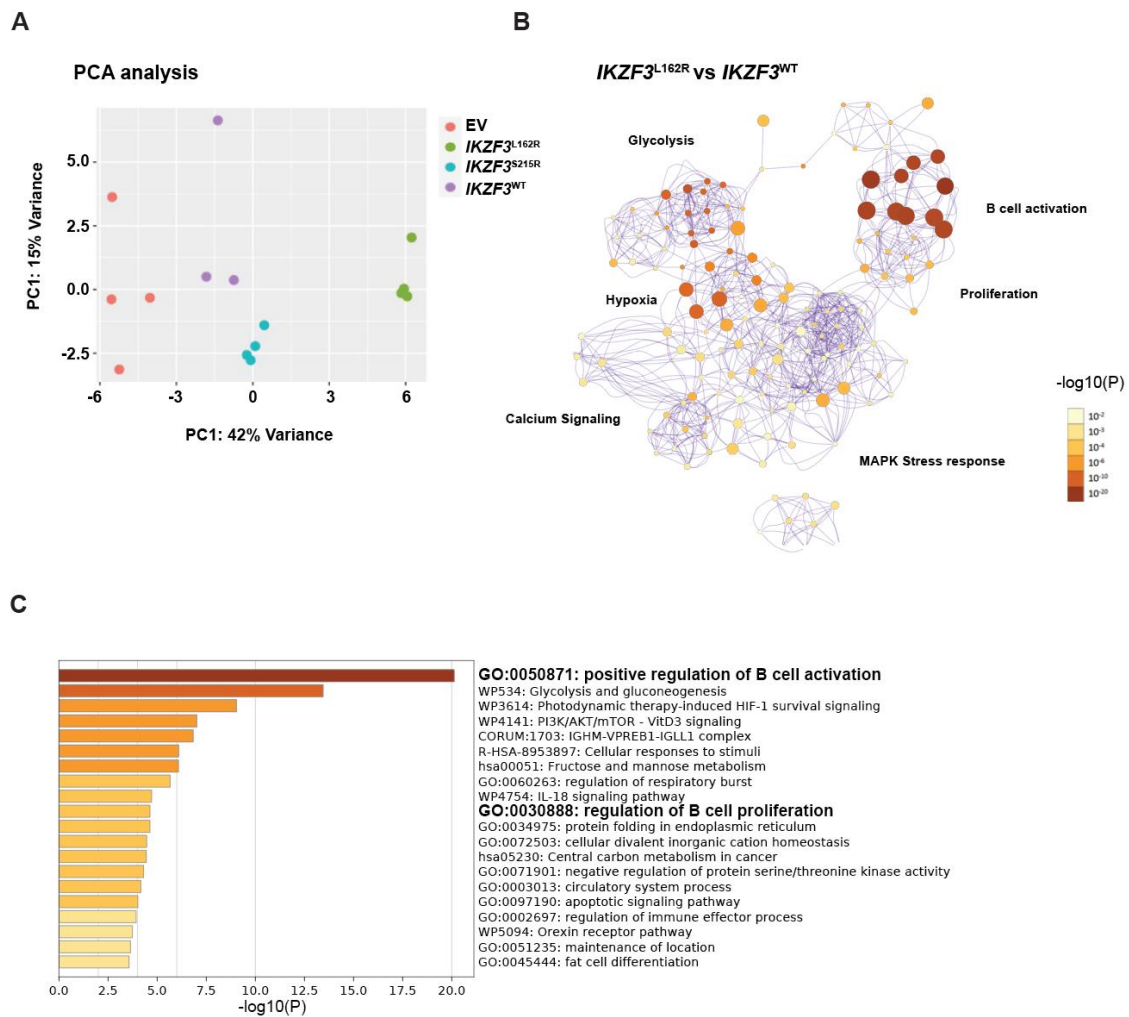
Figure 39- *IKZF3*[L162R] activates FL-like B cells.

A) PCA analysis of RNAseq experiment of FL-like B cells expressing *IKZF3*[WT], *IKZF3*[L162R], *IKZF3*[S215R,] or an EV control. **B**) Network analysis of FL-like B cells comparing *IKZF3*[L162R] vs. *IKZF3*[WT] cells (log$_2$ FC ±0.5, FDR <0.05). Nodes are grouped by -log10(P) values, with highly significant groups of nodes highlighted. **C)** Enrichment analysis comparing *IKZF3*[L162R] vs. *IKZF3*[WT] cells, and performed on the Metascape platform (93), (log$_2$ FC ±0.5, FDR <0.05). **Abbreviations-** FL, follicular lymphoma; FC, fold change; IKZF3, IKAROS family zinc finger 3; EV, empty vector; WT, wild type; GO, gene ontology.

The selective and proliferative advantage of IKZF3[L162R] in FL-like B cells is comparable to the CFU replating phenotype we identified in pre-B cells (section- 3.2.2.3). Therefore, we decided to validate this finding by performing additional RNA seq analysis using pre-B cells from CFUs.

We analyzed sorted CD19$^+$ GFP$^+$ B cells at passage 2 (Emu-BCL2) or CD19$^+$ Thy1.1$^+$ cells from the lineage-specific CFU assay (Emu-BCL2-Mb1-Cre). We first compared Emu-BCL2 derived *IKZF3*^{L162R} CFUs at passage 2 to *IKZF3*^{WT}. We performed this comparison to see if our phenotype in FL-like B cells was similar to pre-B cells. As in FL-like B cells, we identified enrichment in genes relating to B cell activation (**Fig. 40A**).

Similarly, we also sorted CFUs at passage 3 (Emu-BCL2-Mb1-Cre), comparing *IKZF3*^{L162R} CFUs to our GFP control condition from Passage 1. Some studies have suggested that IKZF3^{L162R} can phenocopy increased expression of IKZF3^{WT} (43, 119). We, therefore, wanted to be sure that our analysis of *IKZF3*^{L162R} was not masked by increased *IKZF3*^{WT} expression. In *IKZF3*^{L162R}, we identified enriched genes relating to the adaptive immune response and pre-BCR signaling (**Fig. 40B**). These results were consistent with our previous findings and suggested ongoing B-cell activation.
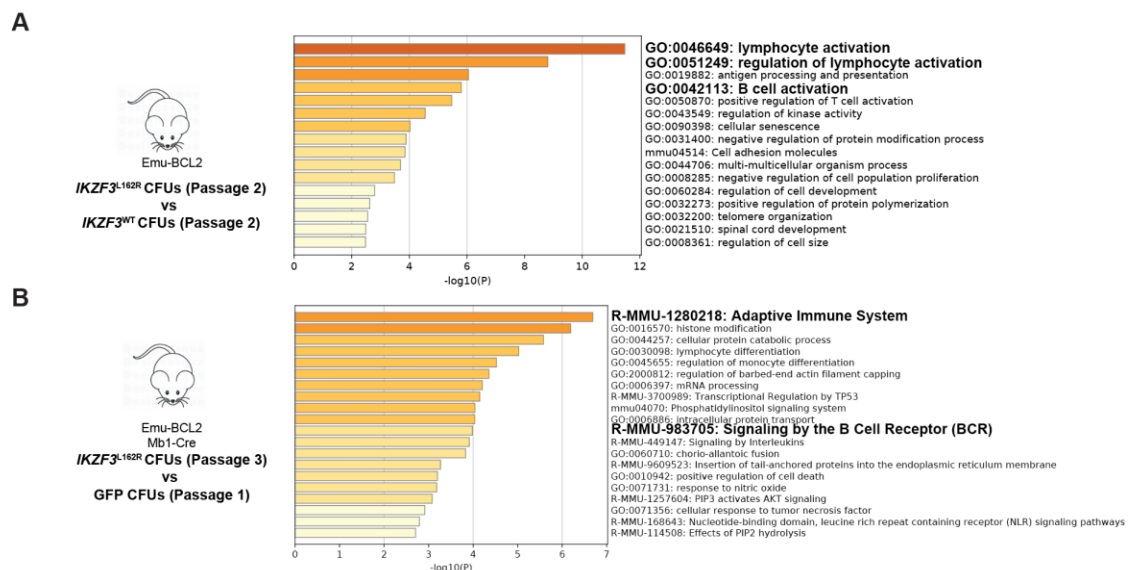
Figure 40- IKZF3^{L162R} activates pre-B cells.

A) RNAseq analysis of pre-B CFUs derived from Emu-BCL2 mice at passage 2 (d14) comparing *IKZF3*^{L162R} vs. *IKZF3*^{WT} and analyzed for gene enrichment using the Metascape platform (N=4, p<0.05, FDR<0.25, log$_2$ FC ±0.5). **B)** RNAseq analysis of pre-B CFUs derived from Emu-BCL2-Mb1-Cre mice at passage 1 *IKZF3*^{EV} (d7) compared to *IKZF3*^{L162R} (Passage 3, d21) and analyzed for gene enrichment using the Metascape platform (93), (N=4, p<0.05, FDR<0.25, log$_2$ FC ±0.5). **Abbreviations-** Cre, Cre recombinase; IKZF3, IKAROS family zinc finger 3, EV, empty vector; WT, wild type; Emu, Immunoglobulin heavy chain enhancer; BCL2, B cell leukemia/lymphoma 2; d, day.

Pre-B cell activation and proliferation is primarily mediated by ongoing pre-BCR signaling. Pre-BCR signaling induces downstream expression of *IKZF3,* which leads to proliferation and differentiation (48, 49).

Lymphoid progenitors give rise to B cell progenitors that differentiate into pre/pro B cells or Hardy Fraction A (Fr. A, LIN⁻ IL7Ra⁺, AA4⁺, B220⁺, Kit⁺), pro-B cells or Fr. B (IgM⁻, B220⁺, CD43⁺, CD24⁺), cycling pre-B cells or Fr. C (IgM⁻, B220⁺, CD43⁺, CD24⁺⁺), resting pre-B cells or Fr. D, (B220⁺, CD43⁻, CD24⁺, IgM⁺) before differentiating into immature B cells Fr. E (IgM⁺, CD19⁺, CD43⁻, CD24⁺) (120-122) (**Fig. 41A**). During these differentiation stages, B cell progenitors undergo productive VDJ recombination of the immunoglobulin heavy chain locus, which leads to expression of pre-BCR components λ5 and VpreB1 (*Igll1* and *Vpreb1*) in Fr.B/C progenitors. Pre-BCR signaling induces proliferation in cycling Fr. C pre-B cells, which then subsequently downregulate the pre-BCR, exit the cell cycle, and undergo light chain rearrangements (Fr. D, resting B Cells) (121, 122). Cycling pre-B cells have nearly unlimited replication potential, and without careful regulation of these developmental steps, genetic lesions can accumulate, leading to malignant transformation (48, 116, 122-124).

We hypothesized that the mutation *IKZF3*^L162R may affect this process, leading to pre-B cell precursors that have increased proliferative capacity. To address this question, we phenotyped our CFUs by FC analysis. At passage 1 we did not notice significant differences between genotypes with three different B cell fractions present (Fr. B, (range-21-30%), Fr. C (58-69%), and Fr. D (7-9%)), in transduced cells (Thy 1.1⁺) (**Fig. 41B**). At passage 4 we consistently found *IKZF3*^L162R CFUs with a Fr. C, cycling pre-B cell phenotype (Fr. B, 3%, Fr. C, 97%, Fr. D, 2%). *IKZF3*^WT also accumulated in Fr. C but had fewer CFUs and failed serial replating beyond passage 4. *IKZF3*^S215R and the GFP⁺ control failed serial replating, and therefore we were unable to phenotype these conditions. These results indicate that *IKZF3*^L162R expression in early pre-B cells induces a Fr. C phenotype. This is characterized by serial replating capacity, increased proliferation, and the inability to further differentiate into Fr. D resting pre-B cells.
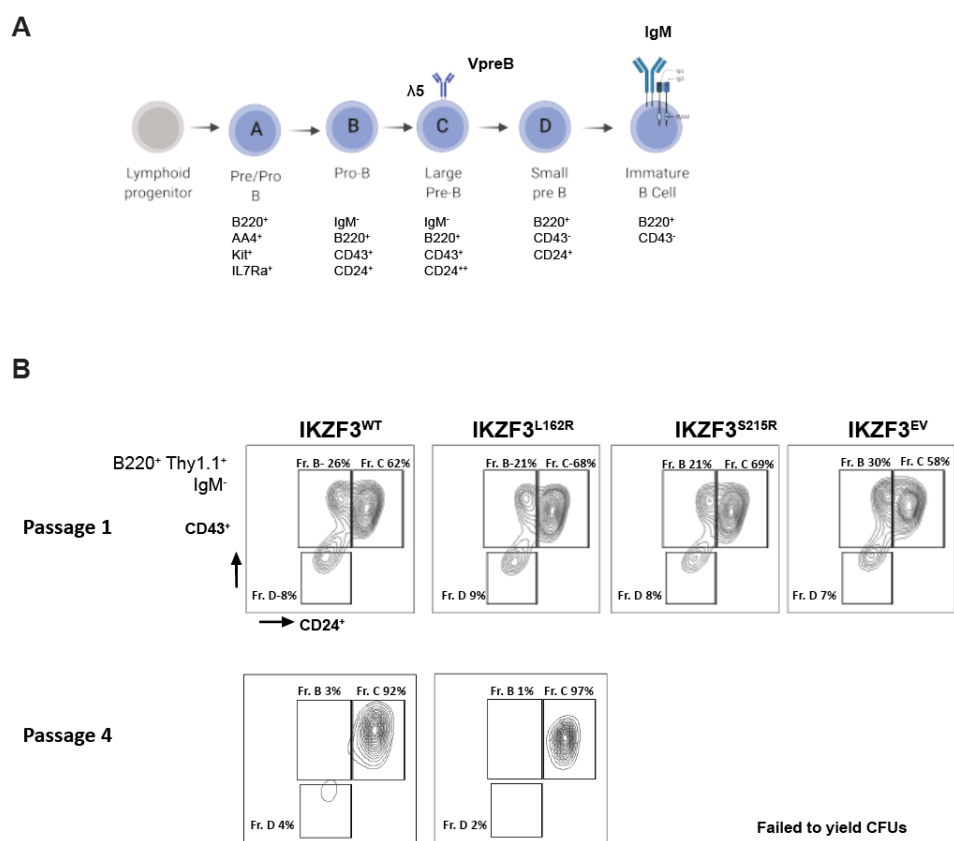
Figure 41- IKZF3^{L162R} induces proliferation in pre-B cells.

A) Overview of mouse pre-B cell differentiation as defined by Hardy's classification (120). **B)** HSPCs from Emu-BCL2-Mb1-Cre mice were transduced with *IKZF3*^{WT}, *IKZF3*^{MUT}, or a GFP control and then serially replated on cytokine-supplemented methylcellulose, that supports differentiation into pre-B cells. Mouse pre-B CFUs were counted weekly. Representative flow cytometry analysis at passage 1 (d7) or Passage 4 (d28) (N=3). At passage 4 only viable cells from CFUs could be analyzed from *IKZF3*^{WT} or *IKZF3*^{L162R}. **Abbreviations-** CFUs, colony forming units; IKZF3, IKAROS family zinc finger 3; SD, Emu, Immunoglobulin heavy chain enhancer; BCL2, B cell leukemia/lymphoma 2; Fr, Hardy fraction; EV, empty vector; WT, wild type. VpreB is encoded by *Vpreb1*, V-Set Pre-B Cell Surrogate Light Chain 1. λ5 is encoded by *Igll1,* immunoglobulin lambda-like polypeptide 1.

To further investigate the underlying mechanism, we used an established Fraction C mouse pre-B cell line (B220$^+$, IgM$^-$, CD43$^+$, CD24^{++}) and retrovirally transduced the cells with *IKZF3*^{WT} or *IKZF3*^{MUT} (125). Western blot analysis of key proteins involved in the pre-B cell signaling cascade revealed increased Syk protein expression in both IKZF3^{WT} and IKZF3^{L162R} expressing pre-B cells (**Fig. 42**). This is consistent with previous studies that have shown that increased expression of *IKZF3*^{WT}, can to some extent phenocopy the gain-of-function mutation, *IKZF3*^{L162R} (43, 126).
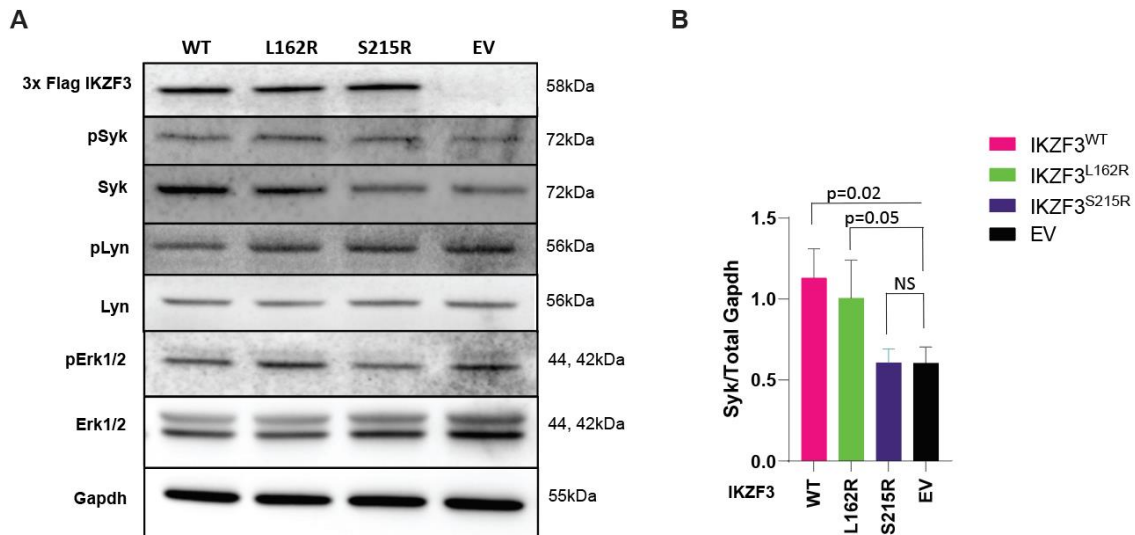
Figure 42- IKZF3^{WT} or IKZF3^{L162R} upregulates Syk in pre-B cells.

A) Western blot analysis from a mouse Hardy fraction C pre-B cell line transduced with *IKZF3*^{WT}, *IKZF3*^{L162R}, *IKZF3*^{S215R}, or an EV control. **B)** Quantification of total Syk levels via densitometry analysis and normalized to Gapdh (N=3, +SD). **Abbreviations**- IKZF3, IKAROS family zinc finger 3; Syk, spleen associated tyrosine kinase; Lyn, Lyn proto-oncogene, Src family tyrosine kinase; Erk1, mitogen-activated protein kinase 3; Erk2, mitogen-activated protein kinase 1; Gapdh, glyceraldehyde-3-phosphate dehydrogenase; EV, empty vector; WT, wild type.

3.2.2.9   IKZF3 regulates SYK expression

We next wanted to verify if IKZF3 alters SYK expression using our established FL-like B cell model. We depleted the feeder cells via magnetic separation and analyzed the expression of BCR signaling components. Again, we saw increased SYK expression in *IKZF3*^{WT} or *IKZF3*^{L162R} expressing cells both at the protein and mRNA level (**Fig. 43A+ B).**

We further checked an additional lymphoma cell line, Karpas 422 (K422). We first stably k/d IKZF3 using a construct that specifically targets the 3' primer untranslated region (UTR) of *IKZF3*. This allows re-expression of IKZF3^{WT}, IKZF3^{MUT}, or an EV control.

Re-expression of 3xFlag tagged IKZF3^{WT} or IKZF3^{MUT} (upper IKZF3 band) allowed us to distinguish the expression of our cDNA construct from the endogenous protein (lower IKZF3 band). We were, therefore, able to successfully verify k/d of endogenous IKZF3, with reduced protein in IKZF3^{WT}, IKZF3^{L162R}, IKZF3^{S215R}, and the EV control, compared to native K422 cells (**Fig. 43C**). Reduced IKZF3 levels also affected SYK protein expression, with a lower level in the k/d + re-expression of EV, compared to native K422 cells.

Re-expression of IKZF3^{WT} or IKZF3^{L162R} (upper IKZF3 band) again resulted in increased SYK protein levels, compared to the other k/d and re-expression conditions (IKZF3^{S215R} and EV), and also native K422 cells. Thus, our results indicate that (i) reduction of IKZF3^{WT} protein levels results in reduced SYK, and (ii) re-expression of IKZF3^{WT} or IKZF3^{L162R} upregulates SYK, thereby rescuing this phenotype.
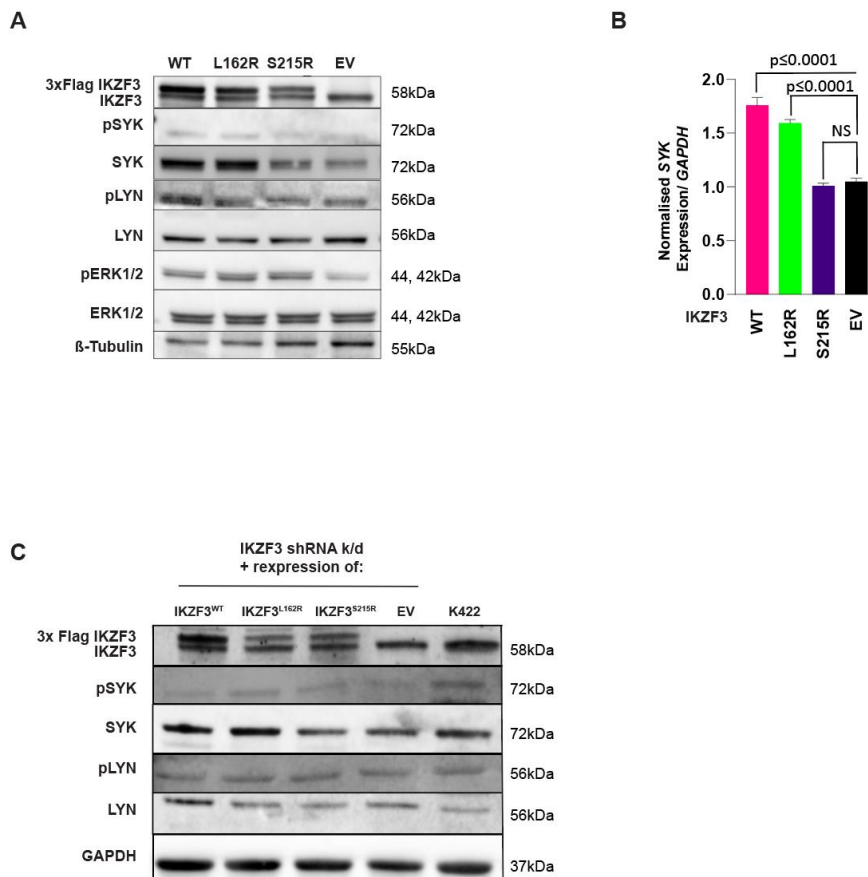
Figure 43- IKZF3 regulates SYK expression.

A) Western blot analysis of FL-like B cells transduced with *IKZF3*^{WT}, *IKZF3*^{L162R}, *IKZF3*^{S215R}, or EV as a control. FL-like cells were co-cultured on FDC feeder cells (YK6-CD40lg-IL-21). The feeder layer was depleted prior by MACS before Western blot analysis **B)** *SYK* expression in FL-like B cells normalized to GAPDH (N=3 mean+ SD). **C)** Karpas 422 cells stably expressing a k/d construct targeting IKZF3's 3' UTR. Cells were then lentivirally transduced with *IKZF3*^{WT}, *IKZF3*^{L162R}, *IKZF3*^{S215R,} or an EV control. Native un-transduced K422 cells were used as a control for IKZF3 k/d efficacy. **Abbreviations**- IKZF3, IKAROS family zinc finger 3; SYK, spleen associated tyrosine kinase; LYN, LYN proto-oncogene kinase; ERK1, mitogen-activated protein kinase 3; ERK2, mitogen-activated protein kinase 1; GAPDH, glyceraldehyde-3-phosphate dehydrogenase; k/d, shRNA mediated IKZF3 knockdown, EV, empty vector; WT, wild type.

3.2.2.10   IKZF3 binds to the SYK promoter

Finally, we wanted to model IKZF3's transcriptional regulation of SYK. We, therefore, performed a luciferase assay with a cloned fragment of the SYK promoter. We used a pGL3 basic vector that lacks a promoter and allows the measurement of *SYK* promoter activity with luciferase (section 2.1.5). As a model system, we used HEK 293T cells which lack endogenous IKZF3 expression.

We co-transfected expression vectors for *IKZF3*^{WT}, *IKZF3*^{MUT}, or an EV control with a cloned fragment of the SYK promoter, in addition to a renilla normalization control. Both IKZF3^{L162R} and IKZF3^{S215R} increased luciferase activity compared to the EV control, whilst IKZF3^{WT} unexpectedly only showed a modest increase in SYK activity (**Fig. 44A**).

IKZF3 can form heterodimers with IKZF1. IKZF1 is a known regulator of SYK, so we wanted to test whether the co-transfection of IKZF1 affected SYK promoter activity (116). Compared to the EV control, IKZF1 is able to increase the transactivation of SYK at its promotor, with the addition of IKZF3 further increasing the activity (**Fig. 44B**). When co-expressed with IKZF1, IKZF3^{WT} or IKZF3^{MUT} increased *SYK* promoter activity. These results were comparable (**Fig. 44A+ B**), with the expression of IKZF1 increasing *SYK* promoter activity further.
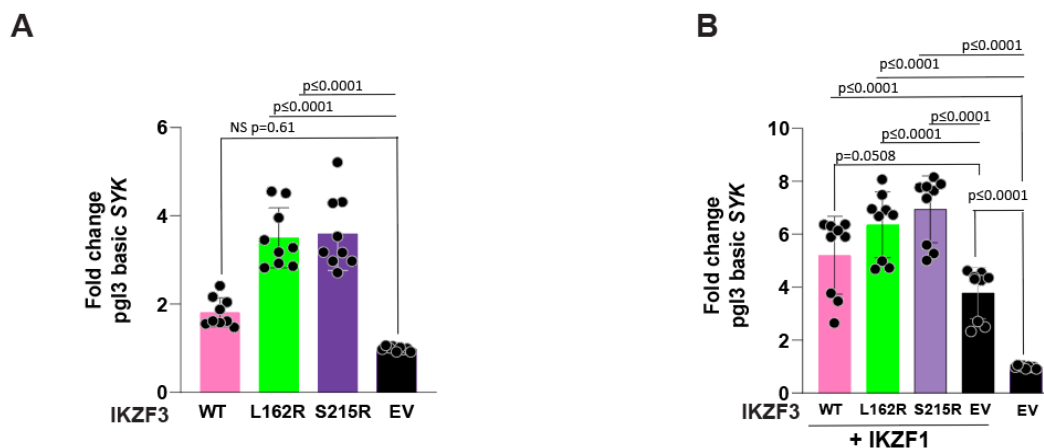
Figure 44- IKZF3^{MUT} binds to the SYK promoter.

A) HEK 293T cells were transfected with a cloned fragment of the *SYK* promoter, in addition to renilla normalization control plasmid, and *IKZF3*^{WT}, *IKZF3*^{MUT}, or an EV control. Firefly luciferase activity was measured after 48 hours and normalized to the Renilla transfection control. Data are displayed as fold change relative to the EV control (N=3 ±SD). **B)** SYK promoter luciferase activity as described above, but including co-transfection with *IKZF1* (N=3 ±SD). **Abbreviations-** IKZF3, IKAROS family zinc finger 3; IKZF, IKAROS family zinc finger 1; SYK, spleen associated tyrosine kinase; EV, empty vector; WT, wild type.

In conclusion, we could show that IKZF3^{L162R} or increased IKZF3^{WT} protein expression is associated with amplified *SYK* mRNA and protein expression in lymphoid cells. In HEK 293T cells, we show that IKZF3 can bind to the SYK promoter and activate expression. However, the upregulation of *SYK* by IKZF3^{WT} or IKZF3^{L162R}, which resulted in increased protein expression in pre-B cells, lymphoma cells, and in our FL-like B cell model cannot be fully explained. The interplay of coactivators (e.g., IKZF1 amongst others) requires further functional investigation using a lymphoid cell model.

4. Discussion

4.1   The molecular ontogeny of follicular lymphoma

4.1.1   Common precursor cells

In my thesis, I first wanted to directly map the molecular ontogeny of FL. We hypothesized that some mutations may precede the *BCL2*/*IGH* translocation and be acquired in HSPCs. These HSPCs would then undergo B lineage commitment and subsequently acquire the BCL2/IGH translocation (subsequent hit model). Our hypothesis is supported by previous work from Horton et al., who showed that *Crebbp* loss in HSPCs can promote lymphomagenesis (66). It is also supported by previous work from our lab, where we reported an *EP300* mutation in CD34$^+$CD19$^-$CD10$^-$ cells from a patient who later developed FL after 8 years with mutations, including *EP300* (65). To date, there is no direct evidence of CPCs in FL. Yet, the targeting of early acquired mutations (CPCs, the presumed origin of relapse) is clinically important as it could offer the chance to eradicate the disease.

In this study, however, my data is consistent with the 'first hit' model of lymphomagenesis. We did not identify any mutations in HSPCs confirmed negative for the BCL2/IGH translocation, suggesting that mutations are acquired after the translocation. The concept of the BCL2/IGH translocation being the first hit in lymphomagenesis is supported by its acquisition in early B cell development and its consistent truncal nature (63, 105, 127).

Although based on a small cohort size, our data provide evidence of the absence of mutations in HSPCs in FL, supporting the idea that the *BCL2*/*IGH* translocation precedes the acquisition of CPC-defining mutations. This concept is highlighted by recent data from Schroers-Martin et al. In this preliminary study presented at the American Society of Hematology conference 2020; they used bone marrow aspirates, peripheral blood, and lymph node samples from patients with *CREBBP* or *KMT2D* mutations (N=6), in their FL tumors. They sorted HSPCs from bone marrow and peripheral blood and observed *CREBBP* mutations only in committed B cells, but not in precursor populations (CD34$^+$/CD20$^-$) or in lymphoid/ myeloid disease. Thus, these data further highlight that HSPCs may not be the precursor reservoir in FL.

4.1.2   Minimal residual disease

Interestingly, our data show that *BCL2*/*IGH* translocated cells can persist and are detectable in blood and bone marrow specimens years after allogeneic transplantation. The absence of CPC-defining mutations (shared mutations between initial diagnosis and relapse) suggests these cells are not contributing to relapse.

Clinically the presence of *BCL2*/*IGH* translocated cells is used as a marker for minimal residual disease (MRD) (128). However, this concept is questionable if cells exist in the periphery that are translocated but don't contribute to relapse (128). Mutation detection in peripheral blood samples would allow better assessment of residual tumor cells that may then contribute to a relapse (129). Furthermore, the advent of more modern NGS technologies allows for a more sensitive comprehensive MRD assessment, including detecting not only the *BCL2*/*IGH* translocation but multiple other targets (e.g., *CREBBP* and *KMT2D* mutations) (130, 131).

4.1.3   CPCs are likely tissue-resident

Another important point is the absence of CPC-defining mutations in B cells that are circulating in the peripheral blood. It is likely that CPCs that are the origin of relapsed disease do not circulate to a sizeable extent but are tissue-resident. This concept fits with the idea that FL CPCs are highly dependent on a microenvironment and are likely tissue-resident, e.g., in the bone marrow or lymphoid tissues (129). This could also explain difficulties in eradicating FL, as the tissue penetration of CD20 antibodies is limited (132).

Additionally, the absence of CPC-defining mutations in *BCL2*/*IGH* translocated cells from HSPC-enriched LMNCs from autologous stem cell transplantations could provide a further explanation for why in vivo rituximab purging prior to transplantation did not improve patient´s outcome (133). Eliminating BCL2/IGH translocated cells from stem cell products only makes sense if these cells are capable of progressing into FL.

4.1.4   Perspective

Understanding how the timing of mutation acquisition contributes to B cell biology and ultimately a disease phenotype is an important open question. Analysis in humans is particularly challenging due to the asymptomatic nature of FL for many years, potentially decades before primary tumor development. Studying the evolution of FL in the human setting has relied on retrospective studies with samples from initial diagnosis and relapse. A comprehensive picture of FL evolution is clinically challenging and would require biopsies prior to the disease onset, which is not feasible.

4.1.5   An unbiased functional in vivo screen to identify drivers of B cell lymphomas

Transposon screens have been used to successfully identify genetic drivers of B and T cell lymphomas (134, 135). Transposons are DNA elements that are mobile and can disrupt gene function via inserting in or near genes. Sleeping Beauty and PiggyBac transposases have been extensively engineered to facilitate this in vivo. Furthermore, the engineering of transposon promoter/enhancer elements allows both loss or gain-of-function mutations depending on the orientation of the transposon and where it is in relation to specific genes (135-137). Therefore, we wanted to perform a screen in the context of an FL mouse model that overexpresses BCL2 (Emu-BCL2) and activates transposition at different stages of differentiation. In this way, we hope to identify cancer genes important for lymphoma development when activated at different stages of differentiation.

We have developed, in collaboration with the laboratory of Marc Schmidt-Supprian, a transposon/transposase screen in 3 different Cre-restricted mouse lines (138). The FL-like Emu-BCL2 mice were crossed with lineage-specific Cre lines (Vav-Cre, Mb1-Cre, Cγ1-Cre) (85-87). These mice were then crossed with mice expressing the transposase (Rosa26^{LSL-PB}) and the transposon (ATP2) (**Fig. 45**).
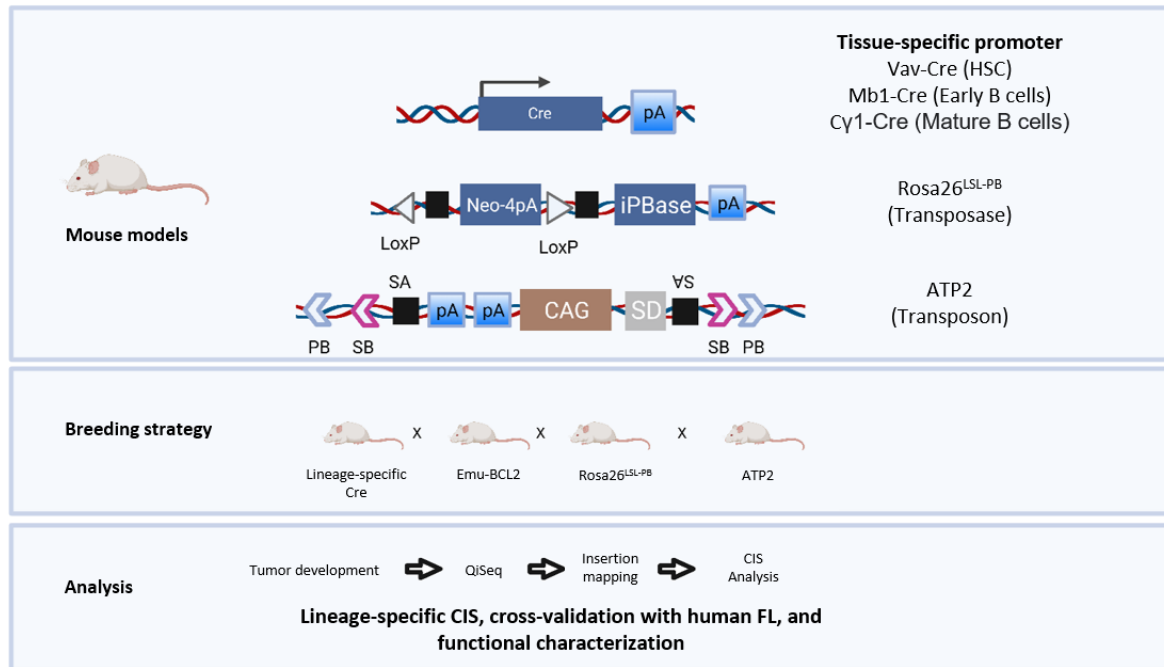
Figure 45- Overview of the ongoing transposon/ transposase forward genetic screen.

Three Cre-restricted mice strains (Vav, Mb1, and Cγ1-Cre) were crossed with Emu-BCL2 mice. These were then crossed to the Rosa 26 [LSL-PB] mice to activate Cre-restricted transposition. Successfully genotyped mice then undergo tumor watch. Tumors are then analyzed via quantitative insertion-site sequencing (QISeq) before insertional mapping and the identification of alterations (136). **Abbreviations-** Cre, Cre recombinase, SD, splice donor; iPBase, insect version of the piggyBac transposase; SA, splice acceptor; CAG, CAG promoter, piggyBac (PB) and Sleeping Beauty (SB).

During the course of my Ph.D., I set up the breeding's and genotyped the mice with a current cohort of 35 mice with all 4 transgenes. We are currently aging correctly genotyped mice, expanding our cohort, and analyzing some initial mice that have developed tumors.

In the context of an FL-like mouse model (Emu-BCL2), these studies will yield new data on how B cell malignancies develop and evolve. While NGS has profiled the landscape of genetic changes, this in vivo screen will expand on the known drivers of lymphoma development (e.g., mutations of *CREBBP* and *KMT2D*), identifying transcriptionally, epigenetically, or post-transcriptionally deregulated genes that are critical players in the development of B cell malignancies.

4.2 *STAT6* mutations in follicular lymphoma

4.2.1 Clonality

As we were unable to identify mutations in HSPCs for functional characterization, we decided to investigate *STAT6* mutations due to their truncal and clonal nature (63, 105, 139). In contrast to Okosun et al., who identified clonal *STAT6* mutations with a high VAF (100%), we found *STAT6* mutations to be both clonal and sub-clonal. This is consistent with other studies, including in both FL and DLBCL (63, 140, 141). Some *STAT6* mutations have also been identified as CPC-defining events, present at relapse and diagnosis, whilst others seem to be important for malignant transformation (63). It is intriguing to speculate the unique biology and selective pressures that may drive clonal or sub-clonal *STAT6* mutations, and they, therefore, represent interesting candidates for functional characterization.

In my thesis, I significantly contributed to our understanding of how *STAT6* mutations drive a self-reinforcing microcircuit. Previous studies have shown that in the presence of IL-4 STAT6 homodimers form a complex with coactivators in the nucleus, including PARP14, forming a STAT6 enhanceosome complex, which drives STAT6-dependent gene expression (36-39). Specifically, I showed in my thesis that:

-STAT6^{D419G} mutations are gain-of-function; demonstrated by my CFU assay/ serial replating phenotype.
-IP demonstrated that STAT6^{D419G} and PARP14 interact/ colocalize.
-qChIP showed that STAT6^{D419G} and not STAT6^{WT} directly binds to the PARP14 promoter.
-FL-like model system recapitulated previous findings, including increased mRNA and protein expression of PARP14 as well as cytokines involved in the re-education of the TME (*CCL17*, *CCL21*).

We propose a model in which, in the presence of IL-4, gain-of-function STAT6^{MUT} and not STAT6^{WT} drives an increase in the levels of *PARP14* in lymphoma cells by directly binding to its promoter and increasing expression. Increased levels of PARP14 then, in turn, drive the assembly of the enhanceosome complex, resulting in increased STAT6-dependent gene expression and thereby amplifying the microcircuit (**Fig. 46**).
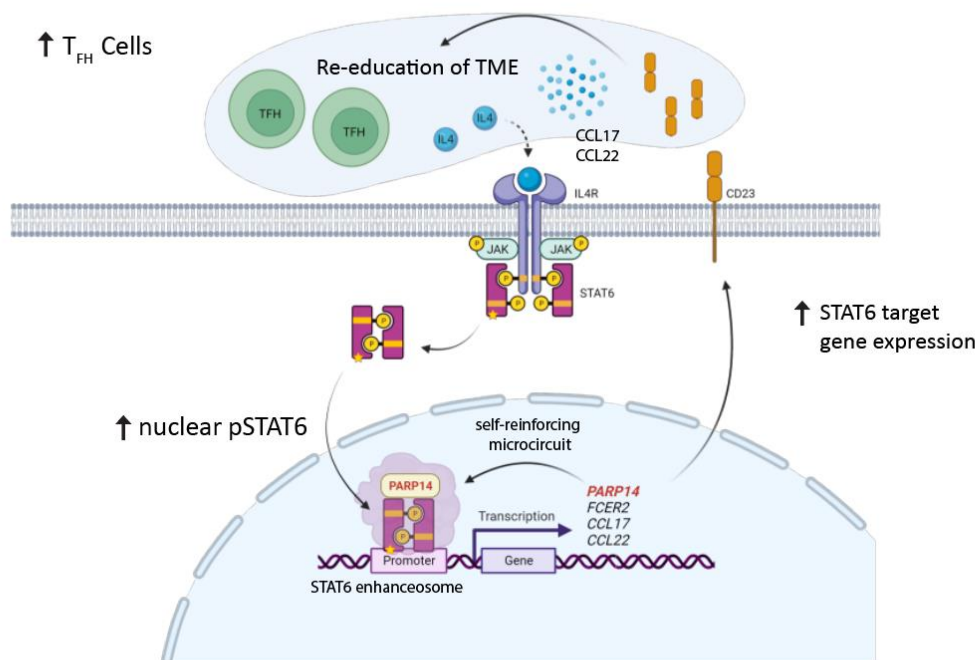
Figure 46- Proposed model-STAT6^{MUT} self-reinforcing microcircuit.

T$_{FH}$ cells produce IL-4, which activates JAK/STAT signaling. Increased JAK/STAT signaling in STAT6^{MUT} cells (indicated by the star) leads to increased pSTAT6, which accumulates in the nucleus driving increased activation of target genes. STAT6^{MUT} but not STAT6^{WT} binds to the PARP14 promoter and upregulates its gene expression. Increased PARP14 promotes the formation of the STAT6 enhanceosome complex, which increases STAT6-dependent gene expression. Increased activation of genes such as *FCER2*, *CCL17*, and *CCL22* leads to increased secretion of chemokines, which in turn attracts more T$_{FH}$ cells, thereby re-educating the tumor microenvironment and further amplifying the microcircuit. This Figure is published in the journal *Leukemia* (108). **Abbreviations-** IL-4, interleukin 4; STAT6, signal transducer and activator of transcription 6; pSTAT6, phosphorylated STAT6; PARP14, Poly(adp-ribose) polymerase family member 14; *FCER2* (CD23), Fc Epsilon Receptor II; *CCL17,* C-C Motif Chemokine Ligand 17; *CCL22,* C-C Motif Chemokine Ligand 22.

We provide further functional data to show that the T$_{FH}$ enriched FL microenvironment (source of IL-4), together with *STAT6* mutations, can drive FL development (56, 142, 143). The increased activation of the *STAT6* signaling cascade in *STAT6*^{MUT}, in turn, not only drives increased *PARP14* expression but also directly regulates and amplifies other *STAT6*-regulated genes, including chemokines CCL17 and CCL22. FL cells produce these chemokines in response to IL-4 stimulation, and they then promote T$_{reg}$ recruitment and the further accumulation of IL-4-producing T$_{FH}$ cells (57). I showed in FL-like B Cells that IL-4 stimulation upregulates *CCL17* and *CCL22* in STAT6^{MUT} cells. Therefore, we hypothesize that chemokine secretion can further drive this regulatory circuit by attracting IL-4-producing T$_{FH}$ cells.

In summary, we show that *STAT6* mutations drive a self-reinforcing microcircuit that amplifies IL-4 induced STAT6 dependent gene activation and results in increased PARP14 levels. Therapeutically targeting PARP14 is, therefore, a promising approach for the treatment of *STAT6*^MUT FL.

4.2.2   PARP14- A novel therapeutic target of STAT6^MUT lymphoma

A recent study demonstrated PARP14s role in IL-4-driven tumorigenesis. Selective inhibition of PARP14 was able to drive a switch from a protumor IL-4 mRNA signature to an anti-tumor inflammatory response (144). Further analysis in our lab also highlighted this link, showing that inhibition of *PARP14* can abrogate the *STAT6*^MUT gain-of-function phenotype (40).

We show that IL-4 is required for *STAT6*^MUT gain-of-function phenotype, including increased target gene expression. IL-4 is a critical survival factor for normal B cells and is often used in short-term ex vivo cultures to improve cell proliferation and survival. Mice models have shown that loss of Parp14 impairs IL-4-induced B cell survival (145). Thus, inhibiting PARP14 in FL cells in the context of an IL-4-rich microenvironment is an attractive therapeutic option that should be investigated further.

4.2.3   Re-education of the tumor microenvironment

The TME in FL has been shown to impact clinical course and treatment outcome (14, 146-148). Yet, due to the inability to model the TME in vitro, the process by which FL cells interact and alter the cells of the microenvironment remains incompletely understood. In our study, we show that patients with *STAT6* mutations have increased IL-4 signaling, which drives increased expression of STAT6 target genes *CCL17* and *CCL22*. We were then able to model this in vitro, showing that there is increased expression of these genes in *STAT6*^MUT FL-like B cells.

Defining how FL cells interact and re-educate cells of the microenvironment offers the chance to further identify therapeutic treatment options that might provide benefit in the context of particular types of cells of the microenvironment.

Our data shows that the *STAT6*^MUT gain-of-function phenotype is dependent on IL-4 stimulation. Therefore, assessing the impact and biological relevance of *STAT6* mutations in patients may only be valuable in the context of an abundant TME, including IL-4-secreting T_{FH} cells. This offers one explanation for why *STAT6* mutations have not been associated with differences in clinical outcomes (13).

4.2.4 Perspective- Unlocking the therapeutic potential of STAT6^MUT lymphoma

In our study, we used an FL-like ex vivo culture to model *STAT6* mutations' gain-of-function phenotype. These FL-like B cells were dependent on growth signals from the FDC feeder layer (YK6-CD40lg-IL21). Unlike lymphoma cell lines, this model system better reflects FLs' dependency on the TME. However, the TME is complex, and it is challenging to develop a model incorporating numerous different cell types ex vivo. Furthermore, in our system, we used tonsil-derived GC B cells, which have a different microenvironment than GC B cells in the lymph nodes.

To better model the TME, recent studies have used primary FL patient samples, developing patient-derived organoid cultures (PDOs). A particular challenge with these models is maintaining FLs in their syngeneic TME (149, 150). In a preliminary study presented at ASH in 2019, Wagar et al. showed that they could propagate PDOs from primary FL and crucially maintain cohesive elements of TME (151). Developing sophisticated models of the TME offers the promise to understand how FL mutations, such as *STAT6,* exploit the TME for their gain-of-function phenotype and then therapeutically target them.

4.2.5 STAT6^MUT target genes

An open question in our study is how *STAT6* mutations may alter DNA binding and target gene selection. A complementary study suggested that the STAT6^D419G mutant has increased binding to STAT6 target genes *CCL17* and *FCER2* (32). Our study indicates that STAT6^D419G binds to novel target genes that STAT6^WT does not bind to (e.g., PARP14). Therefore, a comprehensive ChIP-sequencing experiment in IL-4-stimulated FL-like B cells could identify novel gene targets that may help further define the underlying biology of STAT6^MUT FL.

4.3 *IKZF3*

4.3.1 Clonal gain-of-function *IKZF3* mutations

Unlike *STAT6*, *IKZF3* mutations are primarily clonal. I identified recurrent *IKZF3* mutations with distinct mutation-specific phenotypes when expressed at different stages of B cell development. Therefore, I wanted to functionally characterize these mutations.

In this work, we identified truncal *IKZF3* mutations in FL, analyzing our previously published cohort (17/305 patients), and identifying two hotspot mutations, including the novel S215R mutation and the previously described (L162R) (13, 43).

To assess if the two hot spot mutations were gain-of-function, we again used pre-B CFU assays. To model the molecular ontogeny of the mutations, we expressed them in HSPCs (early acquired event) or pre-B cells (later acquired event). $IKZF3^{L162R}$ showed increased CFUs when expressed in B cells and an outgrowth potential when expressed in FL-like B cells. This is consistent with recent studies that have identified $IKZF3^{L162R}$ as a hotspot gain-of-function mutation in CLL (43).

In contrast, $IKZF3^{S215R}$ mutations showed increased CFU potential when expressed in HSPCs but not in early B cells or FL-like B cells. Unlike *IKZF1,* which is highly expressed in HSPCs, *IKZF3* expression is relatively lower in early progenitors; however, it is highly regulated, peaking in pre-B cells with active pre-BCR signaling (152). IKZF3 forms heterodimers with IKZF1, with recent data showing that IKZF3 mutations can impact IKZF1 transcriptional activity by disrupting DNA binding and altering its selection of target genes (153). Whilst our study did not further investigate the mechanism, altering IKZF1s target gene selection is one hypothesis that could have led to a serial replating phenotype.

The expression of IKZF3 was challenging in both FL-like B cells and lymphoma cell lines. Both lymphoma cell lines and FL-like B cells express high levels of endogenous IKZF3, making it challenging to assess the effects of IKZF3 mutations. $IKZF3^{S215R}$ expression was notably lower than $IKZF3^{L162R}$ in FL-like B Cells, suggesting that expression did not provide a selective advantage. Furthermore, we did not determine any significant phenotype in these cells.

One of the main functions of *IKZF3* is to regulate B cell differentiation from early B cells to plasmablasts (47, 50, 154). The gain-of-function phenotype we observed in HSPCs expressing $IKZF3^{S215R}$ is perhaps context-specific and could depend on the ability of the cells to undergo differentiation. However, this cannot be modeled in our artificial system. Furthermore, given IKZF3s'

low expression in HSPCs and the fact that we did not identify *IKZF3* mutations in HSPCs, we decided to focus on the *IKZF3*^{L162R} mutation.

4.3.2   IKZF3^{WT} is required for B cell proliferation

Targeting IKZF3 with shRNAs, we were able to show in a number of cell lines (N=6) that IKZF3 knockdown reduces B cell growth. We did not determine any significant differences due to mutational status or copy number.

Disruption of IKZF3 via CRISPR-Cas9 further demonstrated in IKZF3^{WT} (Karpas 422) or IKZF3^{S215R} (SU-DHL-16) cells that a certain level of IKZF3^{WT} expression is required for normal B cell proliferation. This concept supports our results that show that IKZF3 mutations in FL are heterozygous.

4.3.3   *IKZF3*^{L162R} mutation provides a selective growth advantage

Our results show that *IKZF3*^{L162R} mutants can drive malignant transformation in FL-like B cells outgrowing a native culture or outcompeting *IKZF3*^{WT} in a competitive growth assay. This is consistent with other studies, particularly in CLL, that have identified this mutation as a driver of malignant transformation (43, 112, 126).

In pre-B cells, the expression of *IKZF3*^{L162R} led to a serial replating phenotype. IKZF3s expression levels steadily increase in response to B cell differentiation with pre-BCR signals leading to a sharp increase in expression (49). Our phenotyping in this study identified *IKZF3*^{WT} or *IKZF3*^{L162R} expressing pre-B cells are in a Fr. C state, characterized by ongoing pre-BCR signaling. At this critical development state, pre-B cells have increased proliferative capacity (48, 116, 122, 155). Disruption of the regulation of pre-B cells due to IKZF3^{L162R} mutation or increased IKZF3^{WT} may lead to a progenitor-like state, characterized by the inability to differentiate into small non-proliferating Fraction D pre-B cells. Yet, the mechanism remains unclear.

4.3.4   IKZF3 regulates B cell activation

B cell activation, proliferation, and BCR signaling were enriched in RNA seq data from IKZF3^{L162R} cells from CFUs or FL-like B cells. IKZF3 is well described as a regulator of B cell activation, and this is mediated via the BCR pathway (43, 48). To this end, we hypothesized that hotspot mutations may disrupt this regulation. Performing immunoblot analysis of the components of the BCR pathway, we identified Syk to be upregulated in mouse Fr. C pre-B cells expressing *IKZF3*^{WT} or *IKZF3*^{L162R} and SYK in human FL-like B cells.

We additionally validated our finding using a lymphoma cell line that was first k/d for IKZF3 before re-expressing IKZF3^{WT} or IKZF3^{MUT} or an EV control. This analysis again revealed upregulation of SYK in IKZF3^{WT} or IKZF3^{L162R} cells, with IKZF3 protein expression level correlating with SYK.

To date, IKZF1/3s role in SYK regulation has been only partially addressed. IKZF1 is known to have an important role in early events in the BCR signaling cascade, with disruption (*Ikzf1*$^{-/-}$ mice) showing reduced Syk protein expression levels (156, 157). Our results are in line with those of *Ikzf1*, suggesting an overlapping or IKZF1/3 complex-mediated regulation of SYK that can be disrupted via IKZF3 k/d.

In our study, we directly show that IKZF3 is able to regulate SYK at the promoter level using HEK 293T cells. Whilst expression and protein analysis showed increased SYK in IKZF3^{WT} or IKZF3^{L162R}, we only observed slight increases in SYK promoter activity in IKZF3^{WT} expressing HEK 293T cells compared to the EV control. In contrast, both mutations showed large increases in SYK promoter activity compared to the EV control. Co-expression of *IKZF3* and *IKZF1* significantly increased luciferase activity and resulted in transactivation, whilst maintaining a similar difference between conditions. These results, therefore, cannot explain increased SYK levels in IKZF3^{WT} or IKZF3^{L162R} pre-B cells or FL-like B cells. However, they highlight that the IKZF1/IKZF3 heterodimer complex can influence the regulation of *SYK* gene transcription, and demonstrate that both IKZF1 or IKZF3 are able to regulate the SYK promoter independently.

In addition to IKZF1, the IKZF1/3 transcription factor complex is known to interact with other cofactors such as MTA2/NuRD, which have overlapping binding sites with IKZF1/3 (158). The absence of such cofactors in HEK 293T cells prevent the effective assessment of IKZF3 mutant's role in SYK regulation. Thus, further experiments using FL-like B cells are required to define the mechanism.

4.3.5 Perspective- Refining the molecular mechanism

Our results indicate that IKZF3 is able to regulate SYK expression at its promoter, with increased activity of IKZF3 mutants. The complex interplay of cofactors was challenging to model in a non-B cell line. Therefore, we propose to develop a luciferase assay to measure SYK promoter activity in lymphoma cells.

Additionally, to complement this approach, qChIP using lymphoma cell lines or FL-like B Cells expressing IKZF3[WT] or IKZF3[MUT], and then qPCR for the SYK promoter region should be performed. This experiment would determine if IKZF3[MUT] binds differently to the SYK promoter region.

4.3.6 Does IKZF3[MUT] differentially regulate genes

Yamashita et al. recently showed that the IKZF3[G159R] mutant has altered DNA binding specificity with over >45,000 differential targets compared to IKZF3[WT] (153). Furthermore, they demonstrated that the IKZF3[G159A] mutant could impair IKZF1 and alter its target gene selection resulting in impaired adaptive immunity. This study shows that IKZF3 mutations can alter target gene selection, yet the specific effects of other recurrent mutations in FL remains to be addressed. We, therefore, purpose to perform ChIP-seq using FL-like GC B cells expressing IKZF3[WT] or IKZF3[MUT] to answer this open question.

4.3.7 Therapeutically targeting IKZF3

Our data shows that targeting IKZF3 by shRNA in lymphoma cells leads to a selective growth disadvantage, with successfully transduced cells being outcompeted over time. We further validated this finding using FL-Like B cells, stably transducing an IKZF3 k/d construct in three independent biological replicates (**Fig. 47A**).
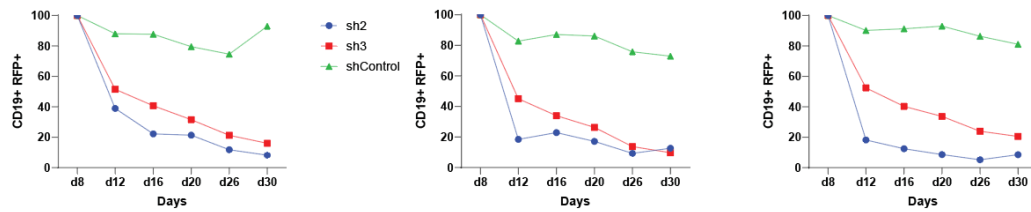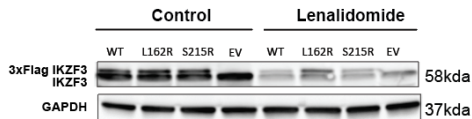
Figure 47- Targeting IKZF3 in FL-like B cells.

A) FL-like B cells expressing *BCL2*/*BCL6* were transduced with an RFP-tagged shRNA construct targeting IKZF3 (sh2 and sh3) in addition to a scrambled control (shControl). Positive cells were measured by flow cytometry for CD19$^+$ and RFP$^+$ positivity over time. **B)** FL-like B cells expressing IKZF3^{WT}, IKZF3^{L162R}, IKZF3^{S215R}, as well as an EV control, were treated with 10 µM lenalidomide or DMSO for 72 hours. Cells were then analyzed by Western blotting. **Abbreviations:** IKZF3, IKAROS family zinc finger 3; BCL2, B cell leukemia/lymphoma 2; BCL6, B cell lymphoma 6; EV, empty vector; WT, wild type; kDa, kilodaltons**.**

Targeted degradation of IKZF3 can also be achieved by treating FL-like B cells with the compound lenalidomide (159). Lenalidomide can slow the growth of FL-like B cells, similar to k/d, with a reduction in IKZF3 protein levels observed by Western blotting (**Fig. 47B**). We observed increased protein levels in IKZF3^{L162R} FL-like B cells by Western blotting. This is consistent with previous studies that have shown that IKZF3^{L162R} mutants are resistant to ubiquitin-mediated proteasomal degradation (159). Yet, whether IKZF3^{L162R} mutants provide lymphoma cells with a selective advantage upon lenalidomide treatment is an open question and should be explored further.

4.4   Summary

In summary, in my Ph.D. thesis, I explored the molecular ontogeny of FL. In the first section of the thesis, we hypothesized that mutations are acquired in HSPCs that then subsequently acquire the *BCL2*/*IGH* translocation, thereby constituting the CPC. However, in carefully controlled experiments, we did not find any mutations in HSPCs, suggesting that mutations are primarily acquired after the *BCL2*/*IGH* translocation in committed B cells. As we were unable to identify mutations in HSPCs for functional characterization, we decided to investigate *STAT6* mutations because they have previously been reported to be primarily truncal and clonal. In this part of my thesis, I further

complemented previous studies, showing that in the presence of IL-4, gain-of-function STAT6^{MUT} and not STAT6^{WT} increase *PARP14* levels in lymphoma cells by directly binding to its promoter and driving its expression. Increased PARP14 levels then drive the assembly/stabilization of the STAT6 enhanceosome complex, resulting in increased STAT6-dependent gene expression. Finally, in the third part of my thesis, I decided to study IKZF3 mutations because a re-analysis of our own FL DNA sequencing data indicated that most of these mutations were truncal. I identified distinct mutation-specific phenotypes when *IKZF3* is expressed at different stages of B cell development. IKZF3^{L162R} induces a proliferative phenotype activating B cells. Functional experiments are still ongoing but suggest that IKZF3^{L162R} disrupts key components of the BCR pathway, such as SYK, to mediate its gain-of-function phenotype.

5. References

1.	Mounier M, Bossard N, Remontet L, Belot A, Minicozzi P, De Angelis R, et al. Changes in dynamics of excess mortality rates and net survival after diagnosis of follicular lymphoma or diffuse large B-cell lymphoma: comparison between European population-based data (EUROCARE-5). The Lancet Haematology. 2015;2(11):e481-91.
2.	Nastoupil L, Sinha R, Hirschey A, Flowers CR. Considerations in the initial management of follicular lymphoma. Community Oncol. 2012;9(11):S53-S60.
3.	Zoellner A, Herfarth K, Herold M, Klapper W, Skoetz N, Hiddemann W. Follicular Lymphoma—Diagnosis, Treatment, and Follow-Up. Dtsch Arztebl International. 2021;118(18):320-5.
4.	Swerdlow SH, Campo E, Harris NL, Jaffe ES, Pileri SA, Stein H, et al., editors. WHO Classification of Tumours of Haematopoietic and Lymphoid Tissues. Geneva, Switzerland: WHO Press; 2008.
5.	Dreyling M, Ghielmini M, Rule S, Salles G, Ladetto M, Tonino SH, et al. Newly diagnosed and relapsed follicular lymphoma: ESMO Clinical Practice Guidelines for diagnosis, treatment and follow-up. Annals of oncology : official journal of the European Society for Medical Oncology. 2021;32(3):298-308.
6.	Michallet A-SAS, Lebras LL, Bauwens DD, Bouafia-Sauvy FF, Berger FF, Tychyj-Pinel CC, et al. Early stage follicular lymphoma: what is the clinical impact of the first-line treatment strategy? Journal of hematology & oncology. 2013;6:45-.
7.	Dreyling M, Ghielmini M, Rule S, Salles G, Vitolo U, Ladetto M. Newly diagnosed and relapsed follicular lymphoma: ESMO Clinical Practice Guidelines for diagnosis, treatment and follow-up. Annals of oncology : official journal of the European Society for Medical Oncology. 2016;27(suppl 5):v83-v90.
8.	Adolph L, Weigert O. Follikuläres Lymphom – Pathogenese, Diagnostik und Therapie. Trillium Krebsmedizin. 2020.
9.	Solal-Céligny P, Roy P, Colombat P, White J, Armitage JO, Arranz-Saez R, et al. Follicular lymphoma international prognostic index. Blood. 2004;104(5):1258-65.
10.	Federico M, Bellei M, Marcheselli L, Luminari S, Lopez-Guillermo A, Vitolo U, et al. Follicular lymphoma international prognostic index 2: a new prognostic index for follicular lymphoma developed by the international follicular lymphoma prognostic factor project. Journal of clinical oncology : official journal of the American Society of Clinical Oncology. 2009;27(27):4555-62.
11.	Bachy E, Maurer MJ, Habermann TM, Gelas-Dore B, Maucort-Boulch D, Estell JA, et al. A simplified scoring system in de novo follicular lymphoma treated initially with immunochemotherapy. Blood. 2018;132(1):49-58.
12.	Oken MM, Creech RH, Tormey DC, Horton J, Davis TE, McFadden ET, et al. Toxicity and response criteria of the Eastern Cooperative Oncology Group. American journal of clinical oncology. 1982;5(6):649-55.
13.	Pastore A, Jurinovic V, Kridel R, Hoster E, Staiger AM, Szczepanowski M, et al. Integration of gene mutations in risk prognostication for patients receiving first-line immunochemotherapy for follicular lymphoma: a retrospective analysis of a prospective clinical trial and validation in a population-based registry. The Lancet Oncology. 2015;16(9):1111-22.
14.	Dave SS, Wright G, Tan B, Rosenwald A, Gascoyne RD, Chan WC, et al. Prediction of survival in follicular lymphoma based on molecular features of tumor-infiltrating immune cells. The New England journal of medicine. 2004;351(21):2159-69.
15.	Huet S, Tesson B, Jais JP, Feldman AL, Magnano L, Thomas E, et al. A gene-expression profiling score for prediction of outcome in patients with follicular lymphoma: a retrospective training and validation analysis in three international cohorts. The Lancet Oncology. 2018;19(4):549-61.
16.	Mlynarczyk C, Fontán L, Melnick A. Germinal center-derived lymphomas: The darkest side of humoral immunity. Immunol Rev. 2019;288(1):214-39.

17.	Allen CD, Cyster JG. Follicular dendritic cell networks of primary follicles and germinal centers: phenotype and function. Seminars in immunology. 2008;20(1):14-25.
18.	Stebegg M, Kumar SD, Silva-Cayetano A, Fonseca VR, Linterman MA, Graca L. Regulation of the Germinal Center Response. Front Immunol. 2018;9:2469-.
19.	Jacob J, Kelsoe G, Rajewsky K, Weiss U. Intraclonal generation of antibody mutants in germinal centres. Nature. 1991;354(6352):389-92.
20.	Mesin L, Ersching J, Victora GD. Germinal Center B Cell Dynamics. Immunity. 2016;45(3):471-82.
21.	Muramatsu M, Kinoshita K, Fagarasan S, Yamada S, Shinkai Y, Honjo T. Class switch recombination and hypermutation require activation-induced cytidine deaminase (AID), a potential RNA editing enzyme. Cell. 2000;102(5):553-63.
22.	Weigert MG, Cesari IM, Yonkovich SJ, Cohn M. Variability in the lambda light chain sequences of mouse antibody. Nature. 1970;228(5276):1045-7.
23.	Tsujimoto Y, Gorham J, Cossman J, Jaffe E, Croce CM. The t(14;18) Chromosome Translocations Involved in B-Cell Neoplasms Result from Mistakes in VDJ Joining. 1985;229(4720):1390-3.
24.	Chiu BC, Dave BJ, Blair A, Gapstur SM, Zahm SH, Weisenburger DD. Agricultural pesticide use and risk of t(14;18)-defined subtypes of non-Hodgkin lymphoma. Blood. 2006;108(4):1363-9.
25.	Liu Y, Hernandez AM, Shibata D, Cortopassi GA. BCL2 translocation frequency rises with age in humans. Proc Natl Acad Sci U S A. 1994;91(19):8910-4.
26.	Roulland S, Faroudi M, Mamessier E, Sungalee S, Salles G, Nadel B. Early steps of follicular lymphoma pathogenesis. Advances in immunology. 2011;111:1-46.
27.	Roulland S, Lebailly P, Lecluse Y, Heutte N, Nadel B, Gauduchon P. Long-term clonal persistence and evolution of t(14;18)-bearing B cells in healthy individuals. Leukemia. 2006;20(1):158-62.
28.	Milpied P, Nadel B, Roulland S. Premalignant cell dynamics in indolent B-cell malignancies. Current opinion in hematology. 2015;22(4):388-96.
29.	Green MR, Kihira S, Liu CL, Nair RV, Salari R, Gentles AJ, et al. Mutations in early follicular lymphoma progenitors are associated with suppressed antigen presentation. 2015;112(10):E1116-E25.
30.	Milpied P, Cervera-Marzal I, Mollichella ML, Tesson B, Brisou G, Traverse-Glehen A, et al. Human germinal center transcriptional programs are de-synchronized in B cell lymphoma. Nature immunology. 2018;19(9):1013-24.
31.	Sablon A, Bollaert E, Pirson C, Velghe AI, Demoulin J-B. FOXO1 forkhead domain mutants in B-cell lymphoma lack transcriptional activity. Scientific Reports. 2022;12(1):1309.
32.	Yildiz M, Li H, Bernard D, Amin NA, Ouillette P, Jones S, et al. Activating STAT6 mutations in follicular lymphoma. Blood. 2015;125(4):668-79.
33.	Ying CY, Dominguez-Sola D, Fabi M, Lorenz IC, Hussein S, Bansal M, et al. MEF2B mutations lead to deregulated expression of the oncogene BCL6 in diffuse large B cell lymphoma. Nature immunology. 2013;14(10):1084-92.
34.	Yildiz M, Li H, Bernard D, Amin NA, Ouillette P, Jones S, et al. Activating STAT6 mutations in follicular lymphoma. Blood. 2015;125(4):668-79.
35.	Pangault C, Amé-Thomas P, Ruminy P, Rossille D, Caron G, Baia M, et al. Follicular lymphoma cell niche: identification of a preeminent IL-4-dependent T(FH)-B cell axis. Leukemia. 2010;24(12):2080-9.
36.	Goenka S, Cho SH, Boothby M. Collaborator of Stat6 (CoaSt6)-associated poly(ADP-ribose) polymerase activity modulates Stat6-dependent gene transcription. The Journal of biological chemistry. 2007;282(26):18732-9.
37.	Hellmuth JC, Louissaint A, Jr., Szczepanowski M, Haebe S, Pastore A, Alig S, et al. Duodenal-type and nodal follicular lymphomas differ by their immune microenvironment rather than their mutation profiles. Blood. 2018;132(16):1695-702.

38.	Mehrotra P, Riley JP, Patel R, Li F, Voss L, Goenka S. PARP-14 functions as a transcriptional switch for Stat6-dependent gene activation. The Journal of biological chemistry. 2011;286(3):1767-76.

39.	Takeda K, Tanaka T, Shi W, Matsumoto M, Minami M, Kashiwamura S, et al. Essential role of Stat6 in IL-4 signalling. Nature. 1996;380(6575):627-30.

40.	Bösl M. Functional characterization of STAT6 mutations in follicular lymphoma. Munich: LMU Munich; 2018.

41.	Bösl MW, Osterode E, Bararia D, Pastore A, Staiger AM, Ott G, et al. STAT6 Is Recurrently and Significantly Mutated in Follicular Lymphoma and Enhances the IL-4 Induced Expression of Membrane-Bound and Soluble CD23. Blood. 2015;126(23):3923-.

42.	Gocho Y, Yang JJ. Genetic defects in hematopoietic transcription factors and predisposition to acute lymphoblastic leukemia. Blood. 2019;134(10):793-7.

43.	Lazarian G, Yin S, ten Hacken E, Sewastianik T, Uduman M, Font-Tello A, et al. A hotspot mutation in transcription factor IKZF3 drives B cell neoplasia via transcriptional dysregulation. Cancer Cell. 2021;39(3):380-93.e8.

44.	Mullighan CG, Zhang J, Kasper LH, Lerach S, Payne-Turner D, Phillips LA, et al. CREBBP mutations in relapsed acute lymphoblastic leukaemia. Nature. 2011;471(7337):235-9.

45.	Sebastian S, Jan MM, Michael K, Christoph R, Alwin K, Sebastian S, et al. EZH2 mutations and impact on clinical outcome: an analysis in 1,604 patients with newly diagnosed acute myeloid leukemia. Haematologica. 2020;105(5):e228-e31.

46.	Cerami E, Gao J, Dogrusoz U, Gross BE, Sumer SO, Aksoy BA, et al. The cBio cancer genomics portal: an open platform for exploring multidimensional cancer genomics data. Cancer discovery. 2012;2(5):401-4.

47.	Morgan B, Sun L, Avitahl N, Andrikopoulos K, Ikeda T, Gonzales E, et al. Aiolos, a lymphoid restricted transcription factor that interacts with Ikaros to regulate lymphocyte differentiation. 1997;16(8):2004-13.

48.	Herzog S, Reth M, Jumaa H. Regulation of B-cell proliferation and differentiation by pre-B-cell receptor signalling. Nature reviews Immunology. 2009;9(3):195-205.

49.	Thompson EC, Cobb BS, Sabbattini P, Meixlsperger S, Parelho V, Liberg D, et al. Ikaros DNA-binding proteins as integral components of B cell developmental-stage-specific regulatory circuits. Immunity. 2007;26(3):335-44.

50.	Wang JH, Avitahl N, Cariappa A, Friedrich C, Ikeda T, Renold A, et al. Aiolos regulates B cell activation and maturation to effector state. Immunity. 1998;9(4):543-53.

51.	Glas AM, Kersten MJ, Delahaye LJ, Witteveen AT, Kibbelaar RE, Velds A, et al. Gene expression profiling in follicular lymphoma to assess clinical aggressiveness and to guide the choice of treatment. Blood. 2005;105(1):301-7.

52.	Glas AM, Knoops L, Delahaye L, Kersten MJ, Kibbelaar RE, Wessels LA, et al. Gene-expression and immunohistochemical study of specific T-cell subsets and accessory cell types in the transformation and prognosis of follicular lymphoma. Journal of clinical oncology : official journal of the American Society of Clinical Oncology. 2007;25(4):390-8.

53.	Harjunpää A, Taskinen M, Nykter M, Karjalainen-Lindsberg ML, Nyman H, Monni O, et al. Differential gene expression in non-malignant tumour microenvironment is associated with outcome in follicular lymphoma patients treated with rituximab and CHOP. British journal of haematology. 2006;135(1):33-42.

54.	Husson H, Carideo EG, Neuberg D, Schultze J, Munoz O, Marks PW, et al. Gene expression profiling of follicular lymphoma and normal germinal center B cells using cDNA arrays. Blood. 2002;99(1):282-9.

55.	Scott DW, Gascoyne RD. The tumour microenvironment in B cell lymphomas. Nature reviews Cancer. 2014;14(8):517-34.

56.	Amé-Thomas P, Le Priol J, Yssel H, Caron G, Pangault C, Jean R, et al. Characterization of intratumoral follicular helper T cells in follicular lymphoma: role in the survival of malignant B cells.

Leukemia. 2012;26(5):1053-63.

57.   Rawal S, Chu F, Zhang M, Park HJ, Nattamai D, Kannan S, et al. Cross talk between follicular Th cells and tumor cells in human follicular lymphoma promotes immune evasion in the tumor microenvironment. Journal of immunology (Baltimore, Md : 1950). 2013;190(12):6681-93.

58.   Bararia D, Hildebrand JA, Stolz S, Haebe S, Alig S, Trevisani CP, et al. Cathepsin S Alterations Induce a Tumor-Promoting Immune Microenvironment in Follicular Lymphoma. Cell reports. 2020;31(5):107522.

59.   Dheilly E, Battistello E, Katanayeva N, Sungalee S, Michaux J, Duns G, et al. Cathepsin S Regulates Antigen Processing and T Cell Activity in Non-Hodgkin Lymphoma. Cancer Cell. 2020;37(5):674-89.e12.

60.   Béguelin W, Teater M, Meydan C, Hoehn KB, Phillip JM, Soshnev AA, et al. Mutant EZH2 Induces a Pre-malignant Lymphoma Niche by Reprogramming the Immune Response. Cancer Cell. 2020;37(5):655-73.e11.

61.   Kumar E, Pickard L, Okosun J. Pathogenesis of follicular lymphoma: genetics to the microenvironment to clinical translation. 2021;194(5):810-21.

62.   Okosun J, Bodor C, Wang J, Araf S, Yang CY, Pan C, et al. Integrated genomic analysis identifies recurrent mutations and evolution patterns driving the initiation and progression of follicular lymphoma. Nature genetics. 2014;46(2):176-81.

63.   Pasqualucci L, Khiabanian H, Fangazio M, Vasishtha M, Messina M, Holmes AB, et al. Genetics of follicular lymphoma transformation. Cell reports. 2014;6(1):130-40.

64.   Tsujimoto Y, Gorham J, Cossman J, Jaffe E, Croce CM. The t(14;18) chromosome translocations involved in B-cell neoplasms result from mistakes in VDJ joining. Science. 1985;229(4720):1390-3.

65.   Weigert O, Weinstock DM. The evolving contribution of hematopoietic progenitor cells to lymphomagenesis. Blood. 2012;120(13):2553-61.

66.   Horton SJ, Giotopoulos G, Yun H, Vohra S, Sheppard O, Bashford-Rogers R, et al. Early loss of Crebbp confers malignant stem cell properties on lymphoid progenitors. Nature cell biology. 2017;19(9):1093-104.

67.   Weigert O, Kopp N, Lane AA, Yoda A, Dahlberg SE, Neuberg D, et al. Molecular ontogeny of donor-derived follicular lymphomas occurring after hematopoietic cell transplantation. Cancer discovery. 2012;2(1):47-55.

68.   Langmead B, Salzberg SL. Fast gapped-read alignment with Bowtie 2. Nature Methods. 2012;9(4):357-9.

69.   Talevich E, Shain AH, Botton T, Bastian BC. CNVkit: Genome-Wide Copy Number Detection and Visualization from Targeted DNA Sequencing. PLOS Computational Biology. 2016;12(4):e1004873.

70.   Dehairs J, Talebi A, Cherifi Y, Swinnen JV. CRISP-ID: decoding CRISPR mediated indels by Sanger sequencing. Scientific Reports. 2016;6(1):28973.

71.   Feng J, Liu T, Qin B, Zhang Y, Liu XS. Identifying ChIP-seq enrichment using MACS. Nature protocols. 2012;7(9):1728-40.

72.   Untergasser A, Cutcutache I, Koressaar T, Ye J, Faircloth BC, Remm M, et al. Primer3--new capabilities and interfaces. Nucleic acids research. 2012;40(15):e115-e.

73.   Cibulskis K, Lawrence MS, Carter SL, Sivachenko A, Jaffe D, Sougnez C, et al. Sensitive detection of somatic point mutations in impure and heterogeneous cancer samples. Nature Biotechnology. 2013;31(3):213-9.

74.   Wickham H. ggplot2: Elegant Graphics for Data Analysis: Springer New York; 2009.

75.   Love MI, Huber W, Anders S. Moderated estimation of fold change and dispersion for RNA-seq data with DESeq2. Genome Biology. 2014;15(12):550.

76.   Andrews S. FastQC: a quality control tool for high throughput sequence data. Babraham Bioinformatics, Babraham Institute, Cambridge, United Kingdom; 2010.

77.   Martin M. Cutadapt removes adapter sequences from high-throughput sequencing reads.

2011. 2011;17(1):3 %J EMBnet.journal.

78.   Parekh S, Ziegenhain C, Vieth B, Enard W, Hellmann I. zUMIs - A fast and flexible pipeline to process RNA sequencing data with UMIs. GigaScience. 2018;7(6).

79.   Dobin A, Davis CA, Schlesinger F, Drenkow J, Zaleski C, Jha S, et al. STAR: ultrafast universal RNA-seq aligner. Bioinformatics. 2013;29(1):15-21.

80.   Hiddemann W, Kneba M, Dreyling M, Schmitz N, Lengfelder E, Schmits R, et al. Frontline therapy with rituximab added to the combination of cyclophosphamide, doxorubicin, vincristine, and prednisone (CHOP) significantly improves the outcome for patients with advanced-stage follicular lymphoma compared with therapy with CHOP alone: results of a prospective randomized study of the German Low-Grade Lymphoma Study Group. Blood. 2005;106(12):3725-32.

81.   Carter SL, Cibulskis K, Helman E, McKenna A, Shen H, Zack T, et al. Absolute quantification of somatic DNA alterations in human cancer. Nature Biotechnology. 2012;30(5):413-21.

82.   Soriano M. Plasmids 101: Gateway Cloning Addgene2017 [Available from: https://blog.addgene.org/plasmids-101-gateway-cloning.

83.   Caeser R, Gao J, Di Re M, Gong C, Hodson DJ. Genetic manipulation and immortalized culture of ex vivo primary human germinal center B cells. Nature Protocols. 2021;16(5):2499-519.

84.   Caeser R, Gao J, Di Re M, Gong C, Hodson DJ. Genetic manipulation and immortalized culture of ex vivo primary human germinal center B cells. Nature protocols. 2021;16(5):2499-519.

85.   Georgiades P, Ogilvy S, Duval H, Licence DR, Charnock-Jones DS, Smith SK, et al. VavCre transgenic mice: a tool for mutagenesis in hematopoietic and endothelial lineages. Genesis (New York, NY : 2000). 2002;34(4):251-6.

86.   Hobeika E, Thiemann S, Storch B, Jumaa H, Nielsen PJ, Pelanda R, et al. Testing gene function early in the B cell lineage in mb1-cre mice. Proc Natl Acad Sci U S A. 2006;103(37):13789-94.

87.   Strasser A, Whittingham S, Vaux DL, Bath ML, Adams JM, Cory S, et al. Enforced BCL2 expression in B-lymphoid cells prolongs antibody responses and elicits autoimmune disease. Proc Natl Acad Sci U S A. 1991;88(19):8661-5.

88.   Rancan C, Schirrmann L, Hüls C, Zeidler R, Moosmann A. Latent Membrane Protein LMP2A Impairs Recognition of EBV-Infected Cells by CD8+ T Cells. PLoS Pathog. 2015;11(6):e1004906.

89.   Bagnoli JW, Ziegenhain C, Janjic A, Wange LE, Vieth B, Parekh S, et al. Sensitive and powerful single-cell RNA sequencing using mcSCRB-seq. Nature Communications. 2018;9(1):2937.

90.   Janjic A, Wange LE, Bagnoli JW, Geuder J, Nguyen P, Richter D, et al. Prime-seq, efficient and powerful bulk RNA-sequencing. 2021:2021.09.27.459575.

91.   Spandidos A, Wang X, Wang H, Seed B. PrimerBank: a resource of human and mouse PCR primer pairs for gene expression detection and quantification. Nucleic Acids Research. 2009;38(suppl_1):D792-D9.

92.   Liao Y, Smyth GK, Shi W. The R package Rsubread is easier, faster, cheaper and better for alignment and quantification of RNA sequencing reads. Nucleic Acids Res. 2019;47(8):e47.

93.   Zhou Y, Zhou B, Pache L, Chang M, Khodabakhshi AH, Tanaseichuk O, et al. Metascape provides a biologist-oriented resource for the analysis of systems-level datasets. Nature Communications. 2019;10(1):1523.

94.   Huggett JF, Foy CA, Benes V, Emslie K, Garson JA, Haynes R, et al. The digital MIQE guidelines: Minimum Information for Publication of Quantitative Digital PCR Experiments. Clin Chem. 2013;59(6):892-902.

95.   van der Velden VH, Cazzaniga G, Schrauder A, Hancock J, Bader P, Panzer-Grumayer ER, et al. Analysis of minimal residual disease by Ig/TCR gene rearrangements: guidelines for interpretation of real-time quantitative PCR data. Leukemia. 2007;21(4):604-11.

96.   Deliard S, Zhao J, Xia Q, Grant SF. Generation of high quality chromatin immunoprecipitation DNA template for high-throughput sequencing (ChIP-seq). Journal of visualized experiments : JoVE. 2013(74).

97.   Subramanian A, Tamayo P, Mootha VK, Mukherjee S, Ebert BL, Gillette MA, et al. Gene set enrichment analysis: A knowledge-based approach for interpreting genome-wide expression

profiles. 2005;102(43):15545-50.

98.	Doulatov S, Notta F, Eppert K, Nguyen LT, Ohashi PS, Dick JE. Revised map of the human progenitor hierarchy shows the origin of macrophages and dendritic cells in early lymphoid development. Nat Immunol. 2010;11(7):585-93.

99.	Ran FA, Hsu PD, Wright J, Agarwala V, Scott DA, Zhang F. Genome engineering using the CRISPR-Cas9 system. Nature protocols. 2013;8(11):2281-308.

100.	Haebe S, Keay W, Alig S, Mohr AW, Martin LK, Heide M, et al. The molecular ontogeny of follicular lymphoma: gene mutations succeeding the BCL2 translocation define common precursor cells. British journal of haematology. 2022;196(6):1381-7.

101.	Bagwell CB, Hill BL, Wood BL, Wallace PK, Alrazzak M, Kelliher AS, et al. Human B-cell and progenitor stages as determined by probability state modeling of multidimensional cytometry data. Cytometry B Clin Cytom. 2015;88(4):214-26.

102.	Albinger-Hegyi A, Hochreutener B, Abdou M-T, Hegyi I, Dours-Zimmermann MT, Kurrer MO, et al. High frequency of t(14;18)-translocation breakpoints outside of major breakpoint and minor cluster regions in follicular lymphomas: improved polymerase chain reaction protocols for their detection. Am J Pathol. 2002;160(3):823-32.

103.	van Dongen JJM, Langerak AW, Brüggemann M, Evans PAS, Hummel M, Lavender FL, et al. Design and standardization of PCR primers and protocols for detection of clonal immunoglobulin and T-cell receptor gene recombinations in suspect lymphoproliferations: Report of the BIOMED-2 Concerted Action BMH4-CT98-3936. Leukemia. 2003;17(12):2257-317.

104.	Wiesner M, Zentz C, Mayr C, Wimmer R, Hammerschmidt W, Zeidler R, et al. Conditional immortalization of human B cells by CD40 ligation. PLoS One. 2008;3(1):e1464-e.

105.	Okosun J, Bödör C, Wang J, Araf S, Yang CY, Pan C, et al. Integrated genomic analysis identifies recurrent mutations and evolution patterns driving the initiation and progression of follicular lymphoma. Nature genetics. 2014;46(2):176-81.

106.	Kridel R, Chan FC, Mottok A, Boyle M, Farinha P, Tan K, et al. Histological Transformation and Progression in Follicular Lymphoma: A Clonal Evolution Study. PLOS Medicine. 2016;13(12):e1002197.

107.	Pasqualucci L, Khiabanian H, Fangazio M, Vasishtha M, Messina M, Holmes Antony B, et al. Genetics of Follicular Lymphoma Transformation. Cell reports. 2014;6(1):130-40.

108.	Mentz M, Keay W, Strobl CD, Antoniolli M, Adolph L, Heide M, et al. PARP14 is a novel target in STAT6 mutant follicular lymphoma. Leukemia. 2022.

109.	Goenka S, Kaplan MH. Transcriptional regulation by STAT6. Immunol Res. 2011;50(1):87-96.

110.	Passerini V, Boesl M, Silkenstedt E, Osterode E, Heide M, Kridel R, et al. PARP14 Is a Novel Therapeutic Target in STAT6 mutant Follicular Lymphoma. Blood. 2018;132(Supplement 1):2842-.

111.	Lu X, Nechushtan H, Ding F, Rosado MF, Singal R, Alizadeh AA, et al. Distinct IL-4-induced gene expression, proliferation, and intracellular signaling in germinal center B-cell-like and activated B-cell-like diffuse large-cell lymphomas. Blood. 2005;105(7):2924-32.

112.	Takahashi K, Vitale C, Bueso-Ramos C, Wang F, Kim E, Zhang J, et al. IKZF3 p.L162R Is a Recurrent Hotspot Mutation in Chronic Lymphocytic Leukemia (CLL). Blood. 2015;126(23):4136-.

113.	Georgopoulos K, Bigby M, Wang J-H, Molnar A, Wu P, Winandy S, et al. The ikaros gene is required for the development of all lymphoid lineages. Cell. 1994;79(1):143-56.

114.	Yoshida T, Georgopoulos K. Ikaros fingers on lymphocyte differentiation. International Journal of Hematology. 2014;100(3):220-9.

115.	Lu G, Middleton RE, Sun H, Naniong M, Ott CJ, Mitsiades CS, et al. The myeloma drug lenalidomide promotes the cereblon-dependent destruction of Ikaros proteins. Science. 2014;343(6168):305-9.

116.	Ferreirós-Vidal I, Carroll T, Taylor B, Terry A, Liang Z, Bruno L, et al. Genome-wide identification of Ikaros targets elucidates its contribution to mouse B-cell lineage specification and pre-B-cell differentiation. Blood. 2013;121(10):1769-82.

117.	Aird EJ, Lovendahl KN, St. Martin A, Harris RS, Gordon WR. Increasing Cas9-mediated

homology-directed repair efficiency through covalent tethering of DNA repair template. Communications Biology. 2018;1(1):54.

118. Kakarougkas A, Jeggo PA. DNA DSB repair pathway choice: an orchestrated handover mechanism. The British journal of radiology. 2014;87(1035):20130685.

119. Yin S, Lazarian G, Ten Hacken E, Sewastianik T, Gohil S, Li S, et al. IKZF3 Overexpression Phenocopies Gain-of-Function Mutation in Chronic Lymphocytic Leukemia. Blood. 2020;136:9.

120. Hardy RR, Carmack CE, Shinton SA, Kemp JD, Hayakawa K. Resolution and characterization of pro-B and pre-pro-B cell stages in normal mouse bone marrow. The Journal of experimental medicine. 1991;173(5):1213-25.

121. Herzog S, Reth M, Jumaa HJNRI. Regulation of B-cell proliferation and differentiation by pre-B-cell receptor signalling. 2009;9(3):195-205.

122. Melchers F, Ten Boekel E, Seidl T, Kong XC, Yamagami T, Onishi K, et al. Repertoire selection by pre-B-cell receptors and B-cell receptors, and genetic control of B-cell development from immature to mature B cells. 2000;175(1):33-46.

123. Mullighan CG, Miller CB, Radtke I, Phillips LA, Dalton J, Ma J, et al. BCR-ABL1 lymphoblastic leukaemia is characterized by the deletion of Ikaros. Nature. 2008;453(7191):110-4.

124. Mullighan CG, Su X, Zhang J, Radtke I, Phillips LA, Miller CB, et al. Deletion of IKZF1 and prognosis in acute lymphoblastic leukemia. The New England journal of medicine. 2009;360(5):470-80.

125. Fisher AG, Burdet C, Bunce C, Merkenschlager M, Ceredig R. Lymphoproliferative disorders in IL-7 transgenic mice: expansion of immature B cells which retain macrophage potential. International immunology. 1995;7(3):415-23.

126. Lazarian G, Yin S, Font-tello A, Ten Hacken E, Sevastianik T, Tom D, et al. KZF-L162R Mutation Affects Splenic Mature B Cell Development and Alters Expression of Aiolos Target Genes. Blood. 2018;132(Supplement 1):668-.

127. Kim T, Tyndel MS, Kim HJ, Ahn JS, Choi SH, Park HJ, et al. Spectrum of somatic mutation dynamics in chronic myeloid leukemia following tyrosine kinase inhibitor therapy. Blood. 2017;129(1):38-47.

128. Pulsoni A, Della Starza I, Cappelli LV, Tosti ME, Annechini G, Cavalli M, et al. Minimal residual disease monitoring in early stage follicular lymphoma can predict prognosis and drive treatment with rituximab after radiotherapy. 2020;188(2):249-58.

129. Huet S, Salles G. Potential of Circulating Tumor DNA for the Management of Patients With Lymphoma. JCO oncology practice. 2020;16(9):561-8.

130. Herrera AF, Armand P. Minimal Residual Disease Assessment in Lymphoma: Methods and Applications. Journal of clinical oncology : official journal of the American Society of Clinical Oncology. 2017;35(34):3877-87.

131. Jung D, Jain P, Yao Y, Wang M. Advances in the assessment of minimal residual disease in mantle cell lymphoma. Journal of Hematology & Oncology. 2020;13(1):127.

132. Smith MR. Rituximab (monoclonal anti-CD20 antibody): mechanisms of action and resistance. Oncogene. 2003;22(47):7359-68.

133. Pettengell R, Schmitz N, Gisselbrecht C, Smith G, Patton WN, Metzner B, et al. Rituximab Purging and/or Maintenance in Patients Undergoing Autologous Transplantation for Relapsed Follicular Lymphoma: A Prospective Randomized Trial From the Lymphoma Working Party of the European Group for Blood and Marrow Transplantation. Journal of Clinical Oncology. 2013;31(13):1624-30.

134. Wartewig T, Kurgyis Z, Keppler S, Pechloff K, Hameister E, Öllinger R, et al. PD-1 is a haploinsufficient suppressor of T cell lymphomagenesis. Nature. 2017;552(7683):121-5.

135. Weber J, de la Rosa J, Grove CS, Schick M, Rad L, Baranov O, et al. PiggyBac transposon tools for recessive screening identify B-cell lymphoma drivers in mice. Nature Communications. 2019;10(1):1415.

136. Rad R, Rad L, Wang W, Cadinanos J, Vassiliou G, Rice S, et al. PiggyBac transposon

mutagenesis: a tool for cancer gene discovery in mice. Science. 2010;330(6007):1104-7.

137.   Rad R, Rad L, Wang W, Strong A, Ponstingl H, Bronner IF, et al. A conditional piggyBac transposition system for genetic screening in mice identifies oncogenic networks in pancreatic cancer. Nature genetics. 2015;47(1):47-56.

138.   Rad R, Rad L, Wang W, Cadinanos J, Vassiliou G, Rice S, et al. PiggyBac transposon mutagenesis: a tool for cancer gene discovery in mice. Science. 2010;330(6007):1104-7.

139.   Kridel R, Chan FC, Mottok A, Boyle M, Farinha P, Tan K, et al. Histological Transformation and Progression in Follicular Lymphoma: A Clonal Evolution Study. PLoS Med. 2016;13(12):e1002197.

140.   Morin RD, Assouline S, Alcaide M, Mohajeri A, Johnston RL, Chong L, et al. Genetic Landscapes of Relapsed and Refractory Diffuse Large B-Cell Lymphomas. Clinical cancer research : an official journal of the American Association for Cancer Research. 2016;22(9):2290-300.

141.   Xian RR, Xie Y, Haley LM, Yonescu R, Pallavajjala A, Pittaluga S, et al. CREBBP and STAT6 co-mutation and 16p13 and 1p36 loss define the t(14;18)-negative diffuse variant of follicular lymphoma. Blood Cancer Journal. 2020;10(6):69.

142.   Calvo KR, Dabir B, Kovach A, Devor C, Bandle R, Bond A, et al. IL-4 protein expression and basal activation of Erk in vivo in follicular lymphoma. Blood. 2008;112(9):3818-26.

143.   Pandey S, Mourcin F, Marchand T, Nayar S, Guirriec M, Pangault C, et al. IL-4/CXCL12 loop is a key regulator of lymphoid stroma function in follicular lymphoma. Blood. 2017;129(18):2507-18.

144.   Schenkel LB, Molina JR, Swinger KK, Abo R, Blackwell DJ, Lu AZ, et al. A potent and selective PARP14 inhibitor decreases protumor macrophage gene expression and elicits inflammatory responses in tumor explants. Cell chemical biology. 2021;28(8):1158-68.e13.

145.   Cho SH, Goenka S, Henttinen T, Gudapati P, Reinikainen A, Eischen CM, et al. PARP-14, a member of the B aggressive lymphoma family, transduces survival signals in primary B cells. Blood. 2009;113(11):2416-25.

146.   Kiaii S, Clear AJ, Ramsay AG, Davies D, Sangaralingam A, Lee A, et al. Follicular lymphoma cells induce changes in T-cell gene expression and function: potential impact on survival and risk of transformation. J Clin Oncol. 2013;31(21):2654-61.

147.   Mondello P, Fama A, Larson MC, Feldman AL, Villasboas JC, Yang Z-Z, et al. Lack of intrafollicular memory CD4 + T cells is predictive of early clinical failure in newly diagnosed follicular lymphoma. Blood Cancer Journal. 2021;11(7):130.

148.   Tobin JWD, Keane C, Gunawardana J, Mollee P, Birch S, Hoang T, et al. Progression of Disease Within 24 Months in Follicular Lymphoma Is Associated With Reduced Intratumoral Immune Infiltration. J Clin Oncol. 2019;37(34):3300-9.

149.   Foxall R, Narang P, Glaysher B, Hub E, Teal E, Coles MC, et al. Developing a 3D B Cell Lymphoma Culture System to Model Antibody Therapy. 2021;11.

150.   Tian YF, Ahn H, Schneider RS, Yang SN, Roman-Gonzalez L, Melnick AM, et al. Integrin-specific hydrogels as adaptable tumor organoids for malignant B and T cells. Biomaterials. 2015;73:110-9.

151.   Wagar LE, Sworder B, Khodadoust MS, Davis MM, Alizadeh AA. Follicular Lymphoma Organoids for Investigating the Tumor Microenvironment. Blood. 2019;134(Supplement_1):2799-.

152.   Schwickert TA, Tagoh H, Gültekin S, Dakic A, Axelsson E, Minnich M, et al. Stage-specific control of early B cell development by the transcription factor Ikaros. Nature immunology. 2014;15(3):283-93.

153.   Yamashita M, Kuehn HS, Okuyama K, Okada S, Inoue Y, Mitsuiki N, et al. A variant in human AIOLOS impairs adaptive immunity by interfering with IKAROS. Nature immunology. 2021;22(7):893-903.

154.   Kuehn HS, Chang J, Yamashita M, Niemela JE, Zou C, Okuyama K, et al. T and B cell abnormalities, pneumocystis pneumonia, and chronic lymphocytic leukemia associated with an AIOLOS defect in patients. Journal of Experimental Medicine. 2021;218(12).

155.   Mullighan CG, Su X, Zhang J, Radtke I, Phillips LA, Miller CB, et al. Deletion of IKZF1 and prognosis in acute lymphoblastic leukemia. 2009;360(5):470-80.

156.   Nera K-P, Alinikula J, Terho P, Narvi E, Törnquist K, Kurosaki T, et al. Ikaros has a crucial role in regulation of B cell receptor signaling. 2006;36(3):516-25.

157.   Trageser D, Iacobucci I, Nahar R, Duy C, von Levetzow G, Klemm L, et al. Pre-B cell receptor-mediated cell cycle arrest in Philadelphia chromosome-positive acute lymphoblastic leukemia requires IKAROS function. The Journal of experimental medicine. 2009;206(8):1739-53.

158.   Lu X, Chu C-S, Fang T, Rayon-Estrada V, Fang F, Patke A, et al. MTA2/NuRD Regulates B Cell Development and Cooperates with OCA-B in Controlling the Pre-B to Immature B Cell Transition. Cell reports. 2019;28(2):472-85.e5.

159.   Krönke J, Udeshi ND, Narla A, Grauman P, Hurst SN, McConkey M, et al. Lenalidomide causes selective degradation of IKZF1 and IKZF3 in multiple myeloma cells. Science. 2014;343(6168):301-5.

6. Acknowledgments

7. Affidavit

Affidavit

Keay, William

_____
Surname, first name

_____
Street

_____
Zip code, town, country

I hereby declare, that the submitted thesis entitled:

The Molecular Ontogeny of Follicular Lymphoma: Identification and Functional Characterization of Selected Truncal Gene Mutations

is my own work. I have only used the sources indicated and have not made unauthorised use of services of a third party. Where the work of others has been quoted or reproduced, the source is always given.

I further declare that the dissertation presented here has not been submitted in the same or similar form to any other institution for the purpose of obtaining an academic degree.

Munich, 06.02.23   William Keay
place, date   Signature doctoral candidate

8. Confirmation of congruency

LMU LUDWIG-MAXIMILIANS-UNIVERSITÄT MÜNCHEN	Promotionsbüro Medizinische Fakultät	MMRS	

Confirmation of congruency between printed and electronic version of the doctoral thesis

Keay, William
_____
Surname, first name

_____
Street

_____
Zip code, town, country

I hereby declare, that the submitted thesis entitled:

***The Molecular Ontogeny of Follicular Lymphoma:
Identification and Functional Characterization of Selected Truncal
Gene Mutations***

is congruent with the printed version both in content and format.

Munich, 06.02.23   William Keay
place, date   Signature doctoral candidate

9. List of publications

Haebe S*, **Keay W*,** Alig S, Mohr AW, Martin LK, Heide M, Secci R, Krebs S, Blum H, Moosmann A, Louissaint A Jr, Weinstock DM, Thoene S, von Bergwelt-Baildon M, Ruland J, Bararia D, Weigert O. The molecular ontogeny of follicular lymphoma: gene mutations succeeding the BCL2 translocation define common precursor cells. **Br J Haematol**. 2022 Mar;196(6):1381-1387. doi: 10.1111/bjh.17990. Epub 2021 Dec 29. PMID: 34967008.

Mentz, M*, **W. Keay*,** C. D. Strobl, M. Antoniolli, L. Adolph, M. Heide, A. Lechner, S. Haebe, E. Osterode, R. Kridel, C. Ziegenhain, L. E. Wange, J. A. Hildebrand, T. Shree, E. Silkenstedt, A. M. Staiger, G. Ott, H. Horn, M. Szczepanowski, J. Richter, R. Levy, A. Rosenwald, W. Enard, U. Zimber-Strobl, M. von Bergwelt-Baildon, W. Hiddemann, W. Klapper, M. Schmidt-Supprian, M. Rudelius, D. Bararia, V. Passerini and O. Weigert (2022). "PARP14 is a novel target in STAT6 mutant follicular lymphoma." **Leukemia**.

Alig, S., V. Jurinovic, M. Shahrokh Esfahani, S. Haebe, V. Passerini, J. C. Hellmuth, E. Gaitzsch, **W. Keay**, N. Tahiri, A. Zoellner, A. Rosenwald, W. Klapper, H. Stein, A. Feller, G. Ott, A. M. Staiger, H. Horn, M. L. Hansmann, C. Pott, M. Unterhalt, C. Schmidt, M. Dreyling, A. A. Alizadeh, W. Hiddemann, E. Hoster and O. Weigert (2020). "Evaluating upfront high-dose consolidation after R-CHOP for follicular lymphoma by clinical and genetic risk models." **Blood Advances** 4(18): 4451-4462.

Adolph, L. C., Q. Fichaux, C. D. Strobl, M. Antoniolli, V. Passerini, **W. D. Keay,** V. Jurinovic, A. Lechner, D. J. Hodson, M. von Bergwelt, M. Subklewe, M. Rudelius and O. Weigert (2021). "CHOP but Not Bendamustine Reverses EZH2 Y641 Mutation Induced MHC-I/II Loss in Human Lymphoma Models." **Blood** 138: 2391. (**ASH conference 2020**)

Antoniolli, M., M. Solovey, D. Bararia, C. D. Strobl, W. D. Keay, J. A. Hildebrand, M. Heide, V. Passerini, L. Wange, W. Enard, S. Thieme, H. Blum, M. Rudelius, S. Bultmann, H. Leonhardt, M. Subklewe, M. von Bergwelt, M. Colomé-Tatché and O. Weigert (2021). "ARID1A Controls a Novel Transcriptional Network Regulating FAS in Follicular Lymphoma." **Blood** 138 (Supplement 1): 3492-3492. (**ASH conference 2020**)

*equal contribution